MULTI-SCALE MODELING
WITH AN INVERSE MAPPING CAPABILITY
FOR DESIGNING BLAST RESISTANT COMPOSITE PANEL
FOR LIGHT WEIGHT VEHICLES

by
John P Kim

A dissertation submitted in partial fulfillment
of the requirements for the degree of
Doctor of Philosophy
(Mechanical Engineering)
in the University of Michigan
2013

Doctoral Committee:

Professor Nickolas Vlahopoulos, Chair
Professor Greg Hulbert
Professor Jwo Pan
Professor David J. Singer

To my wonderful wife, Cindy who always supported and believed in me.

ACKNOWLEDGEMENTS

I would like to take this opportunity to thank for having a very understanding and encouraging research advisor, Professor Nickolas Vlahopoulos, to guide my Ph.D. study. Without his guidance, patience and encouragement, this research work would not be possible. I would also like to thank all my Ph.D. committee members for their time, inspiration and feedback for this study. Thanks to all the staff at the Automotive Research Center at the University of Michigan for allowing genuine chances to present my research in several seminars at the TARDEC and the ARL that gave me irreplaceable feedback. Finally, I would like to thank to my parents and brother Mark for giving me their endless support and providing relief throughout my study.

TABLE OF CONTENTS

LIST OF FIGURES

LIST OF TABLES

ABSTRACT

MULTI-SCALE MODELING WITH AN INVERSE MAPPING CAPABILITY FOR DESIGNING BLAST RESISTANT COMPOSITE PANEL FOR LIGHT WEIGHT VEHICLES

by

John P Kim

Chair: Nickolas Vlahopoulos

Military vehicles emphasize weight reduction for increased fuel efficiency and airborne transportation. Weight reduction and a high level of survivability to blast loads are mutually competing objectives. Composite materials that exhibit good blast resistance characteristics can be employed for reducing weight in vehicles. This dissertation aims to create a computational optimization framework to determine the ply configuration of composite laminate panels of reduced weight and a high level of survivability.

First, research is performed for investigating the performance of a multi-scale simulation process for composite material analysis by integrating a fully coupled Multi-Scale Methods (MSM) framework in both micro-scale (fiber and matrix) and global-scale (vehicle) levels. The MSM framework is based on homogenization and localization between the micro-scale and the global-scale to consider deformation effects on effective material properties of the composites. The functionality of this multi-scale simulation capability and the effort to incorporate micro-constitutive material behavior at high strain

rate loading into the simulation process are studied with associated case studies. Next, an inverse mapping capability for linking desired material properties with the composition of their micro structure in Micromechanics Analysis Code (MAC) in a computationally efficient manner is formulated, and an optimization analysis for identifying the desirable material properties for increasing the blast resistant characteristics is conducted. Finally, an optimization computational framework that can determine the configuration of each ply of a composite laminate panel to achieve the desired blast resistance characteristics at minimum panel thickness is created. A case study demonstrates how the new simulation approach can determine a matrix-fiber configuration and the orientation of the laminates for designing a blast resistant composite panel. Another optimal design case study of a sandwich structural composites panel is performed to present an extended capability of the computational framework.

CHAPTER 1:
INTRODUCTION

Military vehicles emphasize weight reduction for increased fuel efficiency and airborne transportation. Weight reduction and a high level of survivability to blast loads are mutually competing objectives. Composite materials that exhibit good blast resistance characteristics can be employed to reduce weight in vehicles. The work summarized in this dissertation presents the technical elements of a computational optimization process to determine the ply configuration of composite laminate panels to achieve both increased resistance to blast loads and reduced weight. A more detailed discussion of research background is presented in the next section.

1.1: Research Background

The design of vehicles to resist a blast and provide protection to the vehicle and its occupants is of great interest. New combat vehicle designs emphasize weight reduction for increased fuel efficiency and airborne transportation; therefore, a significant effort must be invested to ensure that the vehicle's survivability is not compromised. Currently combat vehicles are subjected to blasts from explosive threats. The recent wars in Iraq and Afghanistan have underlined the importance for increasing the protection of a vehicle's occupant to explosions. In addition to the loss of life, traumatic brain injuries and extremities injuries have been observed (Fischer, 2009; Galarneau et al, 2006). Weight

reduction and high level of survivability are mutually competing objectives. Therefore, significant effort must be invested in order to ensure that the vehicle's survivability is not compromised. Composite materials provide some of the most viable options for manufacturing composite armor that can increase survivability without a significant weight penalty.

In the first part of this research, a new multi-scale simulation for modeling the response of composite armor to explosive threats is presented. The development is based on the integrating BEST and MAC software with commercial finite element solver. This novel multi-scale simulation enables configuring the composite at the matrix-fiber level with consideration of the global deformation effect.

Then, this multi-scale simulation can be used for improving the blast resistance of the composite panel by configuring its properties at the micro-level. The main objective of this second part is to develop an optimization framework that can determine the configuration of each ply of a composite laminate panel for achieving desired blast resistance characteristics at minimum panel thickness. A more detailed discussion of literature and research objectives are presented in the next section.

1.2: Literature Review and Research Objectives

The recent surge of multi-scale modeling related to solid mechanics originated from an unlikely source in the mid-90s, "the reduction of underground nuclear testing by more precise and accurate predictive tools" (Leszczynski and Shukla, 2009). Multi-scale modeling has increased rapidly in recent years using parallel computing power and

experimental capabilities, which is for structure-property relations characterizing to the atomic level. This multi-scale modeling capacitates solving the physical problems, which have important features on multiple scales, by calculating material properties or system behavior on one level with information from a different level. Multi-scale modeling can: reduce product costs through innovations in material, product, and process designs; reduce the number of costly large systems scale experiments; increase product quality and performance by providing more accurate predictions of response to design loads; and aid in developing new materials.

Multi-scale modeling has been researched in different disciplines (solid mechanics, material science, physics, mathematics, biological, and chemistry), and applied to different length scales (from atoms to vehicles). In the field of multi-scale modeling of composites, a micromechanical method of cells has been developed for the analysis of fibrous composites with periodic structure (Aboudi, 1989; Aboudi, 1991). Analysis of composites using the Generalized Method of Cells (GMC), which is the basis of the Micromechanics Analysis Code (MAC) has been developed for the modeling of multiphase periodic composites. Effective constitutive laws that govern the overall behavior of elastic-viscoplastic composite materials within GMC have been established (Paley and Aboudi, 1992; Aboudi, 1995). GMC theory was reformulated for maximum computational efficiency (Bednarcyk and Pindera, 1999; Bednarcyk and Pindera, 2000), and modified for the Integrated multi-scale Micromechanics Analysis Code (ImMAC), which was developed by the NASA Glenn Research Center. ImMAC, which includes the Micromechanics Analysis Code (MAC) with the generalized method of cells, analyzes the thermo-inelastic behavior of composite

materials and laminates (Bednarcyk and Steven, 2002). Examples of the uses of multi-scale modeling in the composites field include: predicting the tensile strength of uni-directional fiber composites, including metal, polymer, and ceramic matrix composites (Xia and Curtin, 2008); acting as a comprehensive framework for adaptive concurrent multilevel computational analysis (Ghosh, 2008); modeling different composite architecture, including particle-reinforced, fiber-reinforced, and woven fabric composites (Kwon, 2008); analyzing composites while considering extreme deformation from blast loads (Karagiozova et al, 2010); and analyzing composites using the commercial finite element solver, LS-DYNA, implemented to model interfacial debonding (Soutis et al, 2011).

However, to date, the capability of multi-scale modeling to analyze composites has been limited to specific phenomena, ranges of the blast loads, and length scales. It cannot be used to analyze extremely large deformation effects on a global scale. In order to consider large deformations, it is important to include strain rate effects in the simulation because the properties of materials under impact differ from those determined under static loading conditions (Hopkinson, 1901). A recent experimental laboratory study on the effect of high strain rate loading conditions emphasized the large inelastic deformation behavior of composites (Wang et al, 2011). A mismatch between the essentially static tensile or compressive test results, for which an approximately linear dependence of flow stress on the logarithm of strain rate occurs, and those higher flow stresses derived from generally more complicated dynamic material test results, also prove the importance of the high strain rate effect (Armstrong and Walley, 2008). Further, high strain rate effects, from the shapes

of pulses produced by explosion and projectile, become more and more important for blast event simulation.

Therefore, it is important to create a new Multi-Scale Methods (MSM) to model the response of a composite panel to these large blast loads deformations. In order to give consideration to high strain rate deformation for blast event simulation, a modified Bodner-Partom model is applied in this work by the creation of new code to implement this micro-scale material model. The increased number of material constants of this micro-scale material model allows much more flexibility in representing viscoplastic, time- and temperature-dependent responses and produces better agreement with the experimental data (Sands et al, 2010).

In the first phase of this dissertation, Multi-Scale Methods (MSM) creation, the LS-DYNA solver, utilizing the BEST synthesis tool, is employed for simulating the soil–explosive–air interaction and calculating accurately the loads on a target structure. In the past, several efforts have been made for modeling explosions and their effect on structures (Gupta, 1999; Bird, 2001; Gupta, 2002; Sun et al, 2006). The BEST process for conducting a complete analysis for the explosive/soil/vehicle/occupant interaction has been made along with validation through comparison to test data (Sun et al, 2006; Zhang et al, 2008). BEST is a synthesis tool with built-in knowledge for preparing the various data files required for conducting the blast simulation, and it is utilized in this research for evaluating the loads from the explosion on the structure and for preparing the LS-DYNA or ABAQUS computations for the vehicle structure. A major advantage of utilizing the LS-DYNA and ABAQUS solvers for blast event simulations instead of CTH hydrocode (McGlaun et al,

1990; Bell and Hertel, 1994) is that LS-DYNA and ABAQUS are commercially readily accessible codes, have a friendly user interface, can exchange data with commercial pre- and post- processors, make interpretation of the structure of the data files easy, and have numerical models for Anthropomorphic Test Devices (ATD) that can be readily integrated in the simulation as part of the vehicle finite element model. BEST provides a series of templates that guide the user in developing the necessary models for the blast event simulations. A capability has been developed for automatically creating the finite element model for the air, the soil, and the explosive, given the structural finite element model for the vehicle. The effect of moisture in the soil properties is considered during the generation of the soil–explosive–air model used by the LS-DYNA solver. Tracers are defined in the model for all structural finite elements, which are on the outer part of the vehicle structure and are subjected to the load from the blast. The data for the pressure load from the explosion comprise the loading for the structural response of the target structure. A methodology was also developed for using the pressure information from the explosion for assigning appropriate velocity and trajectories to projectiles and fragments that are part of the explosive threat. The projectiles are considered along with the blast pressure load to hit the structure, and the response of the structure to the combined loads can be computed.

Sequentially, the ABAQUS Explicit solver coupled with the Micromechanics Analysis Code (MAC) is used for computing the corresponding response of a target structure to the loads from the explosion within the MSM.

In the second phase of this dissertation, a method to use MSM in the optimal design problem is studied. Although the MSM can be used for a micro-level configuration design

of the composites panel to improve the blast resistant capabilities, directly engaging the MSM simulations within the optimization environment for assessing the response of a panel to the blast loads for every different combination of design variables is computationally expensive. Moreover, a large number of different panel configurations must be evaluated during an optimization process. Therefore, in order to consider computational efficiency, an Inverse Material Engineering Algorithm (IMEA) is developed in this work to identify each ply configuration that results into a prescribed set of global mechanical characteristics for a panel. In the final computational framework, which is the last objective of this work and consists of the modified MSM and IMEA, first an optimization analysis is performed using modified MSM to determine the desired mechanical characteristics of a composite blast resistant panel with minimum thickness. Then the composition of each ply (i.e.; volume ratio and fiber orientation) is determined using the IMEA process.

The inverse mapping method has been researched in different fields (e.g., material science, physics, mathematics) to estimate inputs through given outputs. Different from forward problems, which determine output from input, the inverse method capacitates material property determination from output data that has efficiency (Schnur and Zabaras, 1992). In the field of composites, the inverse method has been used recently to determine material properties (Jiang et al, 2007). The IMEA process is proposed to inversely calculate the composition of the composites from optimal designed output data using several composites theories. A more detailed discussion of the overall process of the IMEA is presented in Chapter 3.

In the following paragraphs, the objectives of this work are summarized. There are three stages of this work. The main objective of the first stage is to establish the integration of a fully coupled Multi-Scale Methods (MSM) framework in both the micro-scale (fiber and matrix) and the global-scale (vehicle) levels to model the response of a composite panel to these large deformations (blast loads from an explosive threat). Secondary objectives include extending this MSM capability to consider large deformations from blast load by including strain rate effects.

The objective of the second stage of the work is the creation of an Inverse Material Engineering Algorithm (IMEA), which is based on inverse mapping theory, using several composites theory: nonlinear formulation for high strain rate effect, strength equations for fiber-reinforced composites, and Classic Laminate Theory (CLT). Secondary objectives include validating this IMEA using an optimal design problem to obtain a practical composite blast resistant panel's micro-level configuration design, such as a fiber volume fraction and a layer orientation of the laminated composites.

The objective of the third, and final stage is the creation of an optimization computational framework, which includes modified MSM and IMEA for micro-level configuration design of the composite panel which satisfies the light weight and the strength simultaneously. The optimization analysis using modified MSM is performed first to determine the desired mechanical characteristics of a composite blast resistant panel with minimum thickness. Then, the IMEA process identifies the composition of each ply. Secondary objectives include applying this computational framework to design an optimal

micro-level configuration of the composite panels, and validating the results. A detailed discussion of each objective is presented in the next session.

1.3: Research Contributions

In the area of multi-scale modeling, the proposed optimization computational framework, which enables multi-scale modeling of the composites over large strain rate loading conditions with computational efficiency, is very valuable for designing composite structures and satisfying two ever-present conflicting objectives: lighter weight and strength in performance.

The main contributions of this thesis are:

- The development of a Multi-Scale Methods (MSM) capability based on the coupling of the MAC and ABAQUS Explicit codes. The high strain rate effects from blast load are included in the modeling process by introducing the modified Bodner-Partom model in the MAC calculation.
- The simulation using MSM is time consuming and not suitable for being utilized within a highly iterative design environment. Thus, an Inverse Material Engineering Algorithm (IMEA) is developed to calculate the micro-scale configuration design of the composites, when the effective material property matrix at each time increment are defined.
- An optimization framework is developed for assessing the effective material properties that can minimize the thickness of a panel subjected to a blast

load. Then, the IMEA algorithm is used to identify its physical composition. Case studies demonstrate the utility and value of the new design process.

In the first stage of the research, a fully coupled Multi-Scale Methods (MSM), which has capacities to propagate local phenomena of composites from deformation, is created by coupling the MAC and the ABAQUS Explicit solver module. The Explicit solver of ABAQUS, enabling dynamic analysis with large range of the loads, is coupled with the MAC code, enabling multi-scale computing from the micro level to the global level. A major advantage of this integrated multi-scale simulation process is that it allows propagating information from the constitutive micro-level, such as fiber failures, matrix damage, inelasticity, and interfacial debonding, to the global structural response level. The MAC and the ABAQUS codes exchange information through homogenization and localization simulation processes. During the homogenization process, the MAC code determines the material response at the integration points within each ABAQUS element from Micro-scale (Fiber and matrix level) to Global-scale (Vehicle level) pass through Meso-scale (Laminated composite material level). In essence, MAC operates as a nonlinear constitutive model within ABAQUS, representing the heterogeneous material. In reverse, during the localization process, local stress and strains computed by ABAQUS from incrementally applied loading are applied to the MAC for obtaining updated effective material properties (Figure 1).

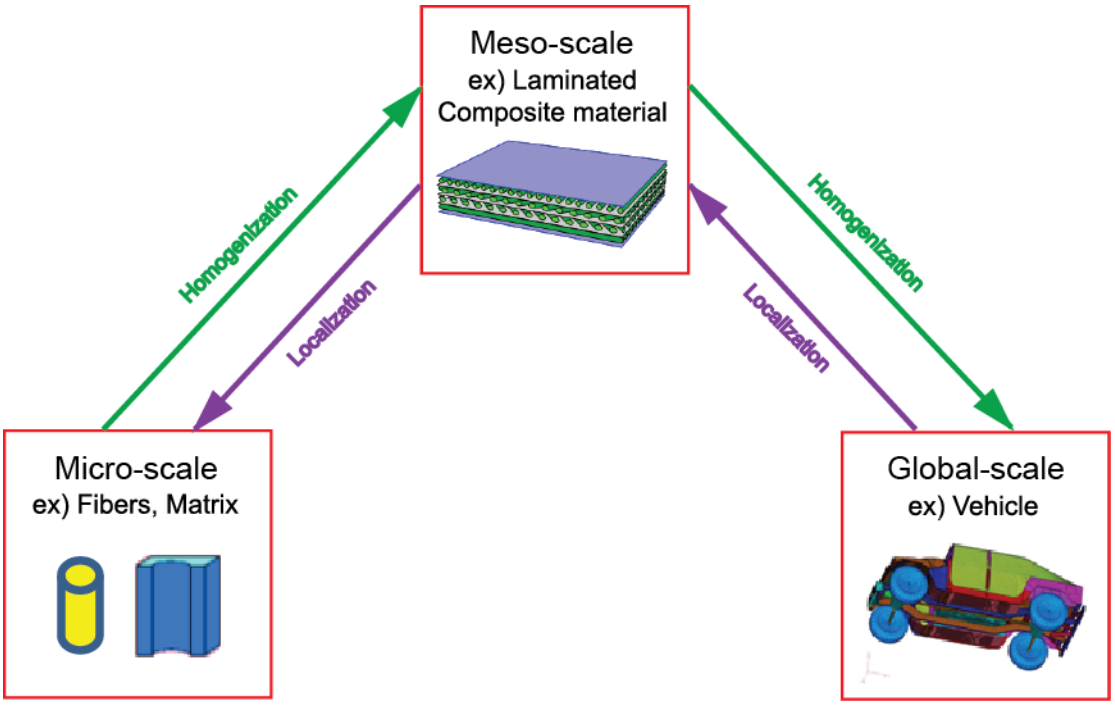

Figure 1: Associated level scales for composite analysis.

The coupling can be done in a fully coupled multi-scale mode and can be also done as a one-way-coupling without global scale deformation effects for demonstration study. In fully coupled mode, at each iteration of each time step, information about the strain field at each integration point of each element is communicated from ABAQUS to MAC. In return, the MAC code computes the constitutive properties and provides their updated values to ABAQUS. In the one-way coupling mode, the MAC code is used for computing the constitutive material properties (assuming no deformation) and provides them as input to the ABAQUS analysis. In order to consider the high strain rate effects in the blast event simulation process, the modified Bodner-Partom model is included instead of the Generalized Viscoplasticity with Potential Structure (GVIPS) model in the MAC calculation. The new user defined micro-scale model for MAC is written to apply a

modified model, and a demonstration case study is performed. This first stage of the work is included in a journal paper, "Development of a Blast Event Simulation Process for Multi-Scale Modeling of Composite Armor for Light Vehicles", accepted by the International Journal of Vehicle Design (IJVD), 2011.

In order to design the micro-level configuration of the composites, the fully coupled MSM can be integrated into the optimization model for global-scale objectives using micro-scale design variables. The only problem is the expensive computational cost of the fully coupled MSM. In the second stage of this research, to overcome the expensive computational cost, the Inverse Material Engineering Algorithm (IMEA), which capacitates the micro-scale configuration design of the composites with global deformation effects, is studied. A modified MSM, capacitates provision of the effective material properties of each time increment of the ABAQUS Explicit calculation by a predicted strain rate. The eliminated iteration processes between the MAC code and the ABAQUS Explicit solver enable one to get the optimized material properties of a certain strain rate condition with efficient computational cost. However, in order to obtain practical design parameters of the micro-level configuration for the composite panel, the material matrix from the modified MSM should be converted to effective design factors, such as the fiber volume fraction and the layer orientation of the laminated composites. The necessity of this conversion is the basis of the IMEA that inversely calculates the material matrix to the micro-scale configuration design factor. This inverse calculation is based on several composites equations, and the feasibility of IMEA is provided with validation case studies that

inversely calculate for the one unknown and compares with given conditions as well as two unknown circumstances.

The last stage links the previous two stages into an optimization computational framework. First, the modified MSM is used for one of the nonlinear constraints in the optimization frame to find optimal material properties and thickness data. Then, through IMEA, I can inversely calculate the formerly obtained optimal result from the first step to the optimal micro-level configuration of the composites panel. A case study demonstrates how the new simulation approach can determine a matrix-fiber configuration and the orientation of the laminates for designing blast resistant composite panel. The second and last stage of the work is included in a journal paper, "An inverse mapping capability for designing blast resistant composite panels through multi-scale modeling", submitted to the International Journal of Vehicle Design (IJVD), 2012.

The additional optimal design case study presents an extended capability of the computational framework for the heterogeneous material sandwich structure. In order to impart significant reinforcement, the energy dissipation is considered using a rubber sandwich structure, which consists of a rubber material between two fiber-reinforced composites panels. Additional layers of adhesive and center material are added, and an optimal design case study is performed using this sandwich structure, which is subjected to a blast pressure load condition. A detailed overview of the dissertation is presented in the next section.

1.4: Dissertation Overview

The body of this dissertation is arranged to follow the stages of the research described above. In Chapter 2, a multi-scale simulation process using the coupled MAC and ABAQUS Explicit solver to compute the response of a structure subjected to a load from an explosion is established. Background on the Micromechanics Analysis Code (MAC) and Multi-Scale Methods (MSM) is presented in section 2.1. and 2.2. A fully coupling sequence of the ABAQUS-MAC solution is presented in section 2.3. In order to demonstrate the type of results obtained by the two coupling approaches, a generic target structure with a V shaped outer bottom, subjected to a load from an explosion, is analyzed using the one-way-coupling approach and the fully coupled method outlined in sections 2.4 and 2.5. Further, a case study associated with the analysis of a generic all-metal structure and a metal-composite structure is also performed and presented in section 2.6. It is demonstrated that the new simulation approach can determine a matrix-fiber configuration and the orientation of the laminates in order to maximize the protection offered by the composite armor while reducing the weight. In addition to the above MSM development, in order to consider the high strain rate effects in the simulation process, the modified Bodner-Partom model is employed instead of the GVIPS in the MAC calculation by using an additionally created micro-scale material code. This is presented in section 2.7. The computational process of the MSM is modified to provide appropriate material property specifications to the appropriate place and to harmonize the units. A simple target structure subjected to an explosive load is analyzed in order to demonstrate the high strain rate effects in the simulation.

In Chapter 3, formulating an inverse mapping capability for linking desired material properties with the composition of their micro structure in MAC in a computationally efficient manner is presented. Background on the multi-scale design optimization is presented in section 3.1. In order to overcome the expensive computational cost of using a fully coupled MSM, which enables the micro-scale configuration design of the composite materials by a simple optimization model with the global-scale objectives and the micro-level design variables, research into an Inverse Material Engineering Algorithm (IMEA) is performed and presented in section 3.2. Two case studies in section 3.3 provide the sequence of the inverse calculation and validation of the IMEA concept.

In Chapter 4, a computational framework that conducts an optimization analysis for identifying the desirable material properties for increasing the blast resistant characteristics is presented. The modified MSM and IMEA are integrated into the framework for the optimization analysis. An optimization computational framework is created by developing MATLAB codes and PYTHON codes to employ the previously developed and validated processes. The organization of the computational framework is discussed in section 4.1 and the functionality of the optimization process is discussed and demonstrated with a composite panel design case study in sections 4.2 and 4.3.

Chapter 5 presents an additional optimal design study of a sandwich structure that consists of heterogeneous materials. Background on the sandwich structure, which intends to increase energy dissipation of the previous design of fiber-reinforced composite panel is discussed in section 5.1. The sandwich structure, which consists of silicon carbide fibrous titanium composites and rubber, can make the structure stronger by using energy

dissipation. An optimal design case study of the sandwich structure is presented in sections 5.2, 5.3 and 5.4.

CHAPTER 2:
A FULLY COUPLED MULTI-SCALE SIMULATION CAPABILITY FOR BLAST ANALYSIS OF THE COMPOSITES

The main objective of this chapter is to document a multi-scale approach for simulating blast events of the composites and to present a demonstration study to validate the approach. As discussed in the introduction section 1.2, material property prediction of the composites during transformation makes it difficult for composites structure design. The motivation behind this work is to see if a micro-scale material property calculation tool, Micromechanics Analysis Code (MAC), can be used with a global-scale structure analysis tool to provide better results for a composite structure analysis. This chapter focuses on developing a Multi-Scale Methods (MSM) by coupling a micro-scale and a global-scale. Secondary objectives include extending the MSM capability to consider the high strain rate effects in the blast event simulation process.

In this chapter, the coupling sequence to enable MSM, is explained. In this study, the LS-DYNA solver, utilizing the BEST synthesis tool, is employed to simulate the soil–explosive–air interaction and to calculate accurately the loads on a target structure. Sequentially, the ABAQUS Explicit solver coupled with the MAC code is used for computing the corresponding response of a target structure to the loads from the explosion. This new framework is necessary for integrating all sorts of tools and combining them into one unified governing framework. This MSM framework is developed first based on

homogenization and localization and its implementation is validated by comparing existing one-way multi-scale and MSM results. The MSM results are compared with previously published bending experiment data using shear stress for evaluation. To consider high strain rate effects, a new user defined micro-scale model, which allows much more flexibility, for MAC is written and a demonstration case study is presented. A more detailed background on Micromechanics Analysis Code is discussed in the next section.

2.1: Background on Micromechanics Analysis Code (MAC)

The Generalized Method of Cells (GMC) forms the foundation of the MAC. This information is discussed in detail in Aboudi and Pindera, 1992 and the core theory is briefly presented here. The GMC is considering a repeating volume-element of a multiphase unidirectional fibrous composite with a periodic structure as the one depicted in Figure 2-(a). This typical repeating volume-element consists of $N_\beta * N_\lambda$ sub-cells and each of these sub-cells is occupied by an elastic-viscoplastic material as Figure 2-(b). The equivalent continuum medium in which the repeating volume-element is represented by the point P as Figure 2-(c) and the representative volume element consists of different elastic-viscoplastic materials, i.e., it represents a multiphase inelastic composite material.

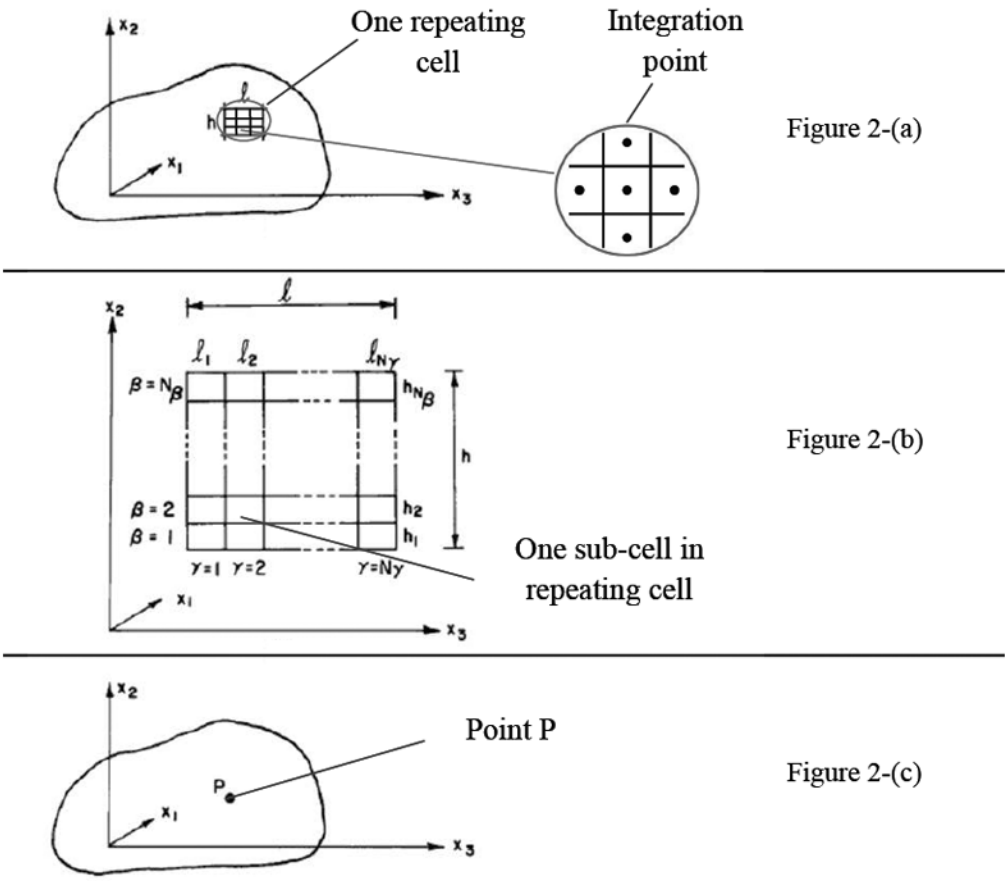

Figure 2: Composite possesses a periodic structure that a representative repeating volume element from (Aboudi and Pindera, 1992).

The micromechanical analysis starts by placing a repeating volume element of the periodic multiphase composite. Then macroscopic average stresses and strains are defined from the microscopic average stresses in sequence. The rate of displacements and tractions continuity conditions at the interfaces between constituents are imposed to eliminate the micro-variables and with micro-equilibrium, the relationship between microscopic strains and macroscopic strains are established through the relevant concentration tensors. Finally,

a set of continuum equations that model the overall macroscopic behavior of the composite are determined.

The outlined micromechanical analysis steps form the basis of micro-to-macromechanics analyses that describes the behavior of heterogeneous media. The resulting micromechanical analysis establishes the overall elastoplastic behavior of the multiphase inelastic composite. This behavior is expressed as an effective elastic-plastic constitutive relation between the average stress, strain, and plastic strain, in conjunction with the effective elastic stiffness tensor B^* (Suquet, 1985; Paley and Aboudi, 1992).

$$\overline{\tau} = B^*(\overline{\eta} - \overline{\eta}^P) \tag{1}$$

, where the effective elastic stiffness tensor B^* is defined by

$$B^* = \frac{1}{hl}\sum_{\beta=1}^{N_\beta}\sum_{\gamma=1}^{N_\gamma} h_\beta l_\gamma C^{(\beta\gamma)} A^{(\beta\gamma)} \tag{2}$$

, where h is the sub-cell height, l is the sub-cell length, $C^{(\beta\gamma)}$ is the elastic stiffness tensor of material in each sub-cell, and $A^{(\beta\gamma)}$ is the concentration matrices at location (β , γ). Location data of the sub-cell, β and γ, are presented in Figure 2. The composite plastic strain-rate tensor for two repeating sub-cells is defined by

$$\overline{\eta} = (\overline{\eta}_{11}, \overline{\eta}_{22}, \overline{\eta}_{33}, 2\overline{\eta}_{23}, 2\overline{\eta}_{13}, 2\overline{\eta}_{12}) \quad , \tag{3}$$

$$\overline{\eta}^P = -B^{*-1}\sum_{\beta=1}^{N_\beta}\sum_{\gamma=1}^{N_\gamma} h_\beta l_\gamma C^{(\beta\gamma)} \times (A^{P(\beta\gamma)}\eta_S{}^P - \overline{\eta}^{P(\beta\gamma)})/(hl). \tag{4}$$

, where $\eta_S{}^P$ represents the plastic strain-rates vector of the sub-cells. The concentration matrices A and A^P are defined as:

$$A = \begin{bmatrix} A_M \\ A_G \end{bmatrix}^{-1} \bullet \begin{bmatrix} 0 \\ J \end{bmatrix} , \tag{5}$$

$$A^P = \begin{bmatrix} A_M \\ A_G \end{bmatrix}^{-1} \bullet \begin{bmatrix} A_M \\ 0 \end{bmatrix} \tag{6}$$

, where matrix A_M represents elastic properties of the material at the sub-cell level, matrix A_G represents geometrical properties of the repeating-cell and matrix J represents interfacial properties of two repeating-cells. The GMC theories implemented within MAC code were reformulated for maximum computational efficiency and for considering deformation history, loading path and loading rate (Bednarcyk and Pindera, 1999). A detailed discussion of the Multi-Scale Methods (MSM) is presented in the next section.

2.2: Multi-Scale Methods (MSM)

The recent surge of multi-scale modeling related to solid mechanics is raised rapidly by parallel computing power and experimental capabilities, which is for the structure-property relations characterizing to the atomic level. In different disciplines (solid mechanics, material science, physics, mathematics, biological, and chemistry), and different length scales (from atoms to vehicles), the multi-scale modeling has been researched. However, to date, the composites analyze capability of multi-scale modeling is limited to specific phenomena and ranges of loads and length scale, and is not capable of analyzing extremely large deformation effects of the composites from blast loads on a global scale. Therefore, it is important to develop a new Multi-Scale Methods (MSM) to

analyze the response of a composite panel to these large deformations (blast loads from an explosive threat).

In MSM, utilizing the BEST synthesis tool, the LS-DYNA solver is employed for simulating the soil–explosive–air interaction and calculating accurately the loads on a target structure. Sequentially, the ABAQUS Explicit solver coupled with the MAC code is used for computing the corresponding response of a target structure to the loads from the explosion. The ABAQUS Explicit solver, which enables dynamic analysis with a large range of the loads, has been coupled with the MAC code, enabling multi-scale computing from the micro-level to the global-level. During the homogenization process, the MAC code determines the material response at the integration points within each ABAQUS element. In essence, MAC operates as a nonlinear constitutive model within ABAQUS, representing the heterogeneous material. In reverse, during the localization process, local stress and strains computed by ABAQUS from incrementally applied loading are applied to the MAC for obtaining updated effective material properties. The formatted MSM capacitates to propagate local phenomena of composites, like fiber failures, matrix damage, interfacial debonding, throughout the structural response. This fully-coupled MSM is used for analyzing blast events.

The coupling can be done either in a fully coupled mode or as an one-way mode (Figure 3). In the former fully coupled mode, at each iteration of each time step, information about the strain field at each integration point of each element is communicated from ABAQUS to MAC. In return, the MAC code computes the constitutive properties and provides their updated values to ABAQUS and iterations are performed to update the

effective material properties. In the latter one-way mode, the MAC code is used for computing the constitutive material properties (assuming no deformation) and provides them as input to the ABAQUS analysis. A more detailed discussion of coupling sequence of the MSM is discussed in the next section.

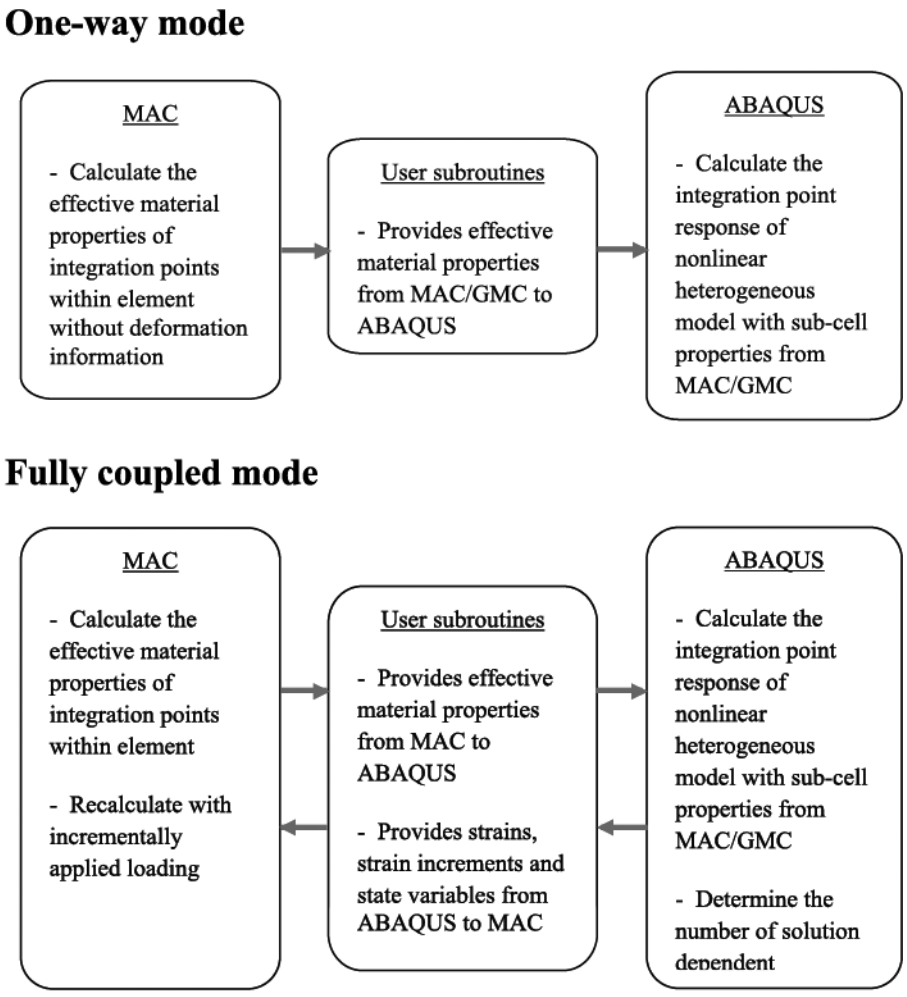

Figure 3: One-way and Fully coupled mode between MAC and ABAQUS solver.

2.3: Fully Coupled ABAQUS-MAC solution sequence

The ABAQUS code can be used in two solver modules of operation, Standard (Implicit) and Explicit. The Standard module is primarily used for monotonic loading and linear or mildly nonlinear problems where nonlinearities are smooth, and the Explicit module is primarily used high-speed dynamic events. In this research, the Explicit module is employed for conducting blast event simulations.

The FEAMAC code, compiled by NASA Glenn Research Center, comprises a fully coupled simulation process between the MAC and the ABAQUS Standard module. FEAMAC consists of ABAQUS/Standard user defined subroutines, as well as subroutines exclusive to the FEAMAC package. Mechanical analysis is achieved through the ABAQUS/Standard subroutine UMAT. For every integration point of each finite element, the UMAT subroutine is called by ABAQUS/Standard, and provides the strains, strain increments, and current values of state variables information to the MAC code. The MAC code then returns a new stiffness and stress state to the UMAT via the FEAMAC subroutine (Figure 4).

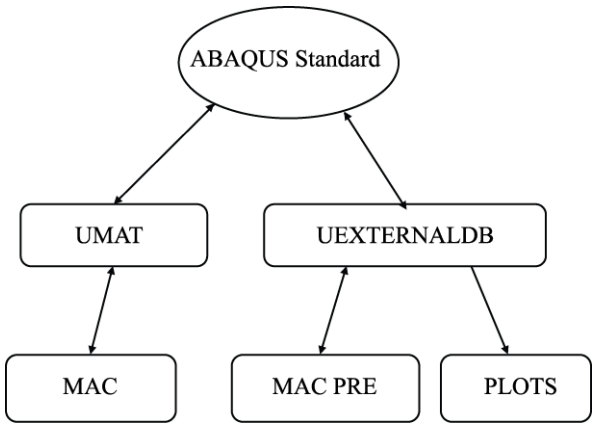

Figure 4: Flow chart describing coupling between ABAQUS Standard and MAC.

However, the computational framework of the Explicit module differs significantly from the Standard one (Figure 5).

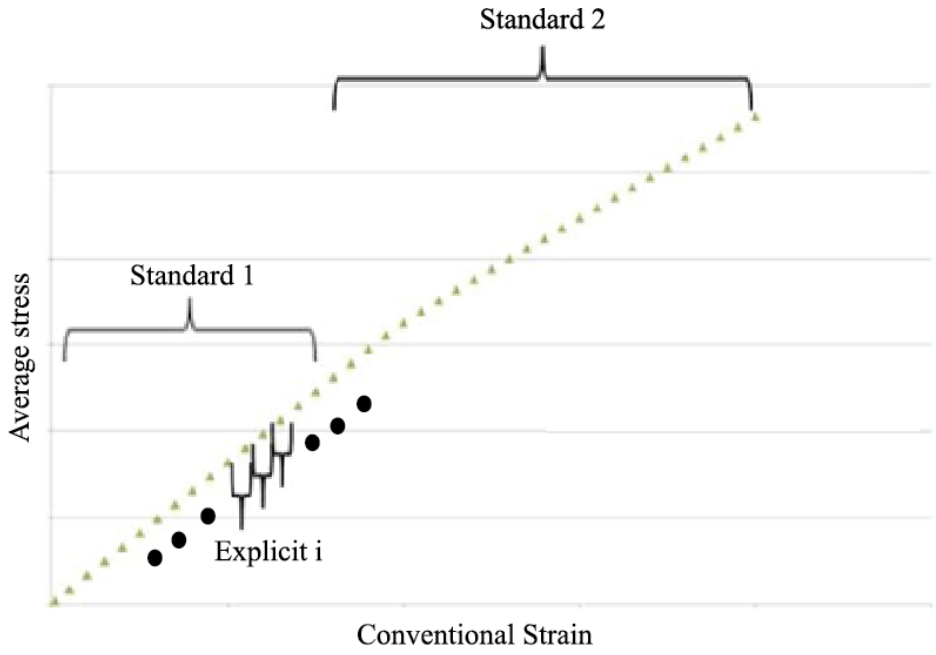

Figure 5: Computational framework difference between Standard and Explicit solver.

In the Standard module, the stress satisfying the constitutive equation is computed first and then a consistent tangent modulus (Jacobian Matrix) is evaluated for the specified time step (ex., Standard 1 or Standard 2 in Figure 5). Sequential iterations are performed until the stress obtained by the consistent tangent modulus satisfies the constitutive equation. Each increment in this analysis consists of at least one iteration that requires the solution of a set of simultaneous equations. The cost per iteration is roughly proportional to the number of degrees of freedom in the model squared. It is difficult to reach consistent tangent modulus for complex constitutive equation using the Standard solver. Further convergence for an

abrupt increase or decrease in the loads is deficient. As a result, the Standard module is primarily used for monotonic loading and linear or mildly nonlinear problems where nonlinearities are smooth. Different from this, in the Explicit module, each increment consists of one group of equations, so no iterations exist and the solution is calculated by explicit time integration step by step (ex., Explicit i in Figure 5). As a consequence, the Explicit module is primarily used in high-speed dynamic events, such as impacts and nonlinear transient analyses. The drawback of the Explicit module is that it is conditionally stable. The stability limit for an Explicit module is that the maximum time increment must be less than a critical value of the smallest transition times for a dilatational wave to cross any elements in the mesh. This limitation induces the expensive computational cost of the fully coupled MSM and precludes using the MSM with micro-level configuration design of composites.

To resolve the difference between ABAQUS Standard solver and Explicit solver, the user subroutine VUMAT in the Explicit module must be used in addition to UMAT (Figure 6).

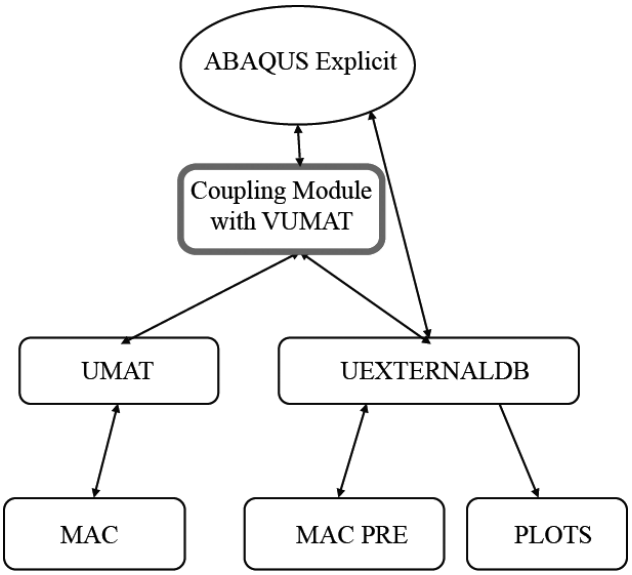

Figure 6: Flow chart describing coupling between ABAQUS Explicit and MAC.

The VUMAT calls for blocks of material calculation points for which the material is defined in a user subroutine and updates the stress states for each material point in the block by looping through all material points in the block. On the other hand UMAT calls at all material calculation points of elements for which the material definition includes a user defined material behavior. Due to this difference, the VUMAT contains one additional column of the material point numbers compared to the UMAT arrays. For instance the stress state in UMAT is represented by the vector "STRESS (NTENS)" where "NTENS" is size of the stress component array, number of direct stress components and shear stress components, while the stress state in VUMAT is represented by the vector "STRESSNEW (NBLOCK, NDIR+NSHR)" where "NBLOCK" is the material point number of a block and "NDIR+NSHR" is size of the stress component array similar to "NTENS". To utilize the existing FEAMAC subroutines to communicate with the MAC code, the VUMAT subroutine is formatted to interact between the existing subroutines and the Explicit module

by updating the stress state for each material point and deformation gradient information and converting them back.

The 'Coupling Module (CM)', which includes formatted VUMAT and other user subroutines to couple MAC and the ABAQUS Explicit module, is created. The new subroutine updates the stress state for each material point and deformation gradient information and converts them back for UMAT-VUMAT conversion. VUMAT is initialized (e.g. STRESS(1) = DBLE(STRESSOLD(K1,1)), DFGRD0(1,1) = DBLE (DEF GRADOLD (K1,1)) and so on) and then calls UMAT to update the material properties with field variable data (e.g. STRESSNEW(K1,1)=SNGL(STRESS(1)).

Other user subroutines for the Standard module, UEXTERNALDB, USDFLD, UVARM, UEXPAN, SDVINI and so on are transformed or reformulated for Explicit module calculation. Since stored data associated with material point is not stored in the Explicit state variable space, which is essential for MAC calculation, an additional several pages of FORTRAN code and PYTHON codes, to resolve an argument related to element number, integration number and so on, were also written. The overall structure of the MSM is created with above sequence as in Figure 7. An initial effective material property, which is calculated using MAC, is transferred from MAC to ABAQUS Explicit solver passing through CM. Then, ABAQUS Explicit solver returns the calculated transformation data to MAC through CM using PYTHON scripts. Iterations are performed to update the effective material properties.

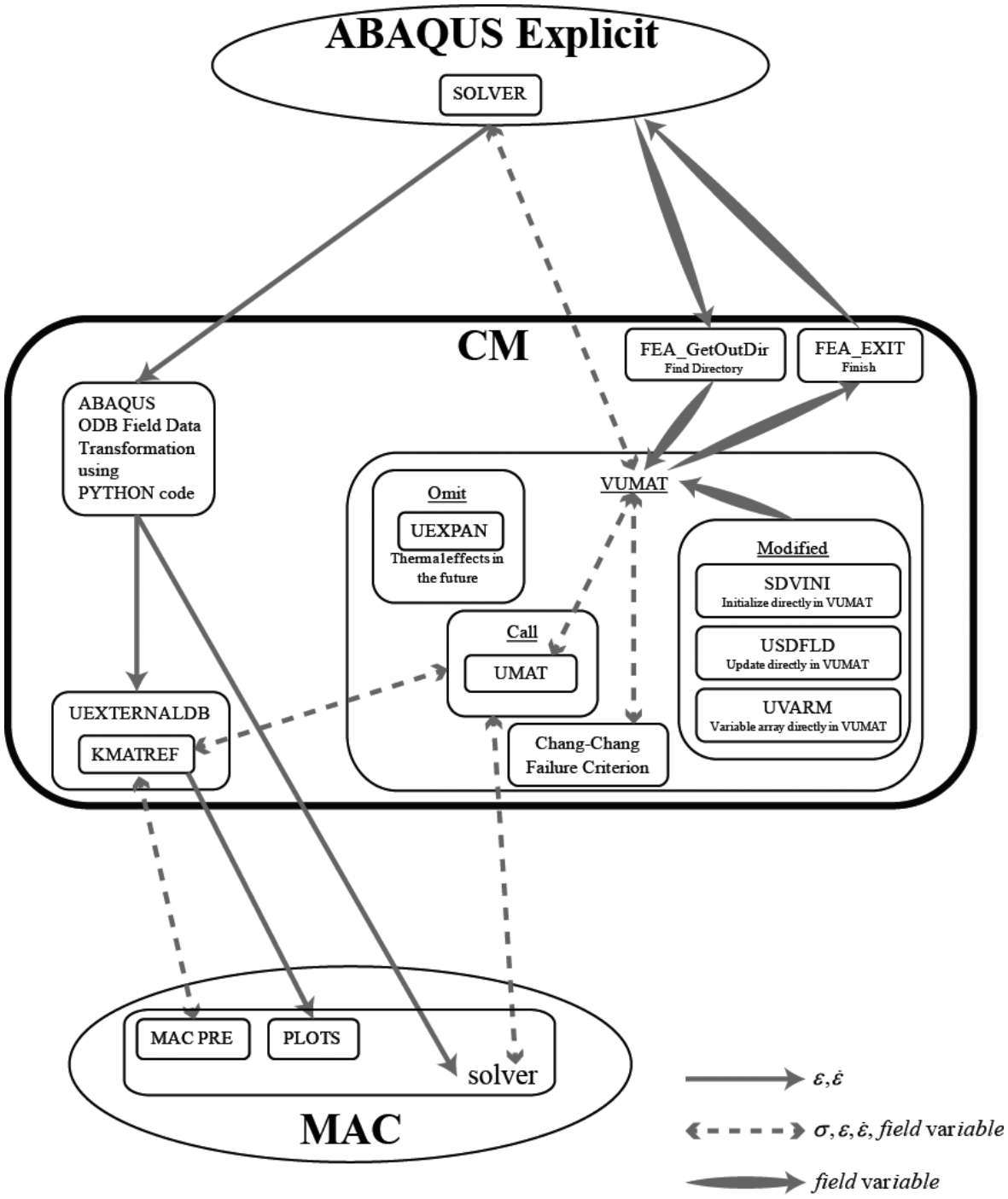

Figure 7: Overall MSM structure and data flow sequence.

The formatted MSM capacitates to propagate local phenomena of composites, like fiber failures, matrix damage, interfacial debonding, throughout the structural response. This fully-coupled MSM will be used to analyze blast events. A case study to demonstrate the appropriate of the MSM is discussed in the next section.

2.4: Case Study Definition

A target structure similar to the one used in the experimental validation presented in reference (Vlahopoulos and Zhang, 2010) is used for the case study presented in this section. The target structure is comprised of a box with a V-shaped outer bottom. The numerical finite element model, which is used in the simulations, is presented in Figure 8. The dimensions of the box are 2m x 2m x 1.8m (1.8m is height), the floor of the box is 0.8m above ground and the tip of the V-shaped outer bottom is 0.5m above ground. The roof and four lateral walls have thickness of 0.01m, the inner floor has thickness of 0.02m, and the outer V-shaped bottom has thickness of 0.03m. The BEST simulation process is used for conducting the analysis for the explosive and the air that surrounds the target structure.

During this simulation, the interface between the structure and the air is considered as a rigid boundary. The simulation computes the pressure time histories at a number of tracer points placed at the interface between each structural elements and the air. During the analysis, the interaction between the explosive, the soil, and the air is computed and the load histories applied on the structure due to the explosion are computed. The BEST process also has the capability to include a user-defined number of projectiles as part of the

explosive threat (Zhang et al, 2008); however, in this case study, the projectile effects are not considered.

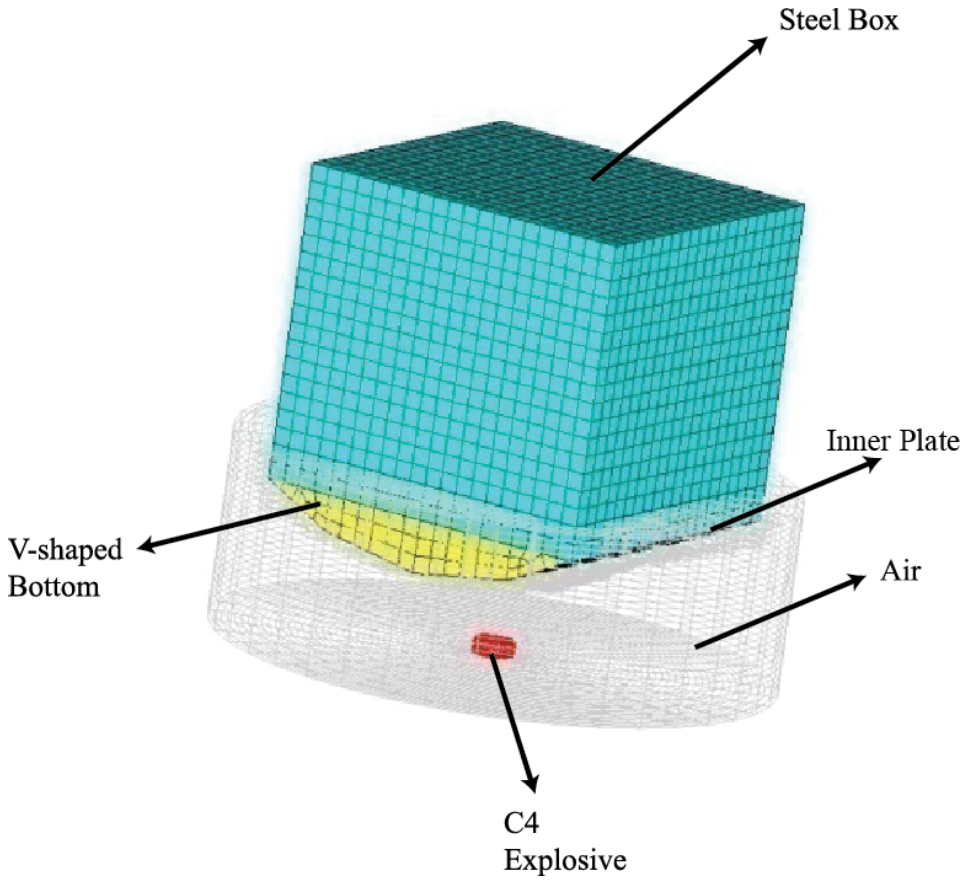

Figure 8: Air-Explosive-Structure model for case study.

To observe the difference between the one-way and fully coupled multi-scale approach, a set of three simulations is conducted first by considering the inner floor and the outer V-shaped bottom structure made out of composite material and the rest of the box made out of steel. Titanium matrix composite material, comprised by silicon carbide (SCS Ultra) fiber-reinforced titanium alloy(Ti-6Al-4V) matrix with 60 percent fiber volume fraction for each cell, is used for the inner floor and the outer V-shaped bottom structure.

The first two simulations are conducted by using the one-way coupling approach and the third simulation is conducted by a fully-coupled MSM. The material properties of steel, fiber, matrix, and the effective composite material properties from the MAC calculation are presented in Tables 1 and 2.

Table 1: Material properties of steel.

	Steel	(unit)
ρ Density	7830	Kg/m^3
E Elastic modulus	$2.05*10^{11}$	N/m^2
υ Poisson's ratio	0.3	-
SigY Yield stress	$0.35*10^9$	N/m^2
Tangent modulus	$0.636*10^9$	N/m^2
Hardening parameter	0 (Kinematic)	-
Failure strain	0.25	%

Table 2: Effective composite material properties evaluated by the MAC code for zero levels of strain.

	SiC	Ti-6Al-4V	unit		Compo-site
ρ Density	3000	4428	Kg/m^3	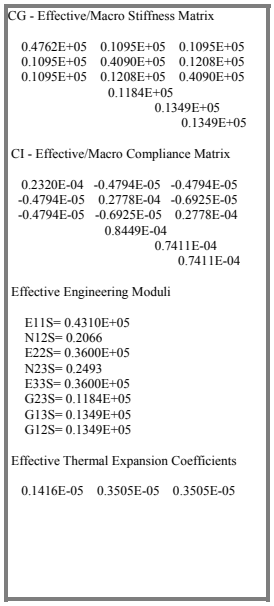 MAC code Calculation Results	3571.6
E1 Axial elastic modulus	$4.15*10^{11}$	$1.18*10^{11}$	N/m^2		$2.97*10^{11}$
E2 Transverse elastic modulus	$4.15*10^{11}$	$1.18*10^{11}$	N/m^2		$2.48*10^{11}$
υ12= υ13 Axial Poisson's ratio	0.14	0.32	-		0.2066
υ23 Transverse Poisson's ratio	0.14	0.32	-		0.2493
G12=G13 Axial shear modulus	$182.05*10^9$	$44.65*10^9$	N/m^2		$93.01*10^9$
G23 Transverse shear modulus	$182.05*10^9$	$44.65*10^9$	N/m^2		$81.63*10^9$
S11 Axial tensile strength	$5.9*10^9$	$1.38*10^9$	N/m^2		$3.36*10^9$
S22=S33 Transverse tensile strength	$0.85*10^9$	$1.38*10^9$	N/m^2		$0.748*10^9$
S12=S13 Axial shear strength	$0.42*10^9$	$0.480*10^9$	N/m^2		$0.370*10^9$
S23 Transverse shear strength	$0.42*10^9$	$0.480*10^9$	N/m^2		$0.425*10^9$
SC11 Axial compressive strength	$3.90*10^9$	$0.825*10^9$	N/m^2		$2.01*10^9$
SC22=SC33 Transverse compressive strength	$3.90*10^9$	$0.825*10^9$	N/m^2		$1.04*10^9$
Failure criterion				Chang-Chang criterion (Chang et al, 1987)	

The pressure load time histories, computed by the BEST process, comprise the loading for all three structural analyses. Figure 9 presents the typical load histories and the flow chart of the process that generates the loads for the structural analysis. Impulsive curve information from BEST is translated to each global-scale structure analysis solver, LS-DYNA and ABAQUS, respectively.

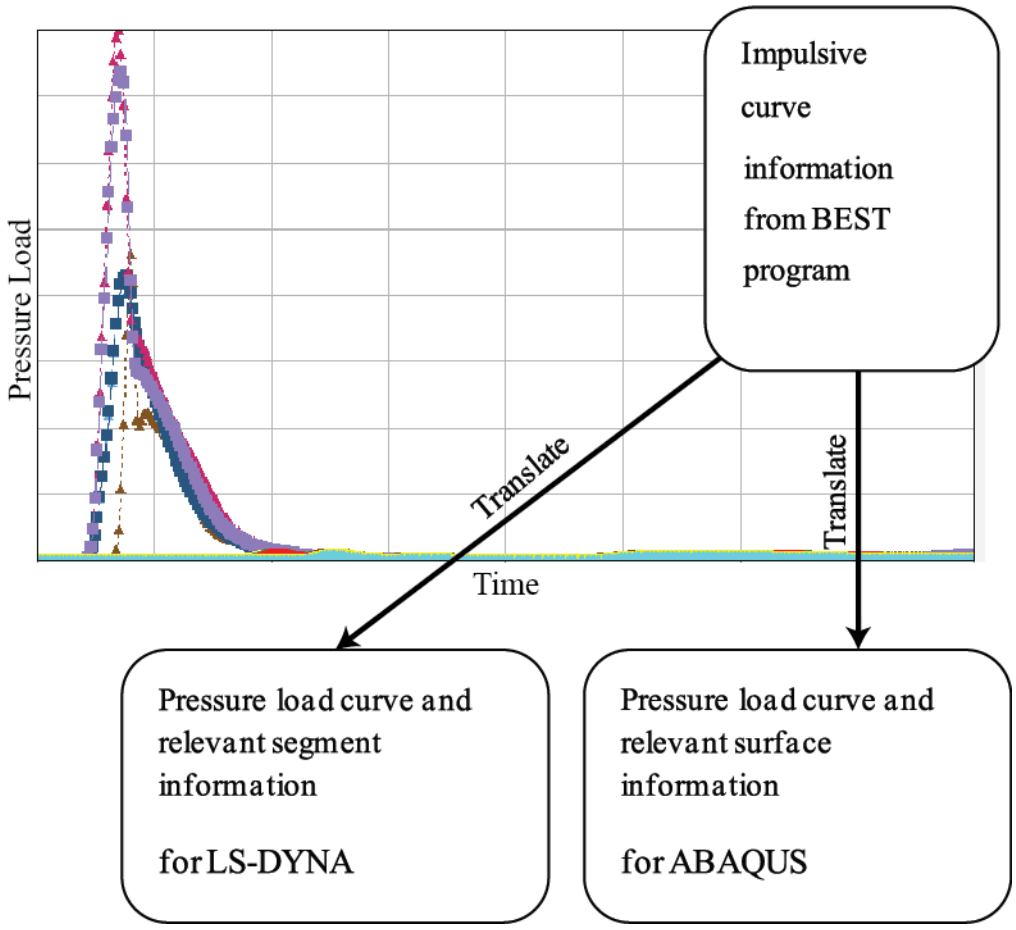

Figure 9: Interpret pressure loading for each solvers.

The first two simulations use the one-way coupling approach. The MAC code is used first for computing the equivalent material properties that correspond to zero levels of

strain (Table 2). Then, the LS-DYNA solver and the ABAQUS Explicit solver are used for computing the response of the structure. The third solution is obtained by using the fully coupled MAC-ABAQUS Explicit solution. The purpose of conducting these simulations is to make certain that all three solutions are comparable. The results of the case study are discussed in the next section.

2.5: Case Study Results - comparison between one-way multi-scale analysis and fully coupled MSM

Three blast event simulations are conducted and the results are compared in this section. Typical results computed by the LS DYNA and the ABAQUS Explicit solvers using the equivalent material properties (summarized in Table 2) are presented in Figures 10-(a) and 10-(b), respectively. Results from the fully coupled MAC-ABAQUS simulation are presented in Figure 10-(c).

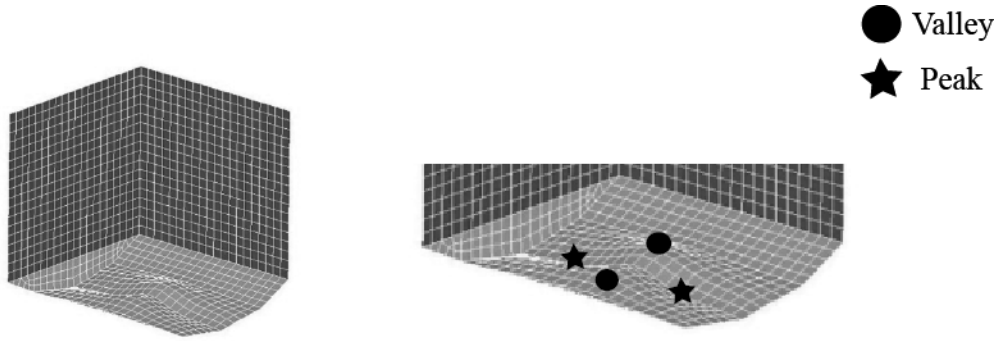

10-(a) One-way coupled analysis
using LS-DYNA

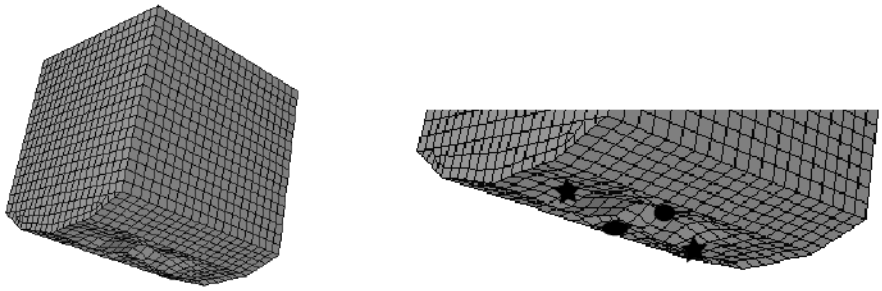

10-(b) One-way coupled analysis
using ABAQUS Explicit

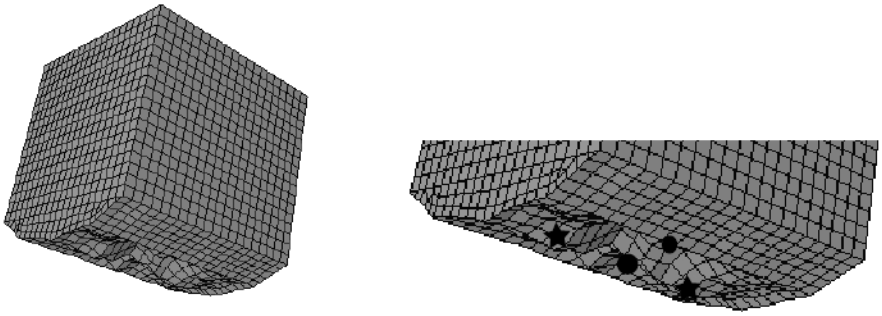

10-(c) Fully coupled analysis
using ABAQUS Explicit

Figure 10: Structure response for blast event simulation.

Although the outer V-shaped shield structure of all three solutions failed, these solutions do produce comparable results. A similar tendency is demonstrated in the response of the outer bottom from all three solutions. Two valleys are created on either side

with respect to the plane of symmetry along the y-direction and two peaks are created on both sides with respect to the plane of symmetry along the x-direction. Since the V-shaped outer shield structure failed rapidly, for comparison, the vertical deformation (z-displacement) of the center node and two valley points in inner plate is measured immediately after the first failure of the inner plate (0.005 sec) and presented in Figure 11 from the three analyses.

The results of the comparison in Figure 11 show that the deformation using one-way coupled LS-DYNA and one-way coupled ABAQUS Explicit are almost identical, and the deformation using the fully-coupled ABAQUS Explicit (MSM) is larger than the previous two results. The difference is fairly small before the first failure, but the gap is expanded after the failure point, and this small difference before the failure between one-way and fully coupled one is used to develop the MSM-INFO framework in Chapter 3.

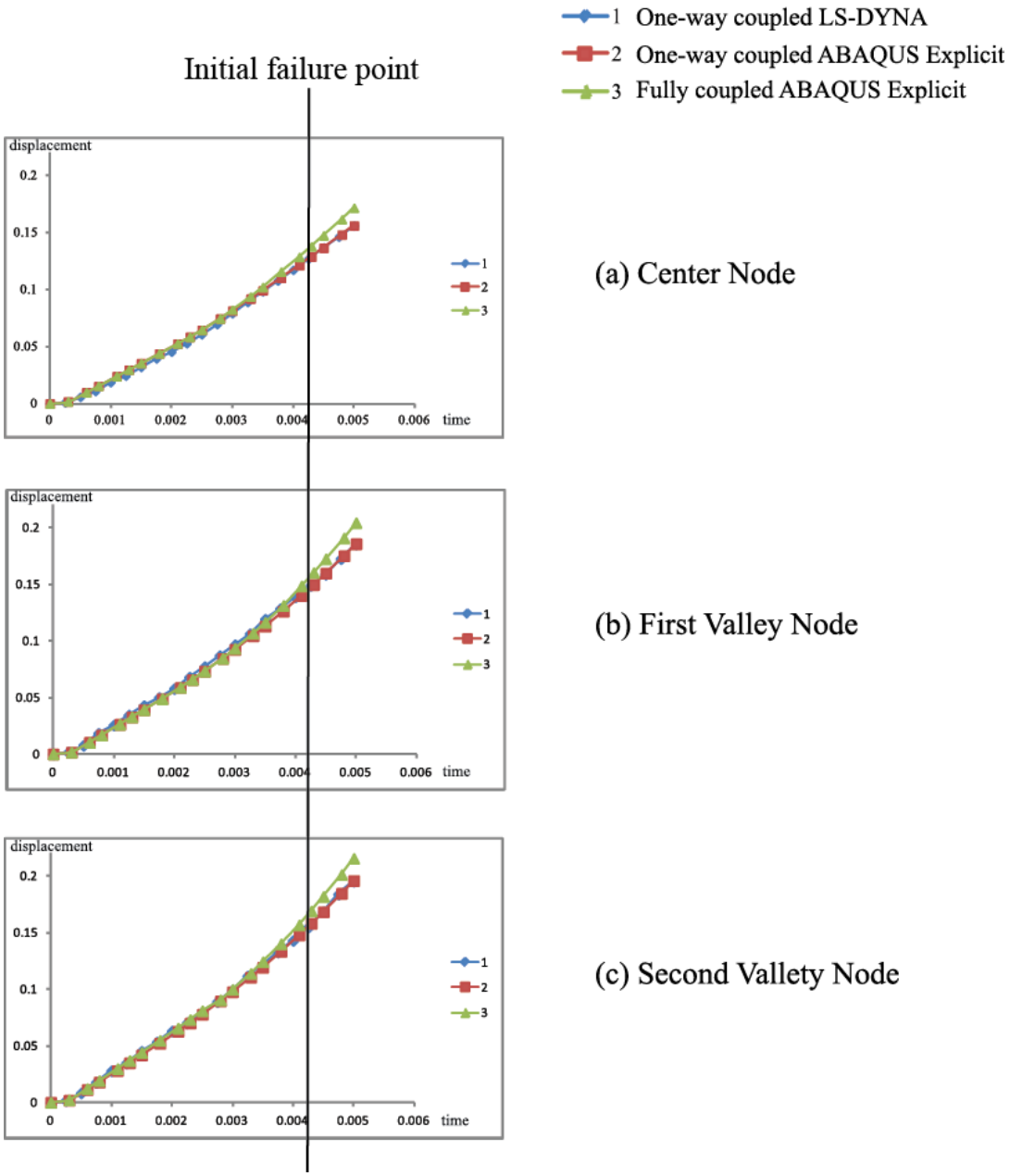

Figure 11: Z-displacement of the nodes.

The results demonstrate comparable values between two one-way coupled analysis results, but larger z-displacement is encountered in the fully coupled MSM analysis result since effective material properties were updated continuously during calculation. The good

agreement observed in the results (as summarized in Table 3) demonstrates the proper implementation and development of the fully coupled MSM capability. The results of the one-way coupled using LS-DYNA (*1) and one-way coupled using ABAQUS Explicit (*2) show the identical value. And, the result using fully-coupled MSM shows larger data comparison between *1 and *2 by 9%.

Table 3: Summary of Z-displacement of the three representative nodes at the final data point.

	One-way coupled using LS-DYNA*1	**One-way coupled using ABAQUS Explicit*2**	**Fully coupled MSM**
Center node z-displacement (m)	0.1558	0.1559	0.1715
% increase of *1	-	0.06 %	9.15%
% increase of *2	-	-	9.09%
Valley node 1 z-displacement (m)	0.1854	0.1856	0.2042
% increase of *1	-	0.11 %	9.21%
% increase of *2	-	-	9.11%
Valley node 2 z-displacement (m)	0.1952	0.1957	0.2153
% increase of *1	-	0.25 %	9.33%
% increase of *2	-	-	9.10 %

To evaluate the results, additional bending and off-axis loading analysis is performed, since it is difficult to acquire the blast event experiment data. The difference between the one-way coupled and the fully coupled MSM analysis is also identified by both of the comparisons using the bending experiment data (Gonzalez and LLorca, 2001; Gonzalez et al, 2004) and the off-axis loading experiment data (Aghdam et al, 2000) condition in Figure 12 and Figure 13. The silicon carbide fiber-reinforced titanium alloy matrix composites with 35% fiber volume fraction is used in the first bending experiment. The same composition of the composites, but with a different fiber volume fraction of 33%, is used in the second off-axis loading experiment. In the both comparisons, the experiment data from literature is represented using the rhombus marked line. The data from the one-way coupled using LS-DYNA and ABAQUS Explicit are represented using the square and the triangle marked line, and they show the significant difference compared to the experiment data. The data from the fully-coupled ABAQUS Explicit (MSM) is represented using the cross marked line, and shows a very good agreement to both the bending and off-axis loading experiment data.

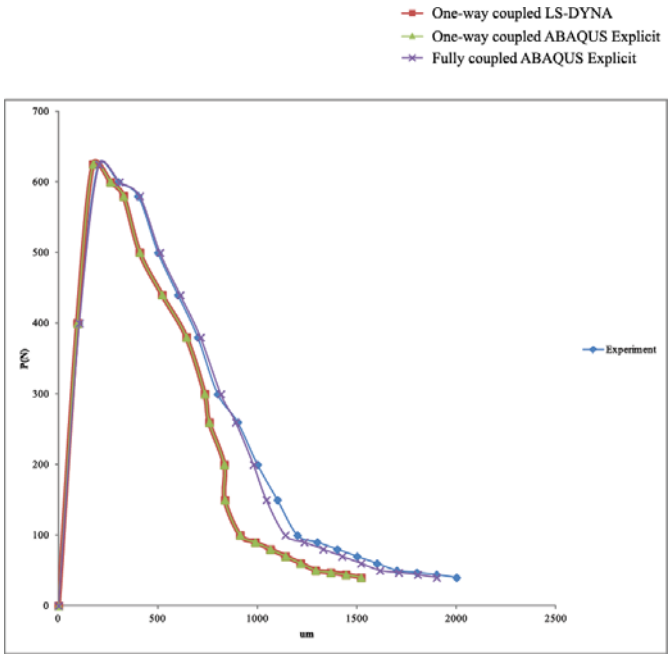

Figure 12: Comparison between FE prediction and bending experimental data.

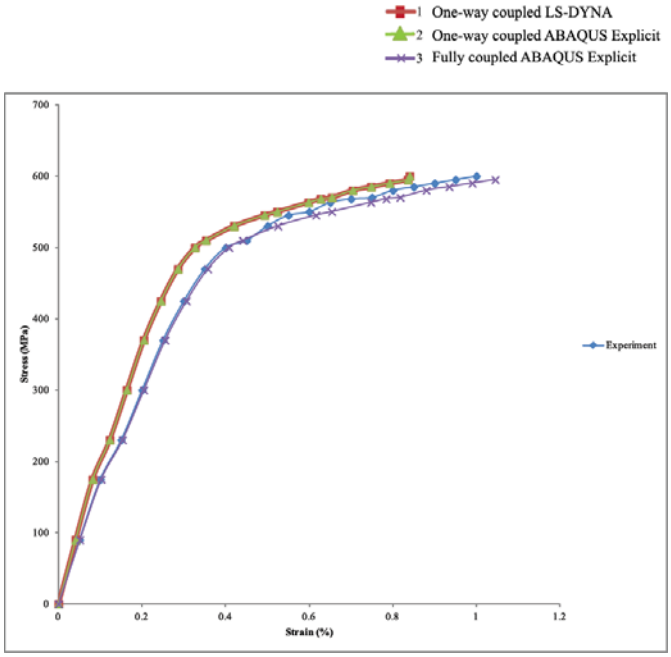

Figure 13: Comparison between FE prediction and off-axis loading experimental data.

Contrary to the one-way coupled analysis results, the fully-coupled MSM analysis result is in good agreement in the whole range of both comparisons, and the appropriateness of the newly created fully-coupled MSM is demonstrated. An additional case study for the utilization of the MSM is discussed in the next section.

2.6: Utilization Case Study

To demonstrate how the new MSM methodology can be used for configuring light weight blast resistant armor, the target structure analyzed in the previous section is subjected to the combined load from 5.352kg of C4 and high velocity projectiles. An all-steel configuration comprises the baseline design. The thickness of the four lateral sides and the roof is 0.01m, and the thickness of the inner floor and the outer V-shaped bottom is 0.015m. The overall weight is approximately 2467kg. In this case study, the micro-scale simulation capability is employed for identifying an inner floor and an outer V-shaped shield configuration made out of composite that offers a similar level of protection with the steel structure. The relative composition of each composite laminate layer cell, the orientation of each laminate layer, and the thickness of each layer can be used as design parameters when determining a double floor configuration that weights less but offers similar protection levels with the one made out of steel. The level of permanent deformation and/or failure of the outer V-shaped bottom floor and the maximum deformation encountered in the center of the inner floor comprise the performance metrics considered in this study. A configuration that reduces the total weight to 2222.3kg is identified. The outer V-shaped bottom floor has 0.03m thickness and the inner bottom

thickness is 0.02m. A configuration of two perpendicular laminated composites is used for the inner floor and outer V-shaped bottom floor. The number of layers and the orientation of each layer are summarized in Table 4.

Table 4: Inner floor and outer V-shaped bottom floor configuration of re-designed composites floor.

	Orientation		Thickness (m)	
	Inner floor	Outer V-shaped bottom floor	Inner Floor	Outer V-shaped bottom floor
Layer 1	0º from x axis in local x-y plane	0º from x axis In local x-y plane	0.010	0.015
Layer 2	90º from x axis in local x-y plane	90º from x axis in local x-y plane	0.010	0.015

The overall deformation encountered in the two structures is presented in Figure 14. The composite outer V-shaped bottom floor failed in both the steel structure and the re-designed composites structure. However, the maximum displacement encountered in the middle of the inner floor is 0.003279m for the steel structure and 0.002348m for the composite. Thus, improved blast resistance characteristics are observed by the composite structure while the weight of the overall structure is reduced. This case study demonstrates how the MSM can be used for configuring blast resistant light weight structures.

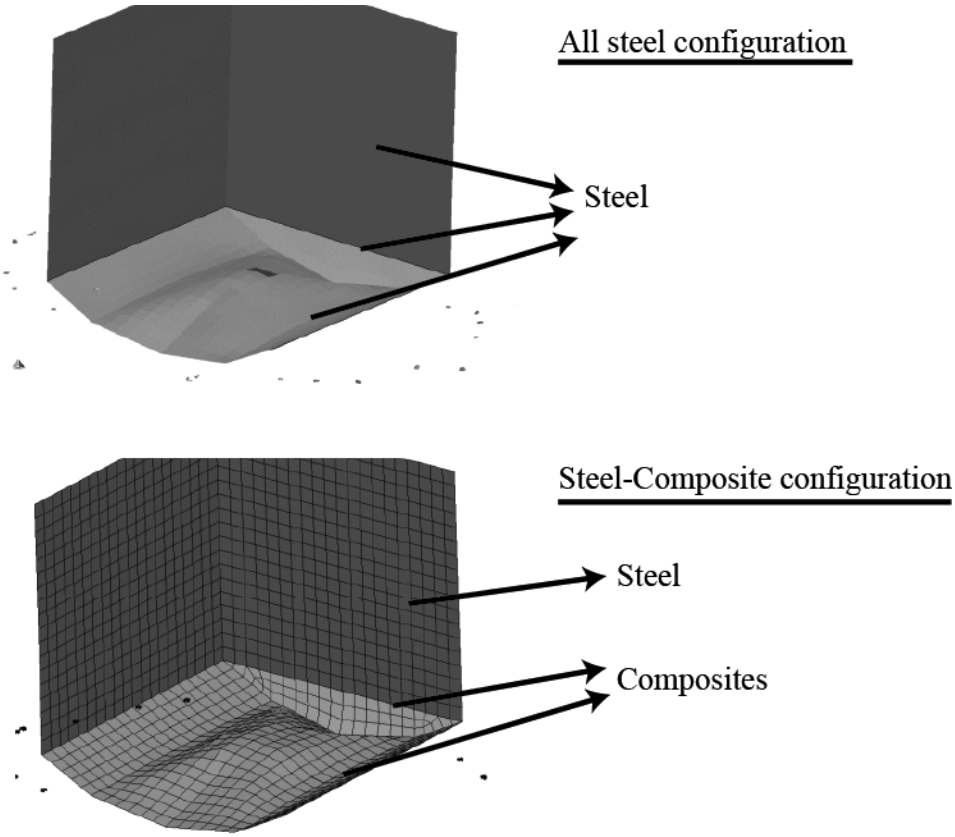

Figure 14: Deformation of steel and steel-composite structures.

An interesting result observed during the utilization study is that different types of load need different micro-scale configurations. The initial velocity load of the projectile shows a better result with parallel fibrous configuration in opposition to a pressure load of the explosion, which needs a perpendicular fibrous configuration for a better result. This result is an effective aid to the upcoming inverse material engineering algorithm research. To consider the high strain rate loading condition of the blast event simulation, a modification of the micro-scale material model is discussed in the next section.

2.7: Extending MSM Capability to High Strain Rate Loading

It is important to include strain rate effects in the simulation because the properties of materials under impact differ from those determined under static-loading conditions (Hopkinson, 1901). A recent laboratory experimental study on the effect of a high strain rate loading condition emphasized the large inelastic deformation behavior (Wang et al, 2011). A mismatch between the essentially static tensile or compressive test results, for which an approximately linear dependence of flow stress on the logarithm of strain rate occurred, and those higher flow stresses derived from generally more complicated dynamic material test results, also prove the importance of the high strain rate effect (Armstrong and Walley, 2008). Further, high strain rate effects from the shapes of pulses produced by explosion and projectile become increasingly more important for blast event simulation.

To consider the high strain rate deformation for blast event simulation, a modified Bodner-Partom model has been considered in this work. The increased number of material constants of this model allows much more flexibility in representing visco-plastic, time-, and temperature-dependent responses, and produces better agreement with the experimental data (Sands et al, 2010). The new user defined micro-scale material model for MAC code is created to apply a modified model and a demonstration case study is performed.

The modified Bodner-Partom model is considered as a substitute of the initial Generalized Visco-plasticity with Potential Structure (GVIPS). A variety of methods have been explored in the past to accurately characterize the strain-rate sensitivity, and time dependent (visco-plastic) response of a Ti matrix. The GVIPS model has a visco-rate dependent behavior, bounded by two rate independent plasticity models; in particular it

approaches either generalized plasticity or classical plasticity depending on whether the internal characteristic time is large or small compared to the loading rate. Other interesting features are: (1) it smoothly reaches a limiting stress asymptote for both monotonic and cyclic loading conditions and (2) if unloaded from the plastic range, upon reloading, it renews plasticity before the attainment of the stress where unloading begins.

Although the lower stress ranges could be accurately modeled with a new set of constants, the new set of constants would then be less accurate in characterizing the higher strain-rate cases. Consequently, to extend the range of the model to include the levels of kinematic hardening that may be problematic in the traditional formulation, the modified Bodner-Partom model was integrated into the fully-coupled MSM. The first assumption in this analysis is the additive decomposition of the total strain, ε_{ij}^{tot}, into elastic, thermal, and inelastic components.

$$\varepsilon_{ij}^{tot} = \varepsilon_{ij}^{el} + \varepsilon_{ij}^{th} + \varepsilon_{ij}^{in} \tag{7}$$

The elastic strain, ε_{ij}^{el}, depends on the current stress state, the elastic modulus E, and Poisson's ratio υ. The thermal strain component, ε_{ij}^{th}, equals the product of the coefficient of thermal expansion and the difference between the current and reference temperatures. The Bodner-Partom (B–P) flow rule governs the evolution of the inelastic strain, ε_{ij}^{in}, using

$$\dot{\varepsilon}_{ij} = \frac{D_0 \exp\{-\frac{1}{2}(\frac{(Z_I + Z_D)^2}{3J_2})^n\} s_{ij}}{J_2} \tag{8}$$

with the two hardening variables, Z^I and Z^D, for the isotropic and directional hardening, respectively. D_0 is the limiting strain rate, s_{ij} are the components of deviatoric stress with J_2 equal to $(s_{ij}\ s_{ij})/2$. The evolution of Z^I and Z^D has similar empirical forms. Each equation consists of a hardening, thermal recovery and temperature rate term, with the recovery rate coefficient for isotropic hardening A_1, the non-work hardened condition state variable Z_1, the isotropic hardening factor Z_2, the maximum value for kinematic hardening, time T, the stress σ and strain ε at visco-plastic constant n, m, and the material parameter r_1, r_2.

$$Z^I = m_1(Z_1 - Z^I)\dot{W}^{in} - A_1 Z_1(\frac{Z^I - Z_2}{Z_1})^{r_1} + (\frac{Z_1 - Z^I}{Z_1 - Z_2})\frac{\partial Z_2}{\partial T}\dot{T} \tag{9}$$

, where

$$\dot{W}^{in} = \sigma_{nm}\dot{\varepsilon}^{in}_{nm} \tag{10}$$

$$, Z^D = \beta_{nm}u_{nm} \tag{11}$$

, where the state variable

$$\dot{\beta}_{ij} = m_2(Z_3 u_{ij} - \beta_{ij})\dot{W}^{in} - A_2 Z_1(\frac{\sqrt{\beta_{nm}\beta_{nm}}}{Z_1})^{r_2} v_{ij} + \frac{\beta_{ij}\partial Z_3}{Z_3 \partial T}\dot{T} \tag{12}$$

$$, u_{ij} = \frac{\sigma_{ij}}{\sqrt{\sigma_{nm}\sigma_{nm}}} \tag{13}$$

and

$$v_{ij} = \frac{\beta_{ij}}{\sqrt{\beta_{nm}\beta_{nm}}}\,. \tag{14}$$

The modified Bodner-Partom model proposed the hardening rate term m_1 to be an exponential function of the state variable for hardening, Z^I, as

$$m_1 = m_{1b} + (m_{1a} - m_{1b}) \exp[-m_{1c}(Z^I - Z_2)] \quad (15)$$

, with the positive material constants m_{1a}, m_{1b}, m_{1c}.

The second modification was made in the constant value of A_1, which also becomes a function of the hardening variable Z^I,

$$A_1 = A_{1b} + (A_{1a} - A_{1b}) \exp[-A_{1c}(Z^I - Z_2)] \quad (16)$$

, with the additional material constants A_{1a}, A_{1b}, A_{1c}

The increased number of the material constants allows much more flexibility in representing visco-plastic and time- and temperature-dependent responses. In the neat matrix form, the modified Bodner-Partom model produces better agreement with the experimental data. This model requires additional modification to account for matrix cracking damage, but the cracking criterion is not needed for the current research step.

In the original fully-coupled MSM, MAC uses the GVIPS model with SI units and substitutes μ, κ, R_α, B_0, B_1, n, p, q, κ_0, B_0', *and* β specifications from the global-level finite element calculation. However, the modified Bodner-Partom model uses English units and needs to present D_0, Z_0, Z_1, Z_2, Z_3, m_1, m_2, n, a_1, a_2, r_1, r_2, Dm_1, Dm_2, Dz_1, Dz_2, *and* Dz_3 specifications. To address this problem, the CM, which fully links the MAC code and the ABAQUS Explicit module, was modified to change the units and assign the appropriate material property specifications by developing a new micro-scale material model within MAC (Figure 15).

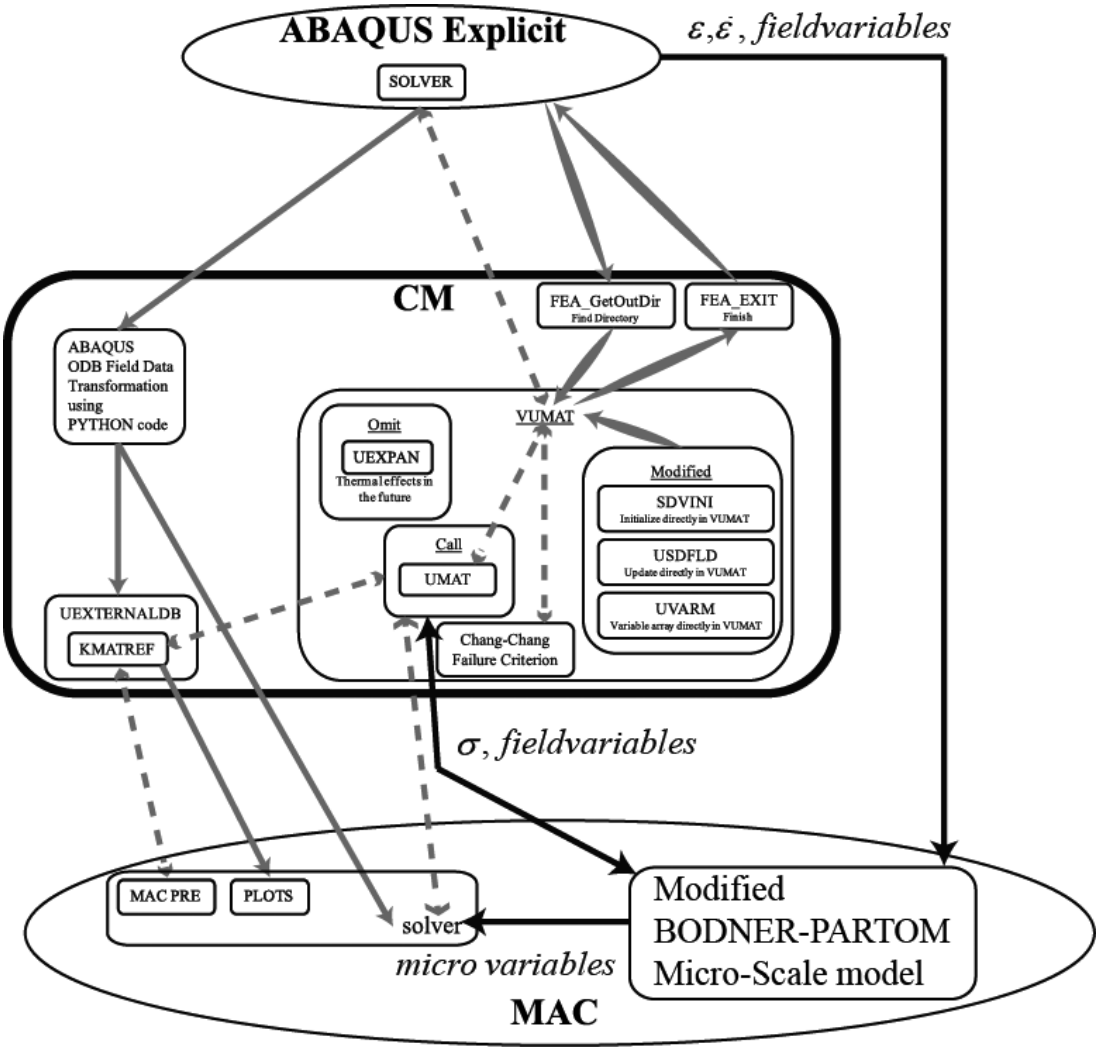

Figure 15: Overall modified MSM structure and data flow sequence.

As shown in Figure 15, a newly developed micro-scale material code engages the effective material properties to the ABAQUS Explicit solver through CM, and obtains the transformation date directly from ABAQUS solver. To demonstrate the modified MSM, a simple pressure load analysis with various strain rates, which has same peak load with different duration, is performed (Figure 16). The simple panel structure using 100 elements

is set up with the 16 pressure load elements. Also, a node has been selected to compare the results from different strain rate conditions.

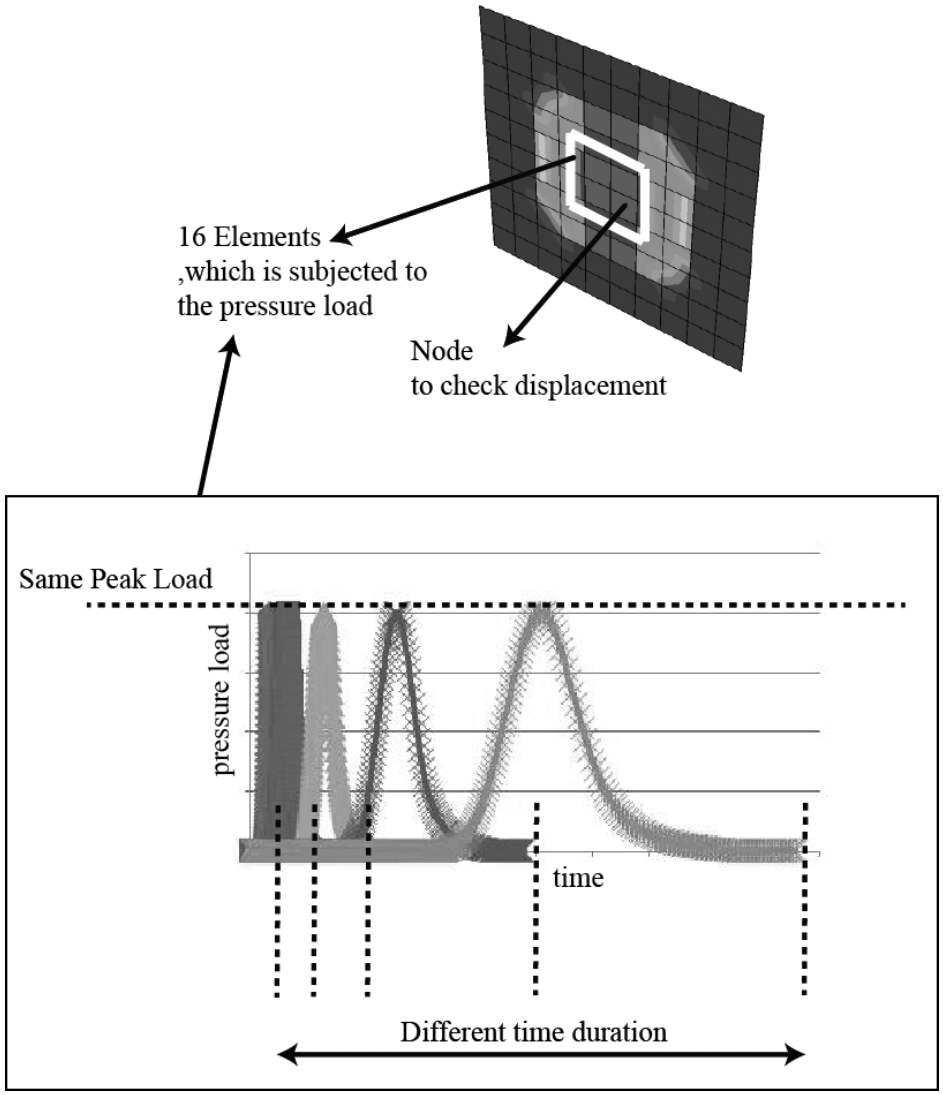

Figure 16: Simple pressure load analysis with different strain rate.

A similar tendency has been observed in the low strain rate in both of the original and modified material model, but dissimilar results have been observed in the high strain rate (Figure 17).

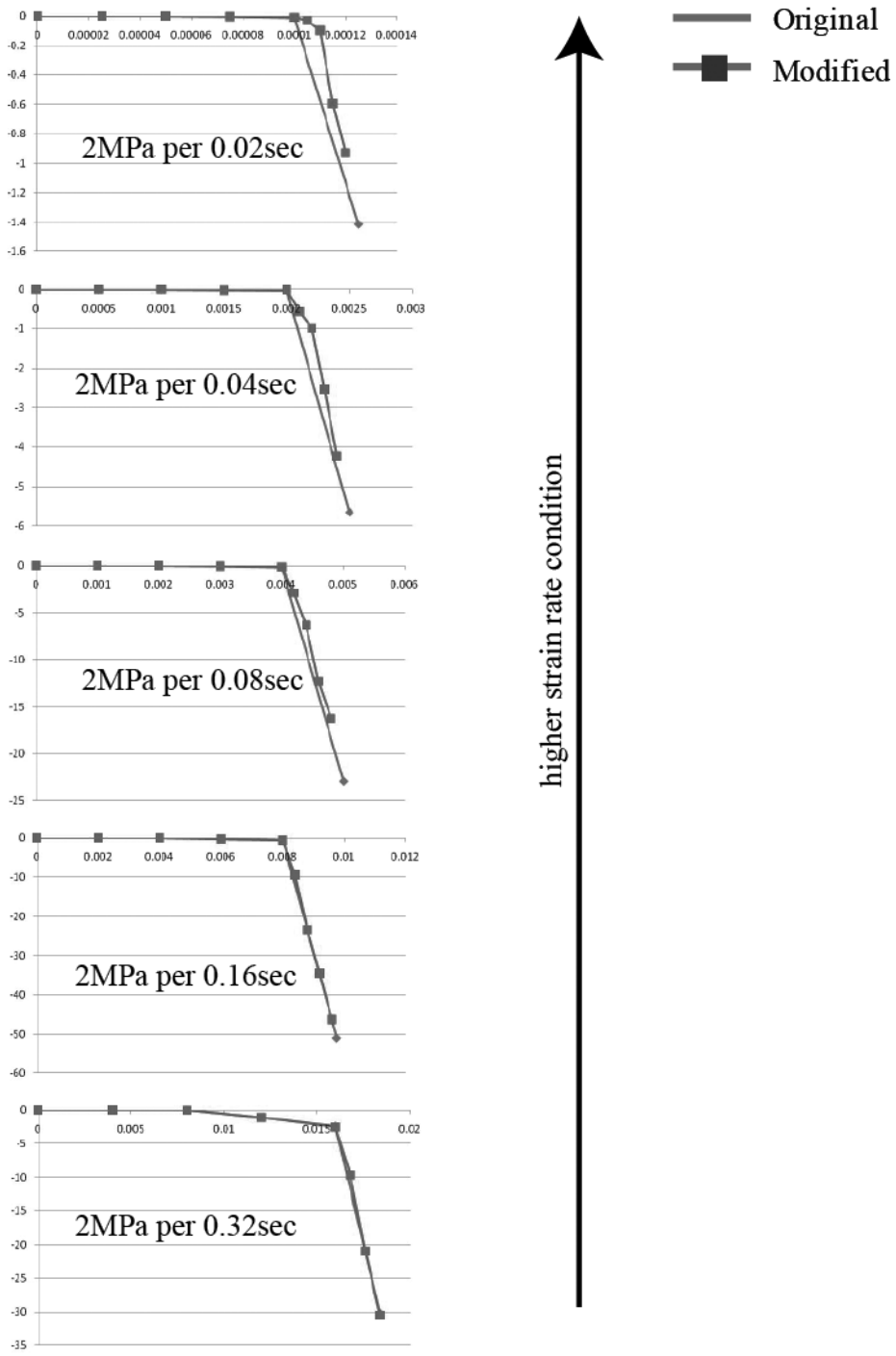

Figure 17: Z-displacement of the specified node for various strain rate condition.

The results of the modified MSM also show better agreement with the results from bending and off-axis loading experiments (Figure 18 and Figure 19), which are used in section 2.5. In both results of the comparison, the experimental data from literature is represented using the rhombus-marked line. The data from the original MSM is represented using the square-marked line, and the data from the modified MSM is represented using the triangle-marked line. The results from the comparison demonstrate that the modified MSM shows better agreement as compared to the original MSM.

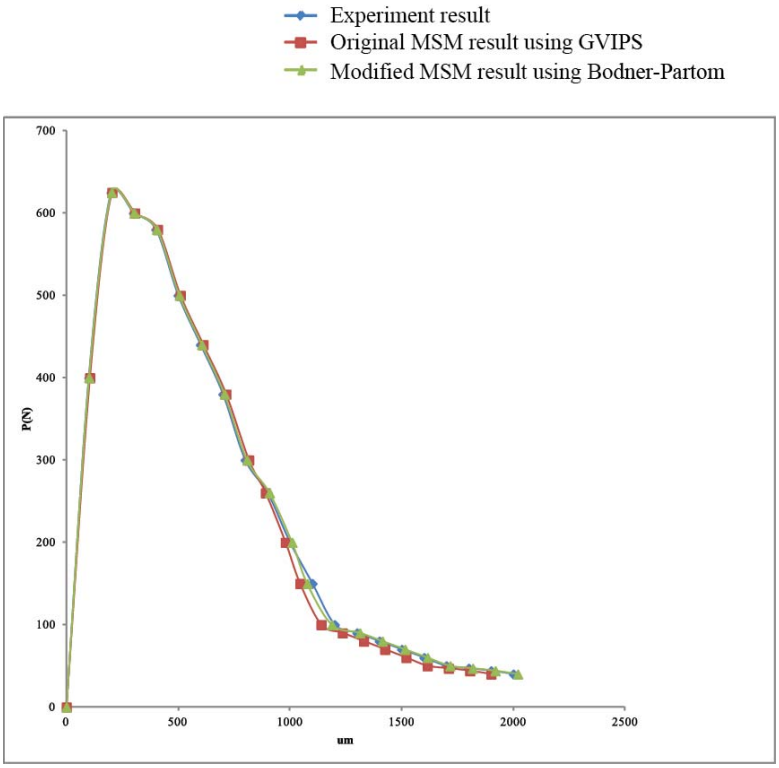

Figure 18: Compare original MSM and modified MSM prediction with bending experiment data.

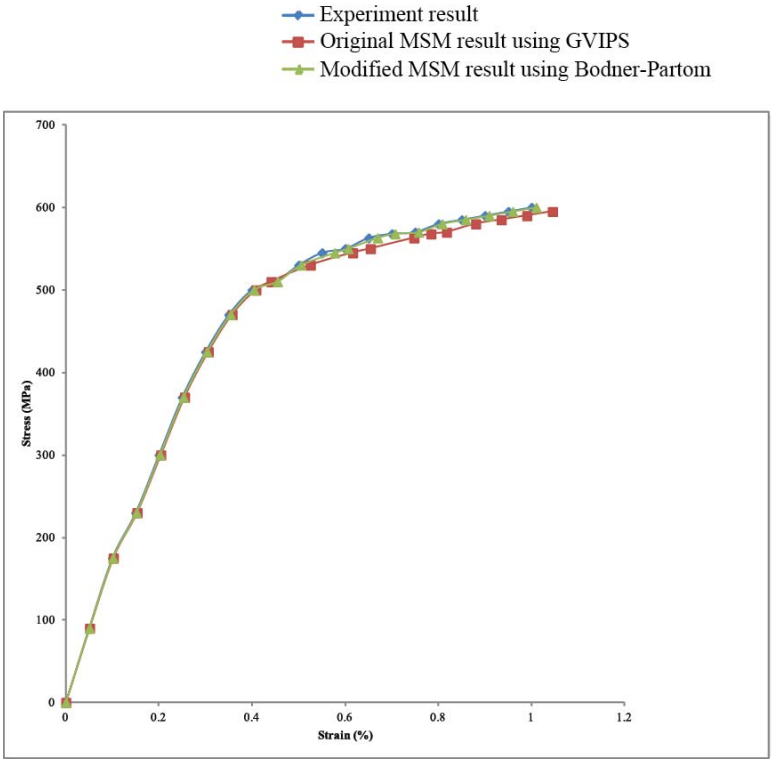

Figure 19: Compare original MSM and modified MSM prediction with off-axis loading experiment data.

This good agreement demonstrates the proper implementation and development of the fully-coupled MSM capability for the high strain rate problem. The newly modified MSM is included within an optimization computational framework and a discussion of the process is presented in the next Chapter.

CHAPTER 3:
INVERSE MAPPING METHODS FOR MULTI-SCALE DESIGN OPTIMIZATION WITH COMPUTATIONAL EFFICIENCY

The objective of this chapter is to document an Inverse Material Engineering Algorithm (IMEA), which capacitates the design of a micro-scale configuration of composites with reduced computational cost. The high computational cost of the fully coupled MSM is caused by the cost of the ABAQUS Explicit solver to achieve stability, and the cost of the iteration process within each time increment in MSM itself. Increasing the time increment size by coarsening the finite element mesh or any artificial inertia or mass penalty technique can reduce the first computational cost. Otherwise, parallel computing using powerful workstations can overcome the cost problem. However, in this work, inverse mapping methods are studied and integrated to increase computational efficiency.

This chapter focuses on developing an IMEA based on the inverse calculation by employing fundamental composites theory to inverse calculations. An optimization analysis, which will be discussed in the next section, is performed first to determine the desired mechanical characteristics of a composite blast resistant panel. Then, the IMEA process identifies the composition of each ply with computational efficiency.

The primary contribution of this chapter is the development of an inverse calculation sequence to enable IMEA. In this study, MSM is modified to eliminate the

iteration process and several composites theories are integrated into the IMEA. The feasibility of the IMEA is demonstrated by validation case studies that compare one inversely calculated unknown with given conditions as well as two unknown conditions. A detailed background on the computational cost problem of the multi-scale modeling using MSM is discussed in the next section.

3.1: Multi-Scale Design Optimization

One method of the micro-scale configuration design of the composites is using the MSM as a constraint component of a simple optimization model. Micro-scale design variables can be achieved with some constraints, such as maximum stress and strain needing to be less than the value at the failure point, and global-scale objectives, such as minimizing the thickness of the blast panel structure. To integrate the fully-coupled MSM within the optimization model, several Python language codes are compiled to access the ABAQUS Explicit data stored in an output database (Figure 20). The micro-scale design variables are directly controlled in the ABAQUS input file, and the MSM framework produces the maximum stress and strain, which can be used for non-linear design constraints within optimization framework. Using a simple optimization algorithm, the optimal configuration design of the composites panel can be achieved using the iterative design optimization framework.

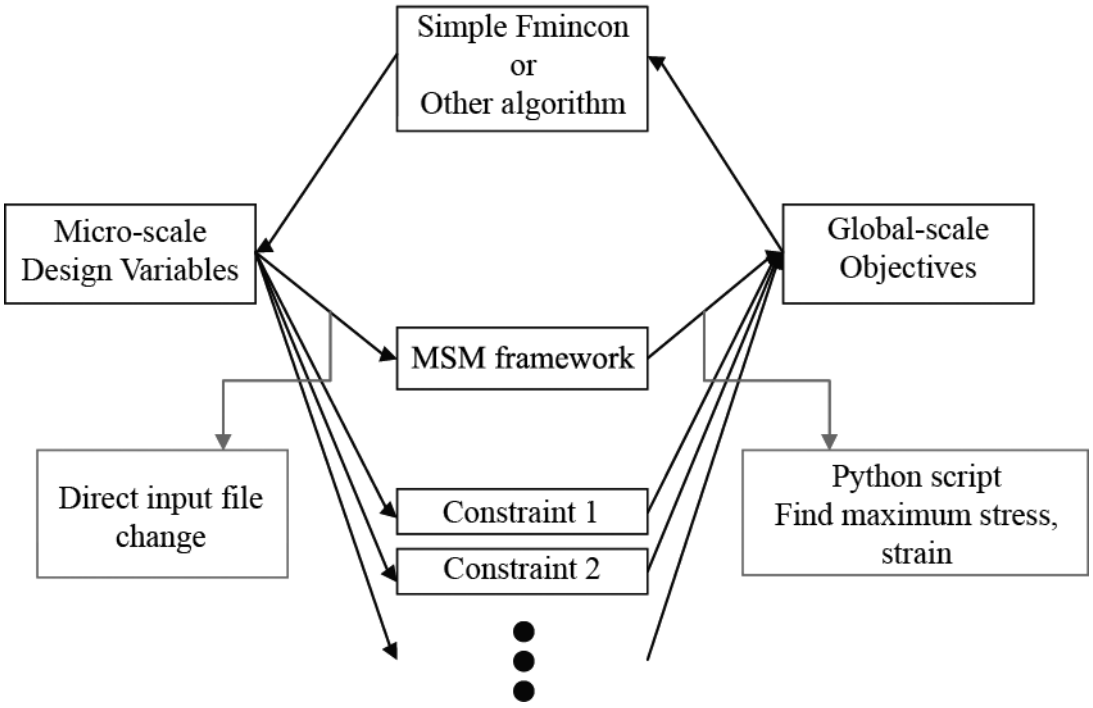

Figure 20: Flow chart of micro-scale configuration using a simple optimization model.

Python is the standard programming language for the ABAQUS solver. In contrast to the unrestricted utilization of the calculation data in the ABAQUS Standard solver, in the ABAQUS Explicit solver needs further scripts to access the data in an output database using ABAQUS scripting interface. An output database generated from an analysis contains both models, which describes the parts and part instances that make up the root assembly, and results data, which describe the results of the analysis. To use calculated results that include stresses and strains, several Python scripts use output to configure the contents of the data. To improve the efficiency of the script itself, objects used to hold temporary variables while the script is executing are created. The object, which holds the variable, improves the script when the script accesses the temporary variable while a loop, and, as a

result, the ABAQUS solver does not need to reconstruct the sequence of objects each time the script accesses a component.

Despite all these efforts to increase efficiency, to achieve stability of the MSM, the maximum time increment needs to be smaller than a critical smallest transition time value to cross any mesh element for an expansion wave (Sun et al, 2000). The computational cost is rapidly increased from the tangent stiffness matrix and occurs at critical divergence, and difficulty of force equilibrium from local instabilities causes interruption to achieve in high strain rate blast event analysis. Because of these reasons, the ABAQUS Explicit solver is applied to MSM to overcome the disadvantages of the implicit solver. ABAQUS has various methods, such as a modal dynamic algorithm for dynamic problems; however, the direct integration method can only provide suitability for nonlinear problems. This cost from integration increases the expensive computational cost of the MSM itself and precludes using the MSM with the micro-level configuration design of composites.

The computational costs are also increased by the iteration process within each time increment and between the MAC and the ABAQUS Explicit module to update effective material properties. This iteration is one of the most important and indispensable parts of the MSM because it considers the global-scale deformation effect from the high strain rate blast load condition in every calculated time increment. This iteration allows propagating information from the constitutive micro-level, such as fiber failures, matrix damage, inelasticity, and interfacial debonding, to the global structural response level for instantaneous blast event simulation.

For such reasons, the computational cost of using MSM as a design constraint in optimization is doubled with optimization cost, and another novel idea to reduce computational cost becomes necessary. A micro-scale configuration design using an optimization frame with a one-way coupled multi-scale method, which has no consideration of the global-scale deformation effects, has been performed as the beginning simple approach, and has been compared with using MSM. Although this frame cannot reduce the computational cost related to first discussed ABAQUS stabilization, the cost from the iteration process of the MSM can be compared. The time increment sizes are selected to provide stability, and optimization results are outputted at each iteration for all the calculations to provide consistent levels. A dual-core CPU workstation with sufficient four Gigabyte RAM memory is used to compare with different quantities of the design variables, and the comparisons are given in Table 5.

Table 5: Computational cost comparisons from iteration process.

Optimization Design variables	**Constraints unit**	**Calculation time (s) per iteration**	**Comparison**
2	One-way coupled (No iteration)	24	1
2	MSM (Iteration)	10,800	450
3	One-way coupled (No iteration)	27	1
3	MSM (Iteration)	12,600	467

To consider the global-scale transformation effect, the iteration process between MAC and ABAQUS makes almost 500 times more computational cost. Since the computational cost from the time increment size of the ABAQUS calculation is

proportional to the increment size, the critical reason of the high computational cost is expected to come from the iteration process. To reduce the computational cost of the MSM, several methods are studied in the next section.

3.2: Inverse Material Engineering Algorithm (IMEA)

Besides depending on high performance parallel computing power to reduce the computational cost of the ABAQUS Explicit solver (just one part of the MSM), other solutions can increase the time increment size by coarsening the finite element mesh or any artificial inertia or mass penalty technique (Macek and Aubert, 1995). As a variant of mass scaling, the addition of virtual mass terms in the mass matrix would decrease the highest frequencies of the system without significant effect to the structural modes. The mass penalty technique includes the ability to preferentially reduce the high-frequency modes with little effect on the low-frequency structural modes and the ability to easily adjust the highest frequencies of the structure. The addition of a stiffness proportional mass matrix to the physical mass matrix preserves the rigid body behavior that is particularly important for systems where part of the structure is stiff and, thus, may basically respond as a rigid body. Improvements in CPU usage without significant loss of accuracy for problems involving moderate dynamic response were established. However, its efficiency is limited to small deflection material non-linear analyses. And again, this improvement can only reduce the computational cost of the one part of the MSM.

Therefore, rather than increasing the time increment size or relying on supercomputers, introducing MSM-INFO as a new module that enables the reduction of

computational cost by eliminating the iteration process between MAC and ABAQUS Explicit solver module is studied. The iteration process was originally used in the MSM to exchange the information through homogenization and localization simulation processes. During the homogenization process, the MAC code determines the material response at the integration points within each ABAQUS element. In essence, MAC operates as a nonlinear constitutive model within the ABAQUS Explicit module, representing the heterogeneous material. In reverse, during the localization process, local stress and strains that are computed by the ABAQUS Explicit module from incrementally applied loading are applied to the MAC for obtaining updated effective material properties. Through the iteration process, effective material properties with the strain rate effect at each time increment can be determined (Figure 21).

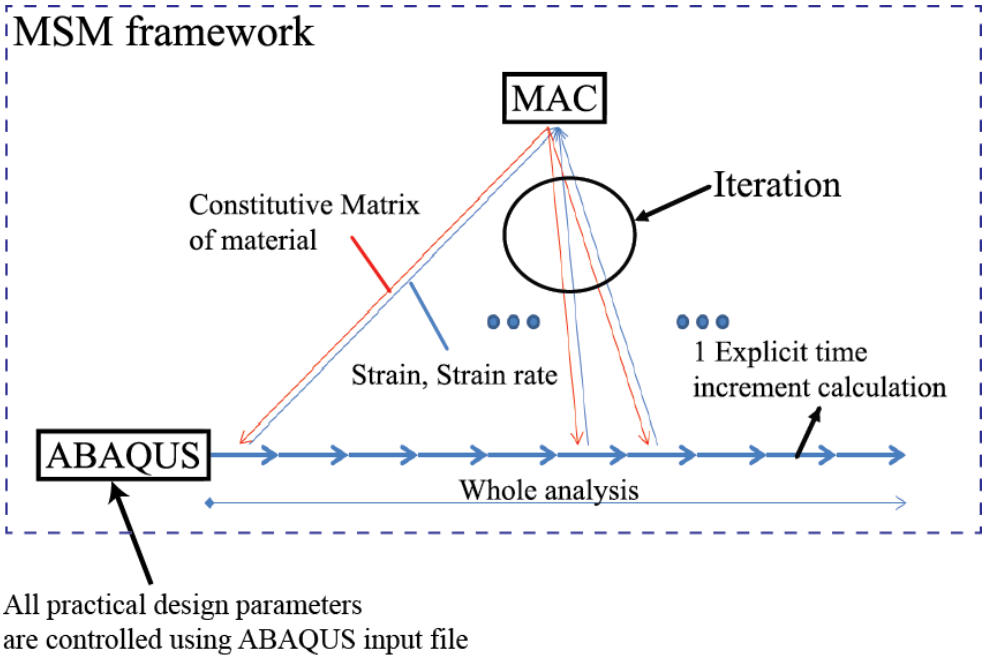

Figure 21: Flowchart for MSM framework.

The idea of the MSM-INFO proceeds from elimination of the iteration process, which is used in consideration of strain rate effects. The difference in the strain rate data between the one-way multi-scale method and MSM is not exceedingly considerable before the subject structure failed in accordance with previous MSM demonstration study in Chapter 2.4. The major concept of the MSM-INFO is that it takes advantage of this similar tendency and uses pre-calculated strain rate data to calculate material properties in each time increment of ABAQUS analysis. Among the 36 pieces of constitutive material property information of the uni-directional fiber-reinforced composite material, six properties (section 4.2) are applied in this work using the symmetrical arrangement and the identical layer thickness design parameter. Because the optimal design cares for a non-destructive structure for a given blast load, this modified framework makes the optimization frame run with computational efficiency in conjunction with consideration of the global-scale deformation effect. To materialize, the material properties variables ought to be controlled in the MAC-INFO module and other variables are controlled in ABAQUS input file, in contrast with all the variables being controlled in the ABAQUS input file as the original method. Using the predicted strain rate information at each time increment, from pre-run one-way multi-scale method, the material properties by the matrix form of the structure can be attained, and this matrix can be utilized for micro-scale configuration design by an inverse calculation using the composite theory (Figure 22).

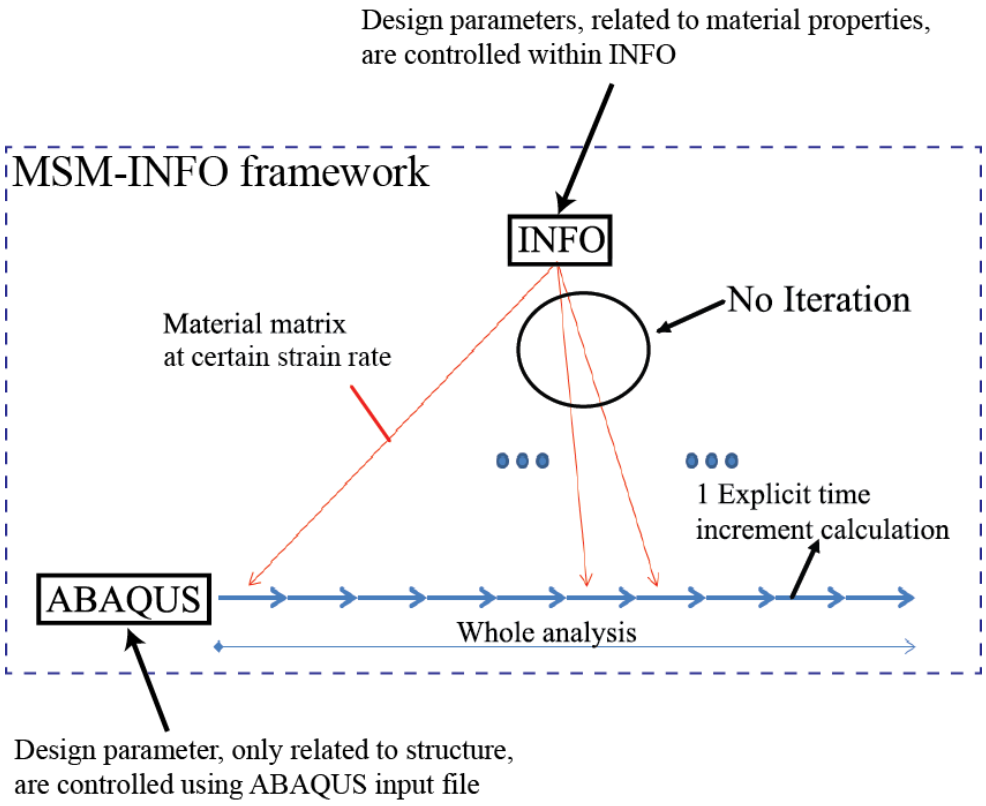

Figure 22: Flowchart for MSM-INFO framework.

The MSM-INFO module capacitates provision of the effective material properties of each time increment using a predefined strain rate from the one-way coupled multi-scale analysis, which is modified with Bodner-Partom micro-scale material model. A strain rate of the each time increment is predefined to reduce the computational cost. The eliminated iteration processes between the MAC code and the ABAQUS Explicit module enable determination of the optimized material properties of a certain strain rate condition with efficient computational cost.

However, to obtain a practical design of the micro-level configuration for the composite panel, the material matrix at a specific strain rate should be converted to effective design factors, such as fiber volume fraction and layer orientation of the laminated

composites. The necessity of this conversion is the basis of the IMEA that inversely calculates the material matrix using MSM-INFO to the micro-scale configuration design factor. This inverse calculation is based on several composites equations, which are provided in the next two sections, and the concept feasibility will be provided with validation case studies that inversely calculate for the one unknown and compares with given conditions as well as two unknown circumstances. The two case studies are discussed in sections 3.3 and 3.4 to provide the sequence of the inverse calculation and to validate the concept.

3.3: IMEA Validation Study with One Unknown - fiber volume fraction

With the material properties matrix and the strain rate information, an inverse calculation capacitates a micro-level configuration by several composite theories included in parentheses. A case study with manual calculation is performed to verify the pre-nominated concept with 0.6 fiber volume fraction composites. To formulate the strain rate effect, the concept of the scaling rule was established, and applied with nonlinear formulation, which is similar to a model commonly used to describe high strain rate behavior (Weeks and Sun, 1998; Matsuoka, 1992). The parameter P, given by power law,

$$P_i = P_1 * \left(\frac{\dot{\varepsilon}_i}{\dot{\varepsilon}_1} \right)^c \tag{17}$$

, is a function of the totally dominated strain rate $\dot{\varepsilon}_i$, with coefficient c from experimental data. However in this study, to demonstrate the IMEA concept, a coefficient c has been obtained (-0.0305) from a simple tensile load analysis with a stress parameter. Three strain

rate conditions with a stress parameter are used to calculate the coefficient using the above power law equation (Figure 23).

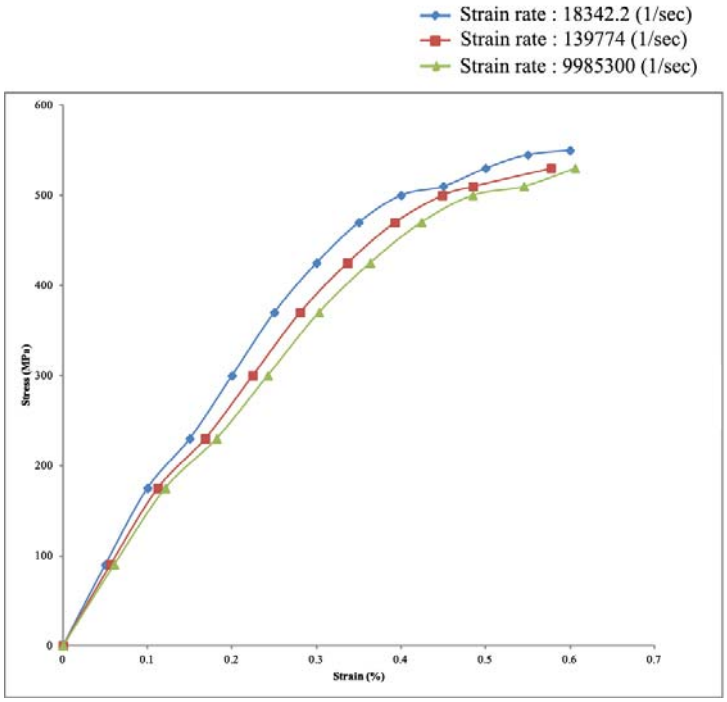

Figure 23: Tensile load analysis to obtain the coefficient.

The effective material properties are calculated using fully coupled MSM with the strain rate information with given fiber volume fraction (V_{fiber} = 0.6). On the other hand, using previously obtained coefficient c, the material property information of the fiber and the matrix are defined for each strain rate condition. The inverse calculations, to find the volume fraction, are performed sequentially (Figure 24) for each strain rate condition by using the simple strength equation for the fiber-reinforced composites (Hale and Kelly, 1972),

$$P_{composite} = (1 - V_{fiber}) \times P_{matrix} + V_{fiber} \times P_{fiber} \tag{18}$$

, with composite parameter $P_{composite}$, the matrix material parameter P_{matrix}, the fiber material parameter P_{fiber}, and the fiber volume fraction V_{fiber}.

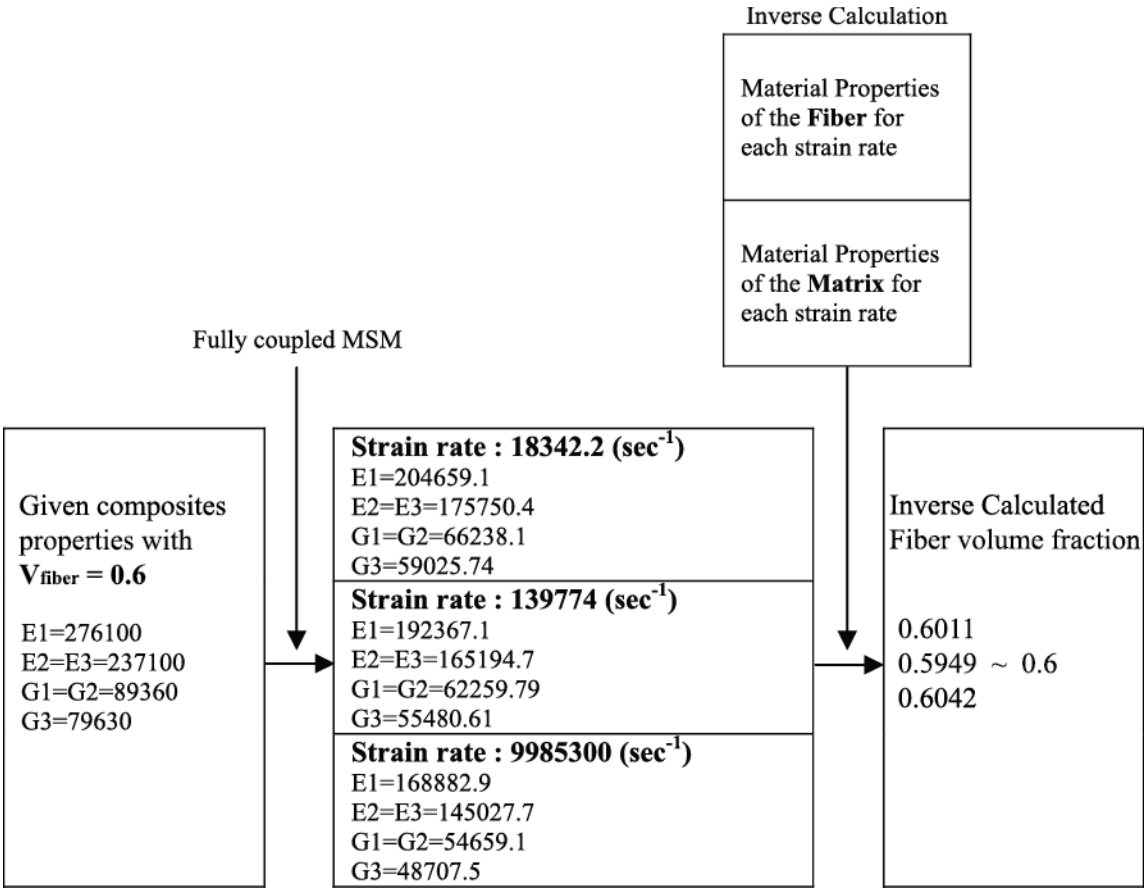

Figure 24: Inverse calculation sequence to find unknown fiber volume fraction.

, and the three inversely calculated fiber volume fractions V_{fiber} of each strain rate condition are determined in Table 6. The results from comparisons show that the inversely calculated fiber volume fractions and the given fiber volume fraction have an identical value.

Table 6: Inversely calculated fiber volume fraction of each strain rate condition.

Strain rate (sec^{-1})	Fiber Volume Fraction	Error (%)
0 (Given)	0.6000 (Given)	-
18342.2	0.6011 (Inverse Calculated)	0.18
139774	0.5949 (Inverse Calculated)	0.85
9985300	0.6042 (Inverse Calculated)	0.70

This good agreement between the given volume fraction and the inversely calculated volume fraction demonstrates the properness of the concept of IMEA for one unknown, fiber volume fraction.

3.4: IMEA Validation Study with Two Unknowns - fiber volume fraction + layer orientation

Another case study with manual calculation is performed to verify the pre-nominated concept with two unknowns using 0.5 fiber volume fraction composites and 0-45-0-45 layer orientation conditions. Aside from the strain rate effect and simple composite strength equations, to formulate the laminate effect, the Classical Laminate Theory (CLT) is used (Ochoa and Reddy, 1992; Gunnink, 1985). In the first sequence, from the given thickness (0.01m), fiber volume fraction (V_{fiber} = 0.5), and laminated orientation condition (Ori : 0-45-0-45), the MSM framework calculates the laminated material matrix at a certain strain rate (Figure 25).

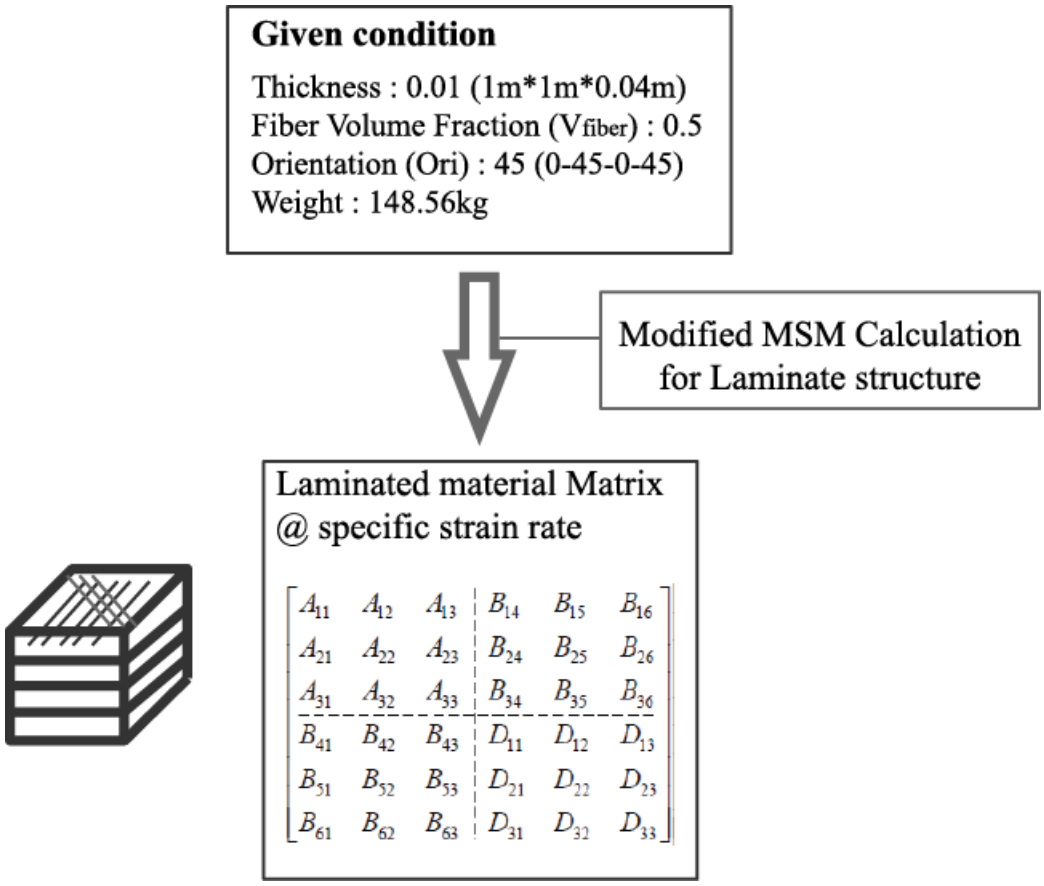

Figure 25: Inverse calculation sequence 1 - Calculate material matrix from given conditions

The material matrix with two unknowns, fiber volume fraction and layer orientation, is calculated from the opposite side using the previous two composite equation, power law equation for strain rate effect, and the additional CLT theory for lamination in the second sequence (Figure 26).

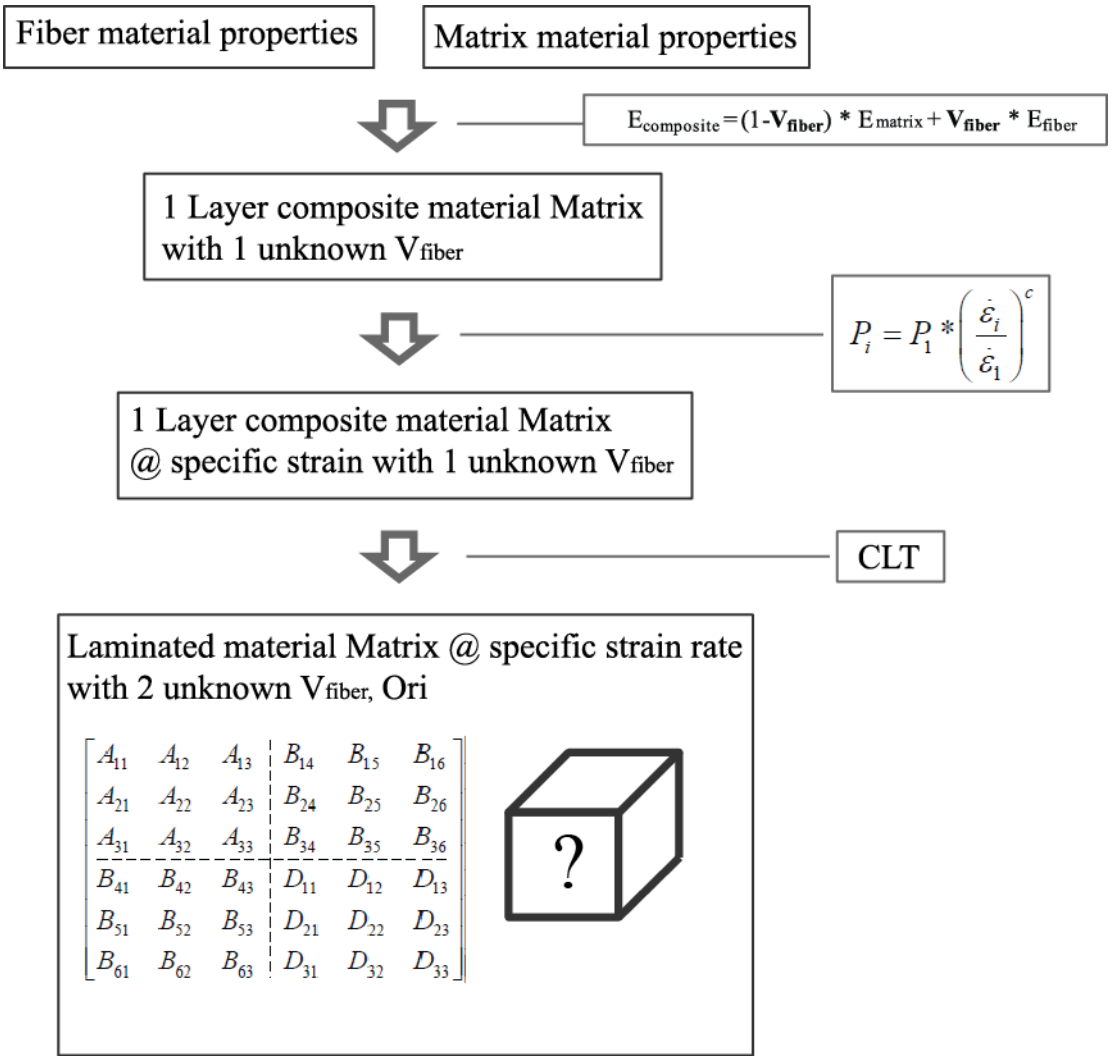

Figure 26: Inverse calculation sequence 2 - Calculate material matrix with two unknowns, fiber volume fraction and layer orientation

The one layer composite material matrix with one unknown fiber volume fraction is calculated using the previous fiber-reinforced composites equation. Then, the one layer material matrix at specific strain rate is calculated using the previous power law equation. The laminated material matrix at a specific strain rate with two unknowns, fiber volume fraction, and laminated orientation is calculated using CLT theory. The material matrix from the first sequence is compared to the material matrix with two unknowns from the

second sequence. The two solution sets are obtained from comparing the matrix from the given conditions against the matrix, which includes two unknowns, and calculated from the material properties of fiber and matrix. The second solution set has been chosen, since it has same blast performance but lighter weight (Figure 27). Since the fiber volume fraction is the only design parameter related to the weight in this case, the larger fiber volume fraction represents the lighter weight. To implement this selection, a simple MATLAB code using a comparison analysis is developed. The process in this work does not need more mathematically calculated boundary conditions, however, several literature studies are considered to apply the conditions for later research (Jiming et al, 2006; Liu et al, 2002; Schnur and Zabaras, 1992).

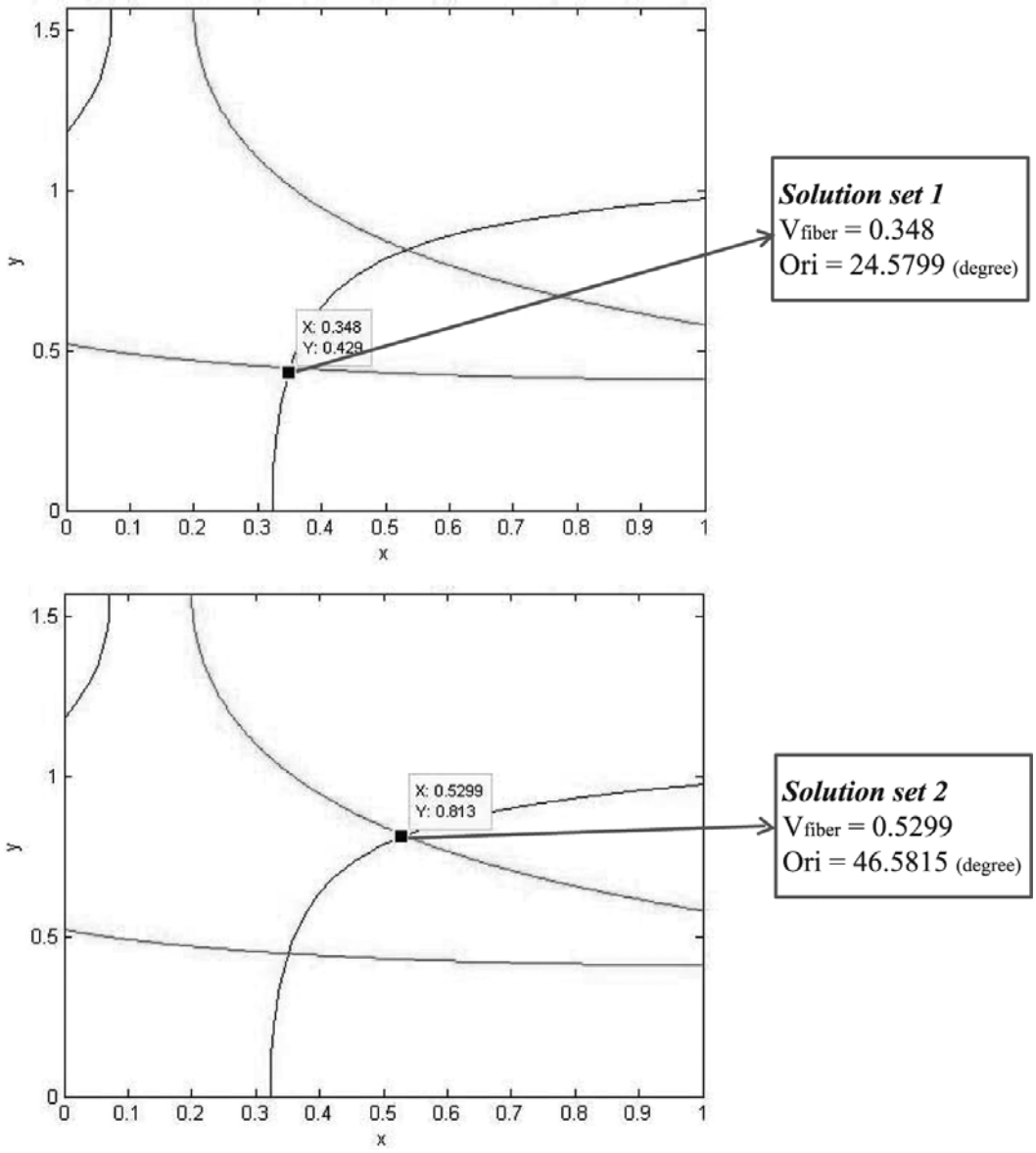

Figure 27: Inversely calculated solution sets at a strain rate 18342.2 (1/sec).

The results at the other strain rate condition are calculated and compared in Table 7. The results from comparisons show that the inversely calculated design parameters and the given conditions are identical.

Table 7: Inversely calculated Volume fraction and Orientation at each strain rate condition.

	Fiber volume fraction		Orientation	
Strain rate	0.5 (Given)	Error	45 (Given)	Error
0	0.5131	0.0262	47.71	0.0602
18342.2	0.5299	0.0598	46.5815	0.0411
139774	0.5299	0.0598	45.4928	0.0110
9985300	0.5299	0.0598	47.3836	0.0530

This good agreement between the given condition and the inversely calculated fiber volume fraction and layer orientation demonstrates the concept feasibility of the IMEA. The validated IMEA concept is compiled in a MATLAB file to use within the computational framework, which capacitates the micro-level configuration design for specific global-level functionality. In the field of the composites, inverse methods are a novel area of study, which include:

- A mixed numerical-experimental identification procedure study estimated with a nonlinear least squares using both the extracted mode shapes and the natural frequencies of the structure (Cugnoni et al, 2007);
- A mixed testing-numerical method study using hybrid genetic algorithm to identify the elastic constants of the composites (Hwang et al, 2007; Liu et al, 2007); and
- An inverse method study using uncertainty in the system to determine the properties of the composites using vector (Jiang et al, 2009).

These hybrid numerical-experimental and uncertainty inverse methods can be included in the IMEA without difficulty, though the computational cost would be also increased. Accordingly, the inverse method using composite equations, which is discussed in sections 3.3 and 3.4, is implemented within the computational framework and additional literature studies to predict a more precise configuration of the composites should be undertaken sequentially. A discussion of the computational framework using an optimization framework and IMEA is presented in the next section.

CHAPTER 4:
A COMPUTATIONAL FRAMEWORK FOR MICRO-LEVEL CONFIGURATION DESIGN OF A COMPOSITES PANEL

The objective of this chapter is to document a computational framework that determines the configuration of each ply of a composite laminate panel to achieve the desired blast resistance characteristics at minimum thickness. Both of the Modified MSM and IMEA are integrated into the framework for the optimization analysis. This chapter focuses on developing an optimization computational framework by developing MATLAB codes and PYTHON codes to employ previously developed and validated processes. In this framework, first an optimization analysis using modified MSM-INFO is performed; then, the IMEA process identifies the composition of each ply.

In this chapter, the developing optimization analysis sequence and the integrating IMEA process is discussed. A case study is performed using an optimal four-layer composite panel design that is subjected to blast pressure load conditions. The results are then compared with the previously discussed multi-scale analysis results. A detailed discussion of the integration of MSM-INFO and IMEA are presented in the next section.

4.1: Integration of MSM-INFO and IMEA into a computational framework

To accomplish the overall objective, the micro-scale configuration design of the composite panel, which has light weight and strength simultaneously, and the

computational framework, which includes MSM-INFO and IMEA concept, were studied. The details are described in a later case study (section 4.2), but three design variables: thickness of the panel, fiber volume fraction of the layer, and layer orientation, are used to perform the initial study.

The MSM-INFO module is used for one of the nonlinear constraints in the optimization framework to find optimal orthogonal material properties and thickness data. A MATLAB file for nonlinear constraints is written using design variables, which are the thickness variable that is controlled in the ABAQUS input file immediately, and the material properties variables that are controlled in INFO module. Through MSM-INFO implementation and applying Python codes, the file calculates a maximum stress and strain of the structure in the entire calculation (Figure 28-(a)). These maximum values are used in two non-linear constraints where maximum stress and strain are less than the value at the failure point, and these constraints are employed in the optimization framework. The objective function of the optimization framework minimizes the thickness of the panel to find the optimal thickness and the material properties information (Figure 28-(b)). The initial point of the optimization is utilized from the result using a pre-nominate optimization framework with a one-way coupled multi-scale method using variables such as thickness and composite material properties. This first step produces the optimal thickness and optimal material matrix information, which needs to be converted for practical design of the micro-scale configuration.

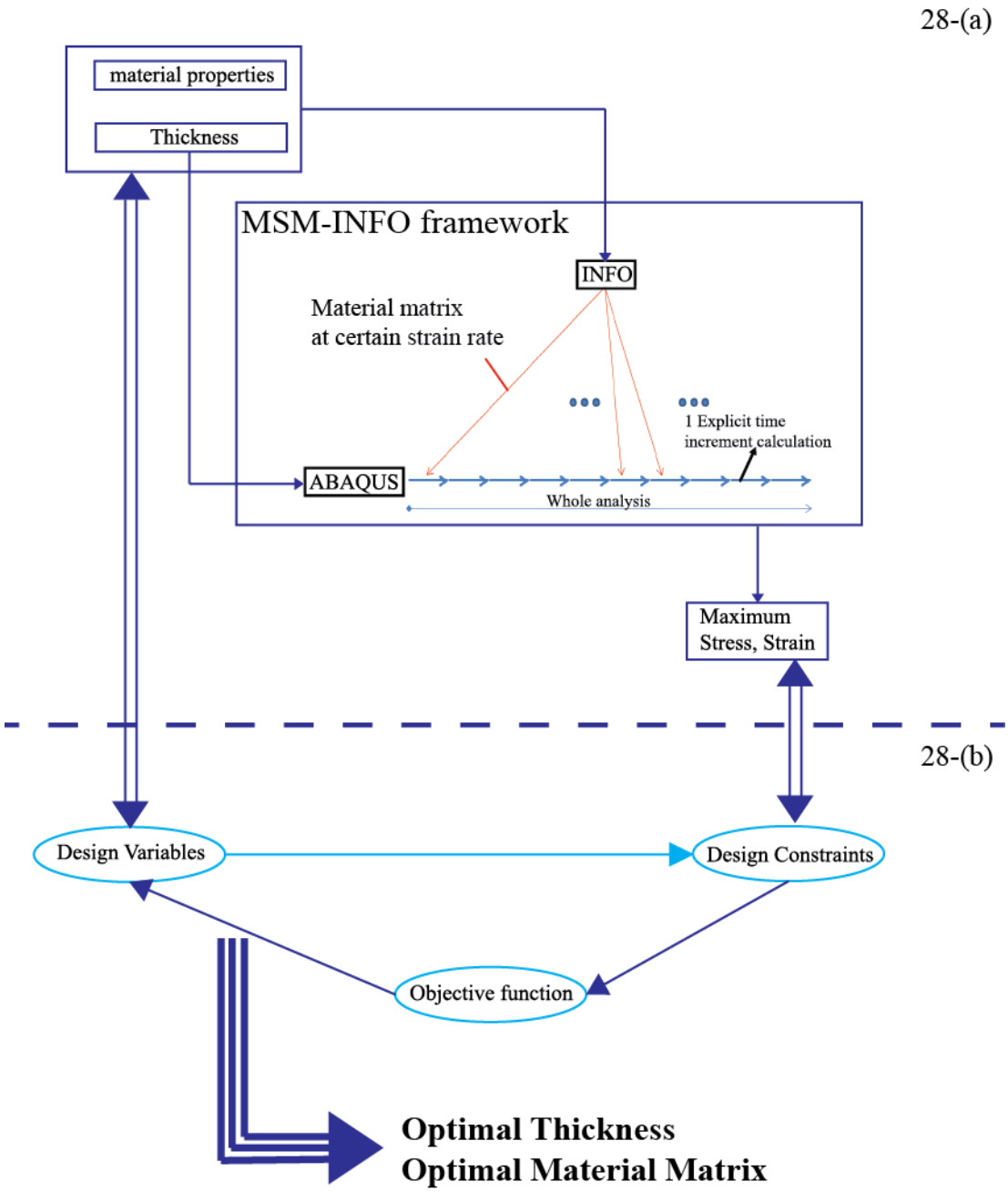

Figure 28: First step of the computational framework, Optimization framework.

Then through IMEA, the formerly obtained optimal result from the first step is inversely calculated to the optimal orientation, fiber volume fraction, and thickness. A non-linear formulation is used to consider high strain rate effect, a simple composite strength

equation, and a Classical Laminate Theory. Through this second step, the computational framework obtains the optimal micro-scale configuration of the composite panel (Figure 29). A case study is discussed in the next section to demonstrate the computational framework.

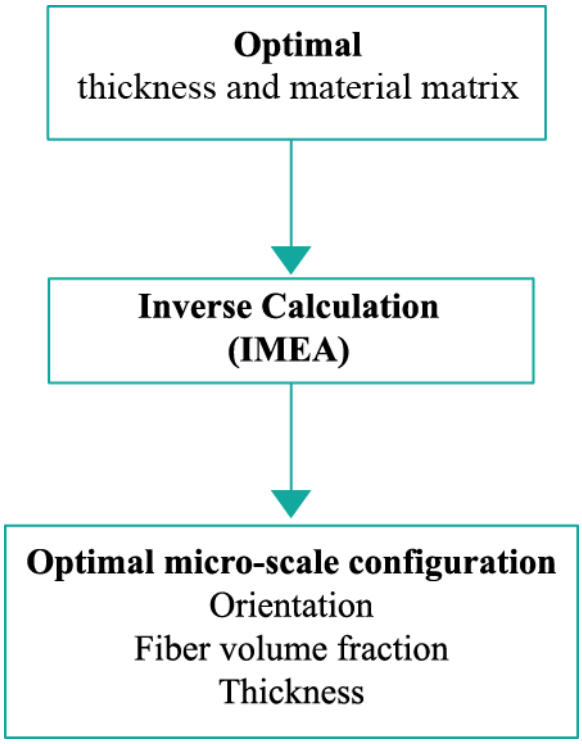

Figure 29: Second step of the computational framework, IMEA framework.

4.2: Optimal Design Case Study Definition - four-layer laminated composite panel

The overall objective of this optimization study is to design a four-layer laminated composite panel that is lightweight and blast resistant. Three design micro-scale variables: thickness of the layer, orientation of the layer, and fiber volume fraction of each layer are

used in this study. The design objective is to find the minimum total thickness of the blast panel, which satisfies the two constraints:

1) the maximum stress needs to be less than the stress at the failure point and

2) the maximum strain needs to be less than the strain at the failure point.

In this study, the optimization is performed with simplified conditions of each layer being of the same thickness, the orientation of the first (a) and third (c) layer being fixed, allowing the second (b) and fourth (d) layer to be oriented between 0 and 90 degrees, and the fiber volume fraction of the each layer being identical (Figure 30). This limitation reduces the 36 material constants of the composite material to the six constants.

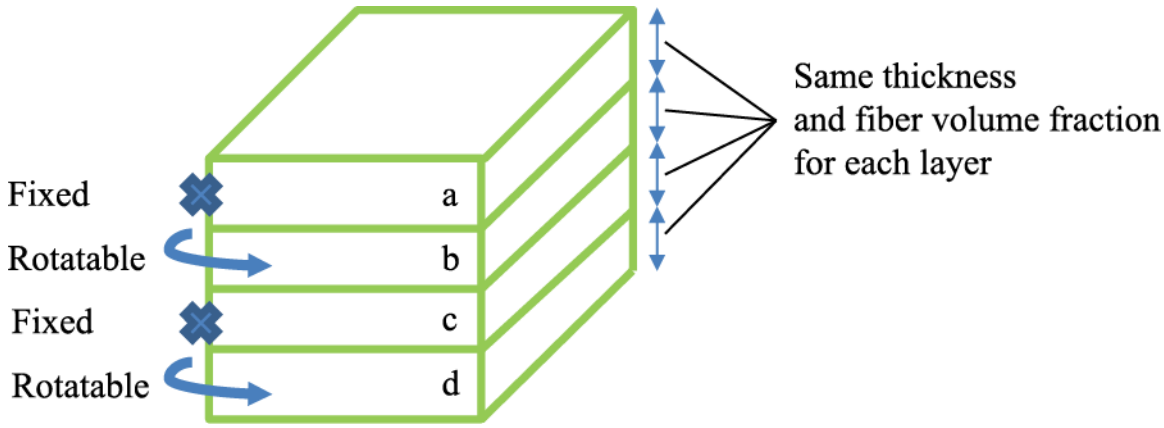

Figure 30: Design variables for four-layer composite panel design optimization.

The FMINCON function of MATLAB is used to find the minimum thickness of the composite panel; seven variables, which include thickness (x(1)) and the six composite material constants (x(2) to x(7)), are used in the optimization frame. The above two non-linear constraints are comprised by a MATLAB code that includes MSM-INFO and PYTHON codes to perform ABAQUS Explicit analysis. To consider failure mechanisms,

the Tsai-Wu failure criteria (Tsai and Wu, 1971) is used in the computational framework for this preliminary study. The matrix failure, F_{matrix}, is given as

$$F_{matrix} = \frac{{\sigma_2}^2}{S_2 C_2} + \left(\frac{\sigma_{12}}{S_{12}}\right)^2 + \frac{(S_2 - C_2)\sigma_2}{S_2 C_2} \tag{19}$$

, with the transverse stress σ_2, the shear stress σ_{12}, the transverse tensile strength S_2, the shear strength S_{12}, and the transverse compressive strength C_2.

, where failure is assumed at

$$F_{matrix} > 1 \tag{20}$$

, and the fiber failure, F_{fiber}, is determined from

$$F_{fiber} = \left(\frac{\sigma_1}{S_1}\right)^2 + \bar{\tau} \tag{21}$$

, with the longitudinal stress σ_1, the longitudinal tensile strength S_1, and the ratio of the shear stress $\bar{\tau}$.

, where failure is assumed at

$$F_{fiber} > 1 . \tag{22}$$

The ratio of the shear stress is determined from

$$\bar{\tau} = \frac{\frac{{\sigma_{12}}^2}{2G_{12}} + \frac{3}{4}\alpha {\sigma_{12}}^4}{\frac{{S_{12}}^2}{2G_{12}} + \frac{3}{4}\alpha {S_{12}}^4} \tag{23}$$

, with the nonlinear shear stress parameter α, and the shear modulus G_{12}.

This macro-mechanical criterion considers multi-directional laminate composite failure as opposed to the micro-mechanical failure criteria, which estimates the ultimate failure. The micro-mechanical failure criterion is more appropriate for initial failure of the composites (Daniel, 2006). The five material properties for the failure theory were calculated by MAC code and three properties were compared with literature (Gundel and Wawner, 1997; Li and Wisnom, 1995) in Table 8.

Table 8: Material properties for the failure theory.

	Longitudinal tensile Strength, S_1 (MPa)	Transverse tensile Strength, S_2 (MPa)	Shear strength, S_{12} (MPa)	Transverse compressive strength, C_2 (MPa)	Nonlinear shear stress parameter, α
MAC result	3360	748	370	2010	0.25
Literature	1252 (measured) 3048 (calculated)	263 (debonding)	269	---	---

A four-layer composites panel design optimization case study is performed using the computational framework, and a detailed discussion is presented in the next section.

4.3: Results - four-layer laminated composite panel

The overall micro-scale configuration of the composite panel design process is performed in two steps with several modules. The first step, Optimization, includes the ABAQUS Explicit solver, BEST software for calculating blast pressure load, and MSM-INFO for providing material information at certain strain rates. From given micro-scale

design variables, the MSM-INFO produces maximum stress and strain. The INFO module provides a material matrix to each of the ABAQUS time increment using strain rate information from pre-run one-way coupled analysis, and the BEST provides blast pressure load history. The maximum stress and strain data is used for non-linear design constraints and the optimization framework produces the optimum results, which needs to be converted for practical design parameter.

The second step, IMEA, includes the inverse calculation (Figure 31). Through the inverse calculation, previous optimum results are converted to the practical design parameter, layer orientation, fiber volume fraction of the each layer, and thickness of the each layer in this second stage.

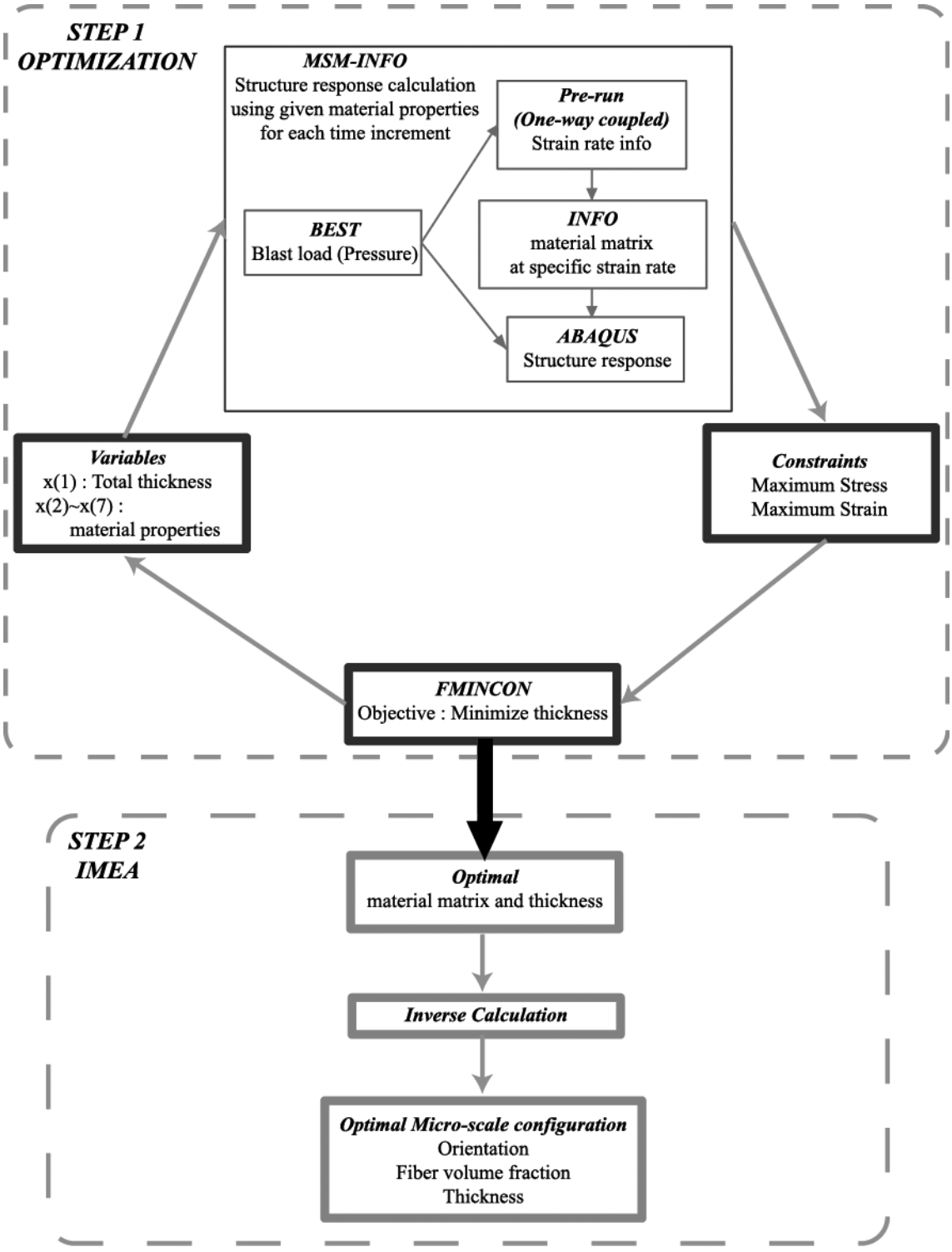

Figure 31: Micro-scale configuration design process.

The starting point of the optimization is from the results of a previously executed simple optimization frame using the one-way coupled multi-scale simulation capability (Kim et al, 2013). The optimum results of the design variables (x(1) to x(7)) are obtained. Sequentially, a micro-level configuration of the composite panel is obtained by the IMEA inverse calculation and the result of the optimal thickness, optimal fiber volume fraction, and the optimal orientation are presented in Table 9. To check the inverse calculation result, comparisons of the maximum displacement measurements and failure checks are performed. Both of the optimization and IMEA results show the identical maximum displacement at the bottom layer, and both results show no failure in the entire structure.

Table 9: Results comparison from the optimization frame and the IMEA frame.

	Step 1: **Optimization**	Step 2: **IMEA**
Starting point	Initial values of x(1)~x(7) have Thickness = 0.10m Fiber Volume Fraction = 0.5 Orientation = 45degree	---
Optimal Value	x(1) = 0.1980 x(2) = 443850 x(3) = 360730 x(4) = 161490 x(5) = 67895 x(6) = 17933 x(7) = 14227	Optimal Thickness = 0.1980m Optimal Fiber Volume Fraction = 0.4006 Optimal Orientation = 0.7077 (40.54 in degree)
Maximum displacement (m) at bottom layer	0.005863	0.005994 (MSM-INFO)
Failure	None	None

The optimal micro-scale configuration design of the composite panel from a result appears as a four-layer composite panel, which has a dimension of 1m width by 1m length by 0.1980 (m) thickness, and each layer of the panel has 0.4006 fiber volume fraction and has 0-40.54-0-40.54 degree layer orientation (Figure 32).

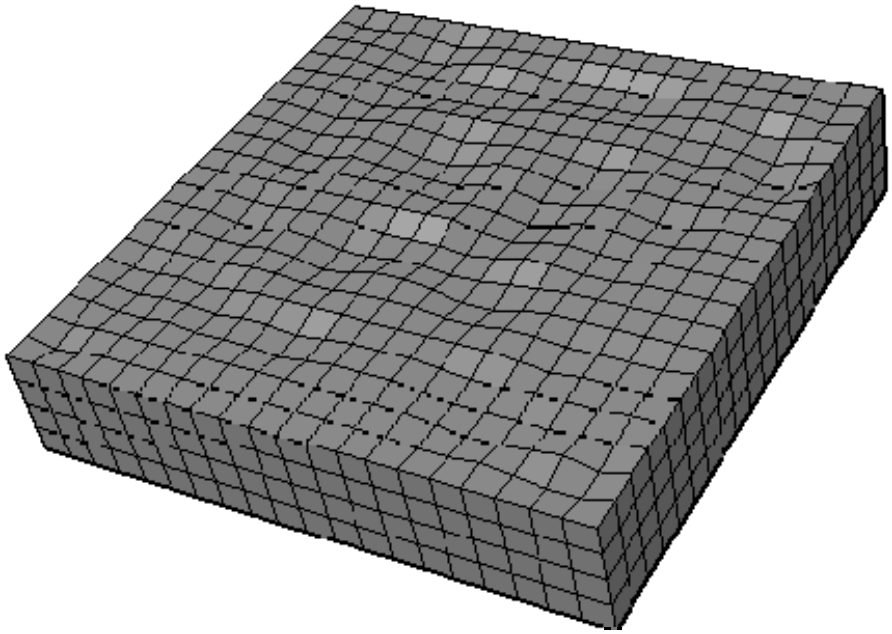

Figure 32: Results from the optimization frame

This optimization result is compared with an early stage fully-coupled MSM result and one-way multi-scale method results using two different solvers in Table 10. The first two results (0.005994, 0.00612) are comparable because both results consider the strain rate effect during calculation. On the contrary, the third and fourth results (0.00512, 0.00498) were different from the first two results because they do not consider the strain rate effects. A good agreement with previously validated fully-coupled MSM result demonstrates the

appropriateness of the overall micro-scale configuration design process. An additional case study using a sandwich panel is presented in the next section.

Table 10: Comparison results using maximum displacement.

	Optimization result	**Fully-coupled MSM**	**One-way ABAQUS Explicit**	**One-way LS-DYNA**
Maximum displacement (m) at bottom layer	0.005994	0.00612	0.00512	0.00498
Failure	None	None	None	None
Strain Rate Effect	Included	Included	Excluded	Excluded

CHAPTER 5:
A CASE STUDY OF A SANDWICH PANEL DESIGN

The objective of this chapter is to present a case study of a sandwich structure that strengthens the fiber-reinforced composite panel discussed in the previous section. To impart significant reinforcement, the roles of energy dissipation are considered by engaging rubber panels to an existing structure. Additional structural stability is expected on the top of the reinforcement. The overall panel structure consists of a hyper-elastic rubber material placed between two four-layer silicon carbide fiber-reinforced titanium alloy matrix composites panels.

This chapter supplements the previously presented computational framework by considering the lamination of dissimilar material using adhesive. Additional layers of adhesive and center material are added and an optimal design case study is performed using the sandwich structure, which is subjected to the blast pressure load condition. The optimal design result of this chapter is compared to the previous results to identify the role of the additional energy dissipative rubber material. A more detailed background on the sandwich structure is discussed in the next section.

5.1: Sandwich Structure

The sandwich structure takes advantage of the various material properties, such as density, high-energy absorption capacity at a low weight, and bend resistance. The physical

phenomena related to the energy absorbing materials has been studied in different disciplines (solid mechanics, material science, physics). In the field of the analysis and design of energy-absorbing materials, the dynamic behaviors of materials are studied, such as metal plates and polymer matrix composites (Goldberg et al, 2005; Binienda, 2004; Cheng and Binienda, 2006), ceramic armors (Lopez-Puente et al, 2005; Sarva et al, 2007), magneto-rheological fluids (El et al, 2002), porous NiTi shape memory alloys (Miyoshi et al, 1999). Also studied are structures capable of resisting blast events (Meyers, 1994; Nesterenko, 2001). The fiber-reinforced composites, addressed in the previous chapter, is undoubtedly a typical high energy-absorbing material, but the sandwich structure can account for other energy dissipate materials, such as a rubber material.

The sandwich structure in this chapter, which consists of a hyper-elastic rubber material placed between two four-layer silicon carbide fiber-reinforced titanium alloy matrix composites, provides a study of the panel design using additional energy dissipative materials. The advantage of the sandwich structure is that it protects the occupant from the explosion. Rubber materials are not only widely used in vibration areas due to its inherent physical characteristic of withstanding large strains and its damping performance, but rubber materials are also used in the protection area as energy absorbing material.

The details are described in a later case study (in section 5.2) with five design variables: thickness of the each three panels (*1, *2, *3 in Figure 33), layer orientation (*4 in Figure 33), and fiber volume fraction of the layer (*5 in Figure 33). A case study applies the previous computational framework with additional codes to implement energy absorbing characteristics of the rubber, using an energy-based hyper-elastic material model

of the Mullins effect (Mullins, 1969) (Figure 33). Several experimental data to apply the Mullins effect were obtained from the literature and are presented in more detail in the next section. Additional layers of the adhesive are employed to consider de-lamination of the heterogeneous materials, which is the rubber and the silicon carbide fiber reinforced titanium composites. A detailed discussion of the case study is presented in the next section.

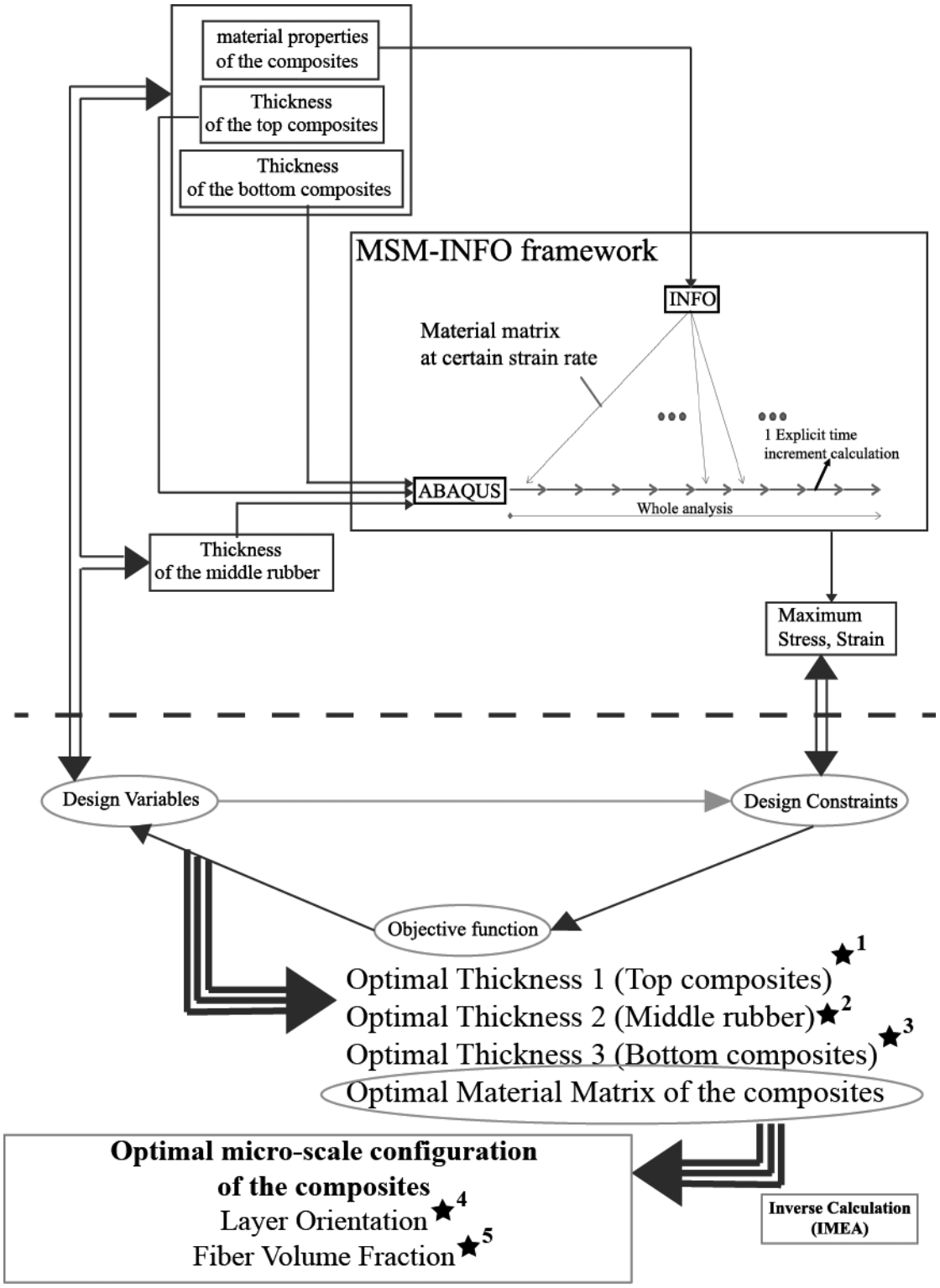

Figure 33: Sequence of the computational framework to design sandwich structure.

5.2: Optimal Design Case Study Definition - sandwich structure

The overall objective of this optimization study is to design a sandwich panel structure that is lightweight and blast resistant. Five design micro-scale variables are used in this study: (1) thickness of the composites on the top, (2) thickness of the rubber in middle, (3) thickness of the composites on the bottom, (4) orientation of the layer, and (5) fiber volume fraction of each layer. The design objective is to find the minimum total thickness of the blast panel, which satisfies the two constraints:

1) the maximum stress needs to be less than the stress at the failure point and

2) the maximum strain needs to be less than the strain at the failure point.

In this study, the optimization is performed with simplified conditions of each layer of the composites on the both sides being of the same thickness, the orientation of the first (a) and third (c) layer being fixed, allowing the second (b) and fourth (d) layer to be oriented between 0 and 90 degrees, and the fiber volume fraction of the each layer being identical. Two additional layers to consider adhesive are located between the top and middle and the middle and bottom, respectively (Figure 34).

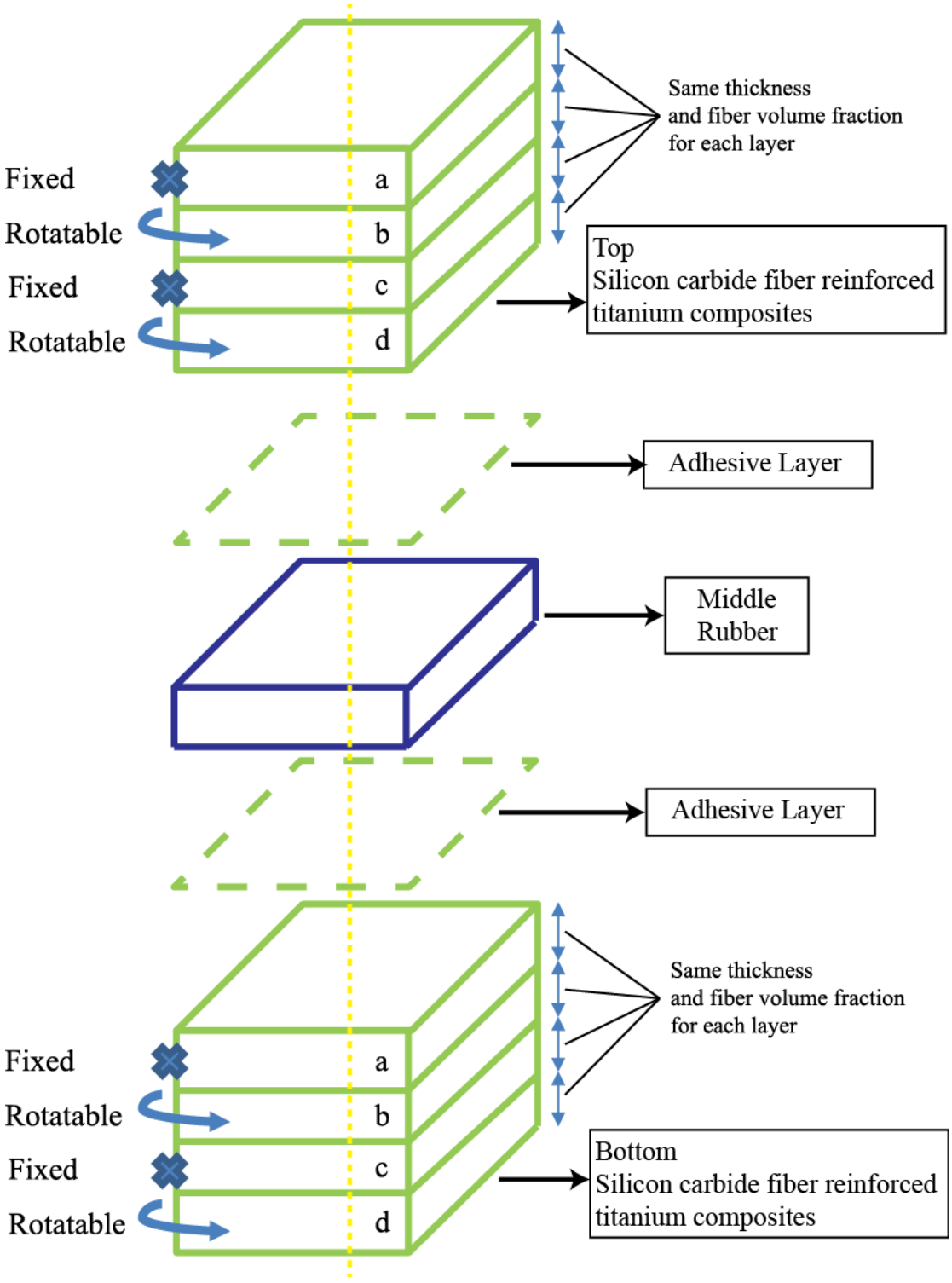

Figure 34: Design variables for sandwich panel design optimization.

The FMINCON function of MATLAB is used to find the minimum thickness of the composite panel as in the previous case study in section 4.2 and nine variables, which include thicknesses of the top, middle and bottom structure (x(1), x(8), x(9)) and material constants of the composites (x(2) to x(7)). The above two non-linear constraints are comprised by a MATLAB code that includes MSM-INFO and PYTHON codes to perform ABAQUS Explicit analysis.

To consider the energy dissipation of the middle rubber structure, a hyper-elastic material characteristic with the Mullins effect is employed. The transient stress-strain response of the rubber under cyclic loading was studied (Mullins, 1969), and ABAQUS solver offers a keyword '*MULLINS' that can be used with '*HYPERELASTIC' to model the energy functioned hyper-elastic material (Bose et al, 2003). The Ogden-Roxburgh model, which forms the basis of the Mullins model, was derived from an energy function in hyper-elasticity, even if that shows history dependence under certain conditions (Ogden and Roxburgh, 1999). The energy function of the model in terms of deformation gradient tensor $\boldsymbol{F}$ is

$$\boldsymbol{U}(\boldsymbol{F},\eta) = \eta\tilde{\boldsymbol{U}}(\boldsymbol{F}) + \phi(\eta) \tag{24}$$

, where U is the deviatoric part of the strain energy function of the material, and $\tilde{U}$ is the deviatoric strain energy function that occurs due to the stress-strain curve, resulting from monotonic loading of the material as non-linear elastic. A damage function, ϕ, quantifies the non-recoverable energy that corresponds to the area between the initial monotonic stress-strain curve and the particular stress-strain curve along which unloading

occurs. The particular damage function, η, includes material parameters. However, when η is active, the particular damage function is determined implicitly in terms of $\boldsymbol{F}$ by the preceding equation; conversely, when η is inactive, the function is assumed to have a value of unity without any loss of generality. The constitutive equation of the Mullins effect has a deviatoric $\boldsymbol{U}_{dev}$ and volumetric parts $\boldsymbol{U}_{vol}$ of the total strain energy,

$$\boldsymbol{U} = \boldsymbol{U}_{dev} + \boldsymbol{U}_{vol} \tag{25}$$

, and using an energy argument function as

$$\boldsymbol{U}(\bar{\lambda}_i, \eta) = \eta \tilde{\boldsymbol{U}}_{dev}(\bar{\lambda}_i) + \phi(\eta) + \tilde{\boldsymbol{U}}_{vol}(\boldsymbol{J}^{el}) \tag{26}$$

, where $\tilde{\boldsymbol{U}}_{dev}(\bar{\lambda}_i)$ is the deviatoric part of the strain energy density of the primary material response, and $\tilde{\boldsymbol{U}}_{vol}(\boldsymbol{J}^{el})$ is the volumetric part of the strain energy density. This energy function extends material compressibility of the Ogdan-Roxburgh model; a validation of the Mullins model is shown in Figure 35 (Paige and Mars, 2004).

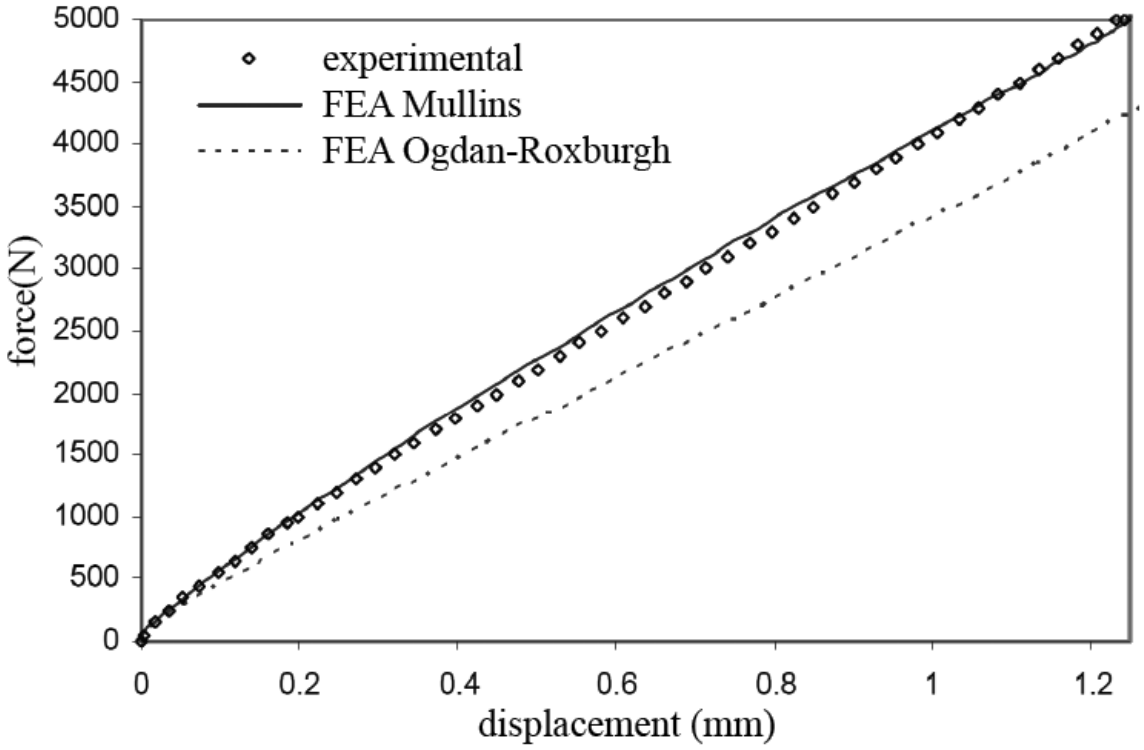

Figure 35: Comparison for Mullins effect (Paige and Mars, 2004).

To apply this energy based hyper-elastic material model within the computational framework, a set of uni-axial test data for filled rubber is found from Cooper Tire and Rubber Company to implement the keyword '*MULLINS' with '*HYPERELASTIC'. To verify that the model works properly within the computational framework, the comparison of the blast analysis results between the Mullins effect and the pure Ogdan-Roxburgh model is performed with an arbitrary design. The details of the design and comparisons are presented in Table 11. The thickness of the top composites, middle rubber, and bottom composites are given as 0.07m, 0.06m, and 0.03m, respectively; the fiber volume fraction of the composites is given as 0.4; and the layer orientation of the composites is given as 0-45-0-45 (degree).

Table 11: Comparison for Mullins effect using the blast analysis results

	Without Mullins effect	**With Mullins effect**
Design of the panel	Top composites thickness : 0.07 Middle rubber thickness : 0.06 Bottom composites thickness : 0.03 Fiber Volume Fraction of the composites : 0.4 Layer Orientation of the composites : 45 (degree) 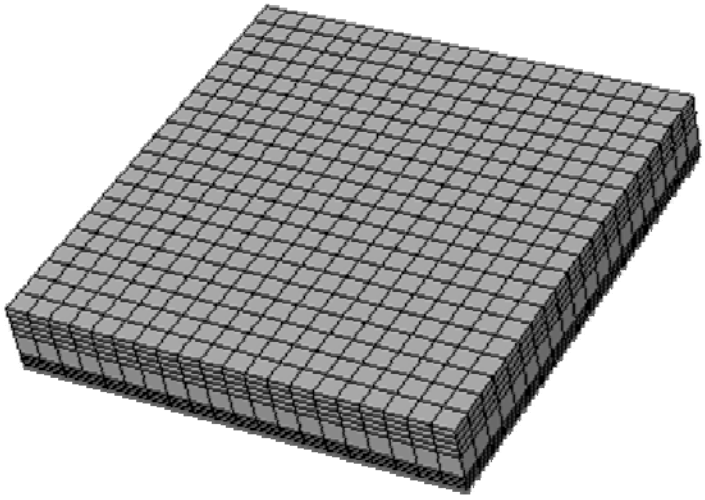	
Results (Bottom composites only)	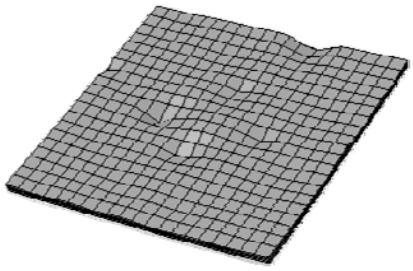	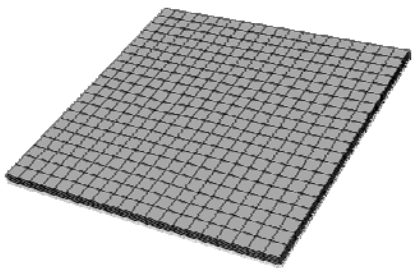
Maximum displacement (m) of the Bottom composites	0.006846	0.00599

Maximum displacement of the bottom composites is measured to compare the results, and the smaller displacement of the Mullins effect shows that the energy dissipation of the rubber is applied appropriately in the model.

Additional considerations when determining the sandwich structure are included in the framework. Cohesive elements (COH3D8) of the ABAQUS solver are used to interface adhesive layer. A traction-separation law with uncoupled behavior between the normal and the shear components defines the elastic response of the interface. The 'Traction Separation' option is selected with a negligibly thin adhesive layer assumption. A sandwich panel design optimization case study using the above-mentioned theories is performed with the computational framework. The FMINCON algorithm is sufficient for nine design variables in this case study, however more design variables would demand advanced inverse techniques, accompanied with expensive computational cost. Therefore, to execute the computational framework much more effectively, additional literature was reviewed on the optimization algorithm and the study of the reliable efficient optimization codes were undertaken sequentially. A more detailed discussion of the results is presented in the next section.

5.3: Results - sandwich structure

The overall micro-scale configuration of the sandwich panel design process is performed in two steps with several modules, as discussed in section 4.3. The first step, Optimization, includes the ABAQUS Explicit solver, BEST software for calculating blast pressure load, and MSM-INFO for providing material information at certain strain rates. The second step, IMEA, includes the inverse calculation. Additionally, two more design variables are used in this case study as in Figure 36. This study follows the same flow as

with the previous four-layer composites panel design case study, but with two additional design variables.

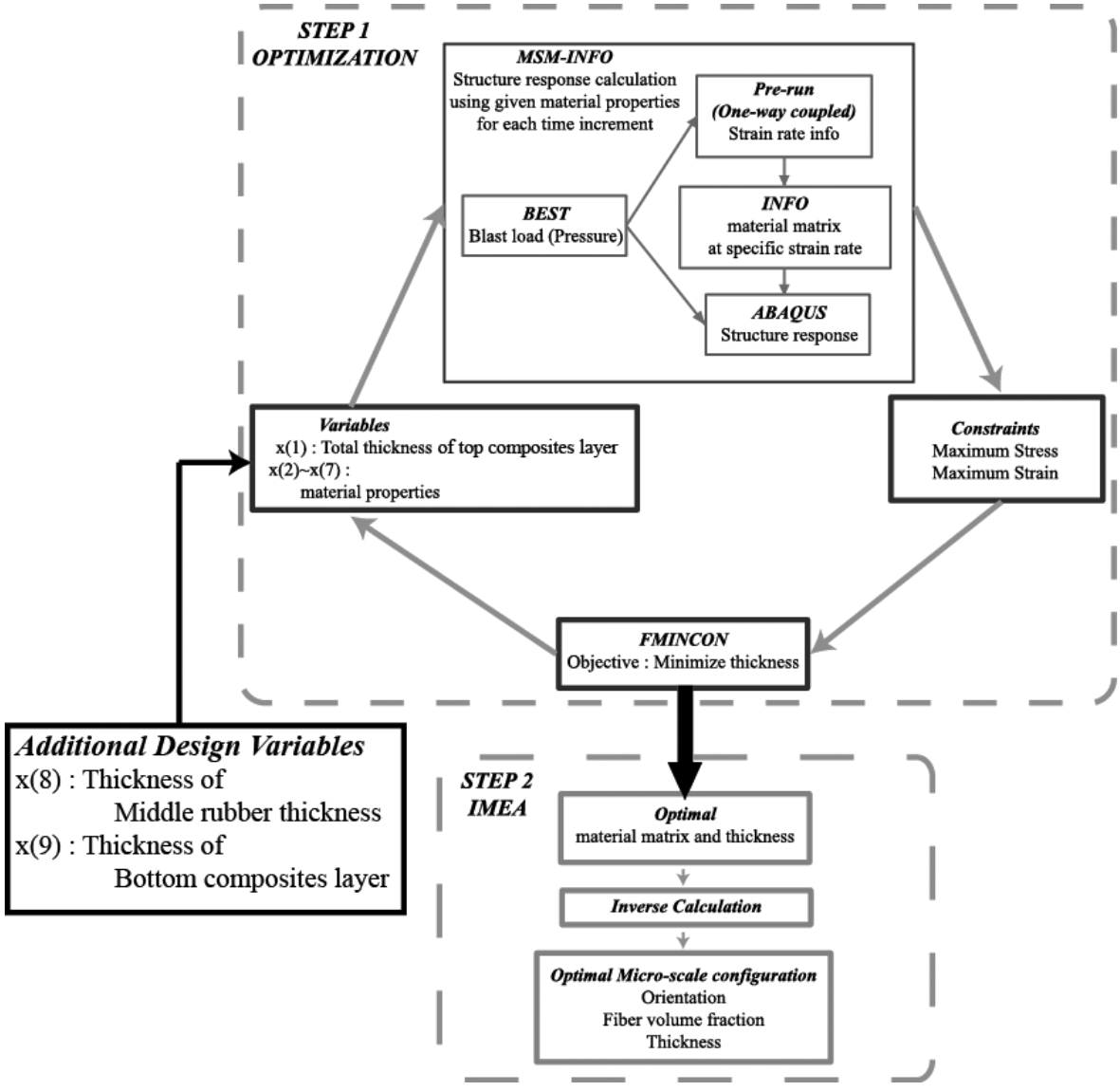

Figure 36: Optimal design process of sandwich panel.

The starting point of the optimization is set up from the results of a previously executed simple optimization frame using the one-way coupled capability (Kim et al, 2013)

for the composite part, and the middle point of the variance is used for the rubber part thickness. The optimal configuration of the composites structure is obtained as x(2) to x(7). Sequentially, a micro-level configuration of the sandwich panel is obtained by the IMEA inverse calculation. Table 12 shows this optimal thickness, fiber volume fraction, and the laminated orientation. To verify the results, maximum displacement measurements and failure checks are performed. Both of the optimization and IMEA results show the identical maximum displacement at the bottom layer, and both show no failure in the entire structure.

Table 12: Results comparing the optimization frame and the IMEA frame.

	Step 1: **Optimization**	Step 2: **IMEA**
Starting point	Initial values of x(1)~x(7) have: Thickness = 0.06m , Fiber Volume Fraction = 0.5 , Orientation = 45degrees x(8) = 0.06 x(9) = 0.06	---
Optimal Value	x(1) = 0.092 x(8) = 0.074 x(9) = 0.053 ---------- x(2) = 442700 x(3) = 360880 x(4) = 161380 x(5) = 67314 x(6) = 17448 x(7) = 14425	Optimal Thickness = 0.219 (m) Optimal Fiber Volume Fraction = 0.3992 Optimal Orientation = 0.7213 (41.32 degrees)
Maximum displacement (m) at bottom layer	0.005324	0.005401 (MSM-INFO)
Failure	None	None

The optimal micro-scale configuration design of the sandwich panel appears as a structure in Figure 37, and has dimensions of 1m width by 1m length by 0.219 (m) thickness (0.092m top composites, 0.074 rubber, 0.053 bottom composites), and each layer of the composite material has a 0.3992 fiber volume fraction and has 0-41.32-0-41.32 degree layer orientation.

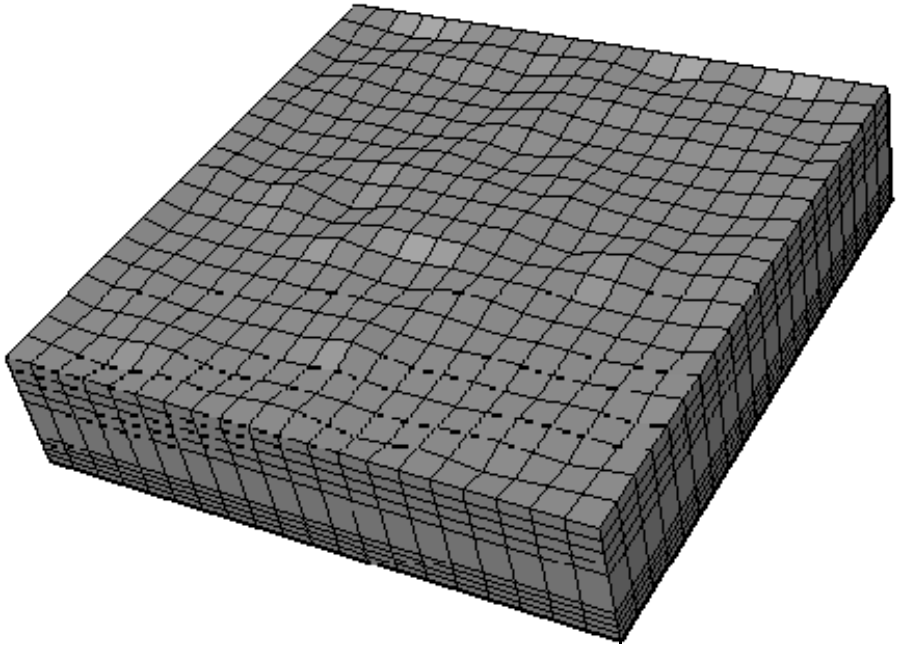

Figure 37: Results from the optimization frame.

This optimization result is compared with an early stage, fully-coupled MSM result to validate the result from evaluated MSM framework in Table 13. Two results, (0.005401, 0.005472), show a comparable result, since both results consider the strain rate effect during calculation. A good agreement with previously validated, fully-coupled MSM results demonstrates the properness of the overall micro-scale configuration design process for the sandwich panel as well as the four-layer composite panel in section 4.3.

Table 13: Comparison results using maximum displacement.

	Optimization result	**Fully-coupled MSM**
Maximum displacement (m) at bottom layer	0.005401	0.005472
Failure	None	None
Strain Rate Effect	Included	Included

Meanwhile, to verify the energy dissipation of the rubber in physics, two additional comparisons are performed. Rubber dissipates energy under cyclic loading through hysteresis caused by friction, stress softening, crystallization, and structural breakdown.

- A friction hysteresis phenomenon is also called internal viscosity where the rearranging molecules due to the load make the sliding of the chains relative to one another. This temperature dependent phenomenon reduces hysteresis when temperature has increased, since the increased mobility makes a reduced viscosity.
- A stress softening hysteresis, also called the Mullins effect (Mullins, 1969) is discussed in section 5.2, refers to a damping characteristics that changes under repeated loading conditions.
- A crystallization hysteresis refers to large extensions and retractions that lead to the crystallized formation regions in the rubber that frequently increases the strength.
- A structural breakdown hysteresis refers to the breakdown of the carbon particles to make the dissipation.

Among the typical hysteresis theories, the first two, friction and stress softening, are employed in this computational framework. Two different physical-based analyses are performed for a comparative analysis using the optimal configuration and blast load from

the previous optimization study. In the first analysis, the rubber material with the Mullins effect is replaced with pure elastic rubber, which refers to zero damping material. In the second analysis, the rubber material is removed and both top and bottom composite material are bonded using an adhesive layer.

The structure design of these physical-based analyses are presented in Table 14, including the previous optimal configuration sandwich panel design, the design with the removed damping from rubber material, and the design with the removed rubber structure. Both conditions were compared to the previous optimal configuration design of the sandwich structure using the maximum displacement of the bottom layer in Table 15.

Table 14: Structure design for comparison analysis.

	Design
Base line **(with dissipation)**	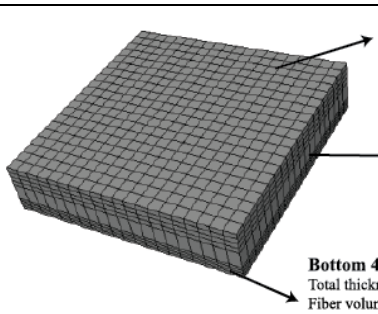 **Top 4-layer composites panel** Total thickness : 0.092 Fiber volume fraction : 0.3992 Layer orientation : 0-41.32-0-41.32 **Middle rubber panel with energy dissipation** Total thickness : 0.074 **Bottom 4-layer composites panel** Total thickness : 0.053 Fiber volume fraction : 0.3992 Layer orientation : 0-41.32-0-41.32
Compare 1 **(without damping)**	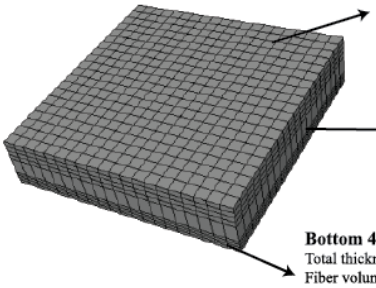 **Top 4-layer composites panel** Total thickness : 0.092 Fiber volume fraction : 0.3992 Layer orientation : 0-41.32-0-41.32 **Middle rubber panel without damping** Total thickness : 0.074 **Bottom 4-layer composites panel** Total thickness : 0.053 Fiber volume fraction : 0.3992 Layer orientation : 0-41.32-0-41.32
Compare 2 **(without rubber)**	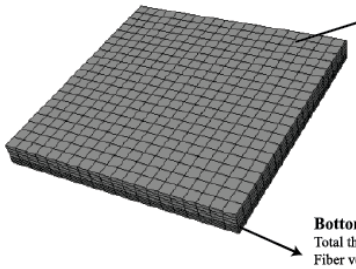 **Top 4-layer composites panel** Total thickness : 0.092 Fiber volume fraction : 0.3992 Layer orientation : 0-41.32-0-41.32 **Without middle rubber panel** **Bottom 4-layer composites panel** Total thickness : 0.053 Fiber volume fraction : 0.3992 Layer orientation : 0-41.32-0-41.32

Table 15: Comparison analysis results for energy dissipation theory.

Base line **(with dissipation)**	Maximum displacement at bottom layer 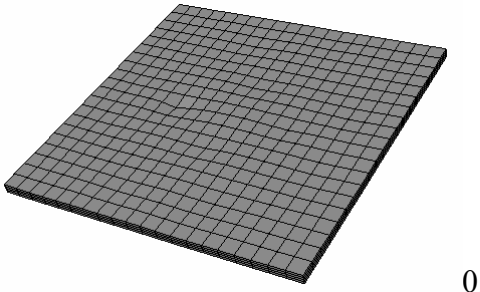 0.005324 (m)
Compare 1 **(without damping)**	Maximum displacement at bottom layer 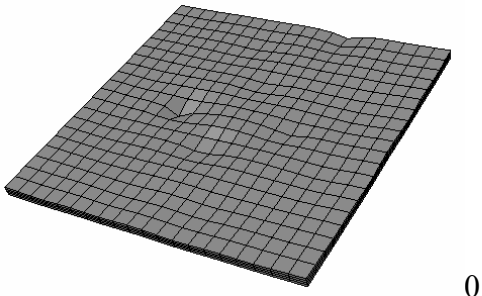 0.006361 (m)
Compare 2 **(without rubber)**	Maximum displacement at bottom layer 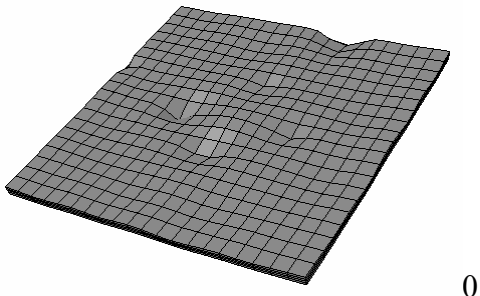 0.007712 (m)

The maximum displacements of the base line, which comprises energy dissipation theory using Mullins effect shows the smallest results, and this comparison analysis presents that our computational framework also possesses the valid physics background of energy dissipation. The optimal design results of the four-layer composites panel and sandwich panel are discussed in detail with comparison in the next section.

5.4: Comparison between four-layer composite panel and sandwich panel results

The optimal design result of the four-layer composites panel from section 4.3 is compared to the optimal sandwich panel design from section 5.3 in this section. Both optimal designs originate from the same global-scale design objective, which is to find the minimum thickness of the panel and the same constraints, which are 1) the maximum stress needs to be less than the stress at the failure point and 2) the maximum strain needs to be less than the strain at the failure point.

The optimal design of both panels (Figures 38 and 39) indicates that the maximum displacement is at the bottom layer. Table 16 compares the optimal design, weight, maximum displacement at the bottom layer, and the failure status in the overall structure in both structures.

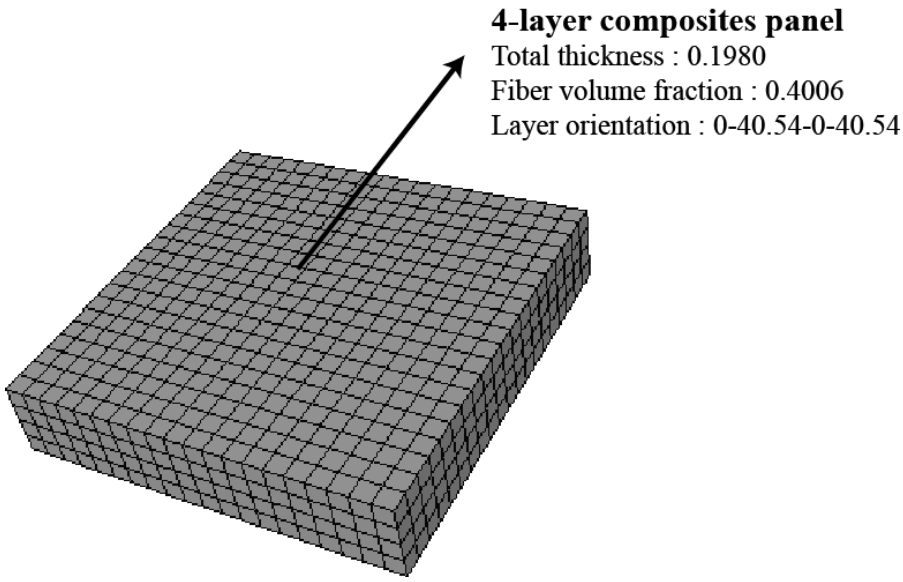

Figure 38: Optimal design of the four-layer composites panel.

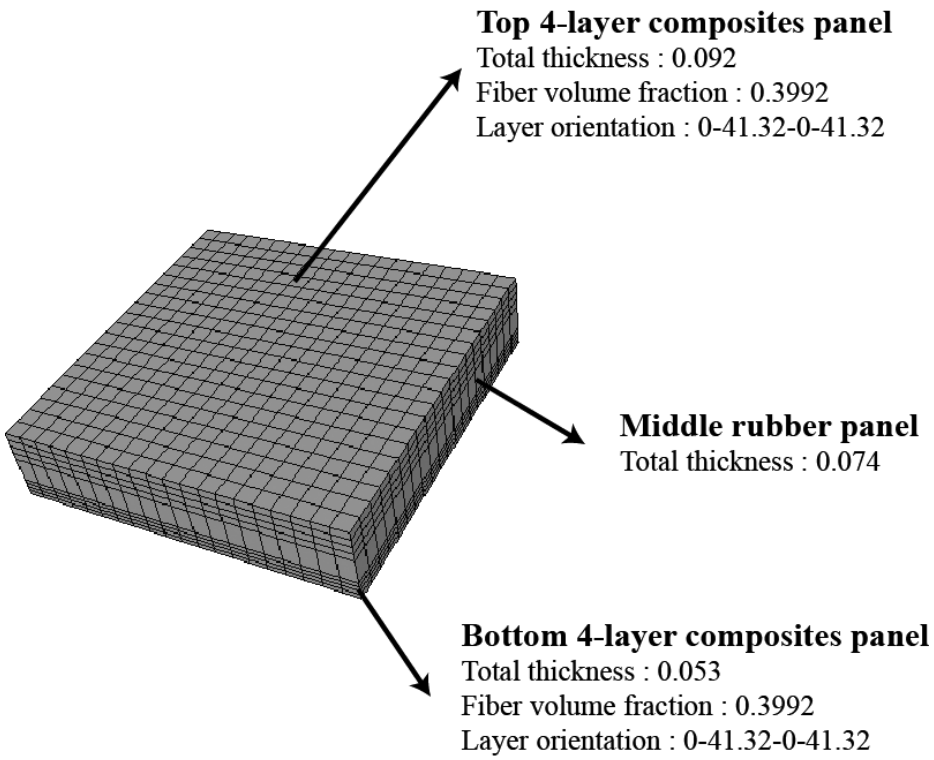

Figure 39: Optimal design of the sandwich panel.

Table 16: Comparison between two optimal panel designs.

	Four-layer composites panel	**Sandwich panel**
Optimal design	**Total Thickness : 0.1980 (m)** Fiber Volume Fraction of the composites : 0.4006 Layer Orientation of the composites : 0.7077 (40.54 in degree)	**Total Thickness : 0.219 (m)** Fiber Volume Fraction of the composites : 0.3992 Layer Orientation of the composites : 0.7213 (41.32 in degree)
Total weight	**763.872 (kg)**	**640.802 (kg)**
Maximum displacement	0.00586 (m)	0.005401(m)
Failure	None	None

In contrast to expectations, the total thickness of the optimal sandwich panel was observed as larger than the total thickness of the four-layer composites panel. An additional

middle rubber panel should have enlarged the energy dissipation more than the four-layer silicon carbide fiber-reinforced titanium composites panel. However, as observed in the maximum displacement comparison, the rubber panel dissipated less energy than expected. From these results, the optimal design of the sandwich panel does not function properly.

However, the overall objective of this work is (1) to develop a computational framework that determines the configuration of the panel to achieve the desired blast resistance characteristics at minimum thickness and (2) to extend the framework's capabilities from the sole composites material structure to the heterogeneous material structure. Furthermore, if the design objective is changed from determining the thickness minimization to the weight minimization, then the optimal design of the sandwich structure is improved, as verified in the total weight comparison in Table 16. Various possibilities of this computational framework are summarized in the next Chapter.

CHAPTER 6:
CONCLUSIONS AND RECOMMENDATIONS

The preceding pages contain an exploration of how the computational framework changes the process of designing the blast resistance panel to satisfy mutually competing objectives, weight reduction, and a high level of survivability. Specific conclusions from this exploration and a set of recommendations for future work are presented in this last chapter.

6.1: Conclusions

In this research, the creation of a fully-coupled Multi-Scale Method (MSM) through coupling between the MAC code and the ABAQUS Explicit solver module is presented. With the ability to conduct blast event simulations, MSM for composites is integrated in these simulations for including constitutive material properties of composites in the analysis and propagating information from the micro cell level to the global structural level. Additional developments for high strain rate analyses have been performed using a new micro-scale material model as well. For the micro-level configuration design of the composite, an Inverse Material Engineering Algorithm (IMEA) approach with reduced computational cost is presented. The iteration process between the MAC code and the ABAQUS Explicit module is substituted by the MSM-INFO module, which uses the strain rate information. The possibility and reality of the approach is demonstrated by the manual

inverse calculation validation study, and the algorithm is developed accordingly. The computational framework, which includes the optimization frame and the IMEA frame, is developed, and the results of the framework are presented. The optimal micro-scale configuration design of the composite panel is calculated, which satisfies the lightness and blast resistance requirements simultaneously. An additional optimal design study of the sandwich panel using the same design objective and constraints is presented, and the results are compared to the previous composite panel design.

The newly developed computational framework is highly valuable for designing composite material structures and satisfying two ever-present conflicting objectives: lighter weight and strength in performance. Further, modification of the IMEA extends the variety of the design variable using mathematically defined boundary conditions, advanced hybrid numerical-experimental inverse techniques, and uncertainty inverse methods, as discussed in Chapter 3. A simple modification in the optimization algorithm and the optimization sequence allows this frame to have more computational efficiency, as discussed in Chapter 4. Moreover, this framework has outstanding applicability to structures that consist of heterogeneous materials, as discussed in Chapter 5.

One important conclusion of this research is that this new computational framework enables multi-scale modeling of the composites over large strain rate loading conditions. Not only are the blast event simulations considered, but also various load conditions can be applied to the design of micro-scale configurations of the composites. Design parameters other than those used in this research, such as different kinds of raw material for the fiber and the matrix, variables for particle-reinforced composites, and different structures of the

panel, can also be included into the computational framework without difficulty for the design of the composites with computational efficiency. This novel optimization computational framework not only capacitates multi-scale modeling of the composites panel, but also accommodates multi-scale design optimization of many different structures. Optimal micro-scale design variables that satisfy global-scale design objectives and constraints can be calculated together without computational cost problems.

6.2: Recommendations for Future Work

The results showed the feasibility of the proposed multi-scale modeling process for optimally designing blast resistant composite panels for lightweight vehicles using a computational framework. In the future, to extend the capabilities of the computational framework and to bring this process to the full implementation, the following research tasks are recommended:

Task 1: Improvement on the IMEA considering increased design variables of the complicated material model.

Based on the results in Chapter 3, all design variables from the four-layer composite panels are limited to identical layer thickness, partially fixed layer orientation, and specific fiber-reinforced composite structures. Therefore, more theories for composite materials discussed in section 3.2 should be included to extend the capabilities of the overall design process. The advanced hybrid numerical-experimental inverse technique and uncertainty inverse methods would extend the capability. Since the increase of the design variables will

require an improved boundary condition in the inverse calculation, a more mathematically extended inverse mapping algorithm should be included to facilitate the multi-scale design optimization.

Task 2: Improvement on the design optimization process for greater efficiency.

With the current optimization framework using a fundamental optimization code 'FMINCON', the computational efficiency of the computational framework has to be limited under certain conditions. Increased micro-scale design variables, complicated boundary conditions, and advanced inverse techniques make the computational framework more expensive. Accordingly, the performance aspect of the optimization algorithm should also be considered. To accomplish this aspect, use verified and reliable efficient optimization codes to obtain an optimal design result with reduced computational cost using an iterative algorithm, a random gradient approximation, or a heuristic algorithm.

Task 3: Performance test of the computational framework using various structures of the blast resistant panel.

Finally, without the performance test of the panel design process using the computational framework, all of the claims in terms of the superiority of the proposed computational framework would still be questionable when compared to other types of panels or the same type of panel as designed by other processes. Thus, the performance test is critically significant for the potential use of this proposed multi-scale optimal design process.

REFERENCES

1. Aboudi J., "Mechanics of Composite Materials", Unified Micromechanical Approach, Elsevier, Amsterdam, 1991.

2. Aboudi J., "Micromechanical analysis of composites by the method of cells", Appl. Mech. Rev. 42, 193-221, 1989.

3. Aboudi J., "Micromechanical analysis of fully coupled electro-magneto-thermo-elastic multiphase composites", Smart Materials and Structures, Vol. 10, 867-877, 2001

4. Aboudi J., "Micromechanical Analysis of Thermo-inelastic multiphase short-fiber composites", Composite Engineering, Vol. 5, No.7, Elsevier, 839-850, 1995.

5. Aboudi J., Pindera M. J., "Micro mechanics of metal matrix composites using the generalized method of cells model (GMC)", Mechanics of Materials 14, Elsevier, 127-139, 1992.

6. Aboudi J., Pindera M. J., Arnold S. M., "Higher-order theory for periodic multiphase materials with inelastic phases", International Journal of Plasticity 19, 805–847, 2003.

7. Aboudi J., Pindera M. J., Arnold S. M., "High-Fidelity Generalization Method of Cells for Inelastic Periodic Multiphase Materials", NASA/TM 211469, 2002.

8. Aboudi J., Pindera M. J., Arnold S. M., "Linear Thermoelastic higher-order theory for periodic multiphase materials", Journal of applied mechanics, Vol. 68, 2001.

9. Aghdam M. M., Pavier M. J., Smith D. J., "Micro-mechanics of off-axis loading of metal-matrix composites using finite element analysis", International journal of solids and structures 38, 3905-3925, 2001.

10. Armstrong R. W., Walley S. M., "High strain rate properties of metals and alloys", International Material Reviews, Vol.53, No.3, 105-128, 2008.

11. Arnold S. M., "Differential continuum damage mechanics models for creep and fatigue of unidirectional metal matrix composites", NASA technical memorandum 105213, 1991.

12. Arnold S. M., Pindera M. J., Wilt T. E., "Influence of fiber architecture on the inelastic response of metal matrix composites", International journal of plasticity, Vol.12, No.4, 507-545, 1996.

13. Arnold S. M., Pindera M. J., Wilt T. E., "Influence of fiber architecture on the inelastic response of metal matrix composites", international journal of plasticity, Vol. 12, 507-545, 1996.

14. Assaad M., Arnold S. M., "An Analysis of the Macroscopic Tensile Behavior of a Nonlinear Nylon Reinforced Elastomeric Composite System Using MAC/GMC", NASA/TM 209066, 1999.

15. Auricchio F., Taylor R. L., "A generalized visco-plasticity model and its algorithmic implementation", computers and structures, Vol. 53, 1994.

16. Baik K. H., " Tensile Failure Behavior of SiC/Ti-6Al-4V Composites Manufactured by Plasma Spraying Route", Materials Transactions, Vol. 47, No. 11, 2815 to 2820, 2006.

17. Bansal, N. P., "Handbook of Ceramic Composites", NASA Glenn Research Center, Kluwer Academic Publishers, 2005.

18. Bednarcyk B. A., "An inelastic micro/macro theory for hybrid smart/metal composites", Composites: Part B 34, 175–197, 2000.

19. Bednarcyk B. A., "Discussion of woven fabric composite material model with material non-linearity for non-linear finite element simulation by tabiei and jiang", international journal of solids and structures 38, 2001.

20. Bednarcyk B. A., "Modeling Woven Polymer Matrix Composites With MAC/GMC", National Aeronautics and Space Administration, Glenn Research Center, 2000.

21. Bednarcyk B. A., Arnold M. J., "A New Local Failure Model With Application to the Longitudinal Tensile Behavior of Continuously Reinforced Titanium Composites", NASA/TM 210027, 2000.

22. Bednarcyk B. A., Arnold M. J., Aboudi J., Pindera M. J., "Local field effects in titanium matrix composites subject to fiber-matrix debonding ", International Journal of Plasticity 20, 1707–1737, 2004.

23. Bednarcyk B. A., Arnold S. M., "A New Local Debonding Model With Application to the Transverse Tensile and Creep Behavior of Continuously Reinforced Titanium Composites", NASA/TM 210029, 2000.

24. Bednarcyk B. A., Arnold S. M., "Micromechanics-based deformation and failure prediction

25. Bednarcyk B. A., Arnold S. M., Lerch B. A., "Fully Coupled Micro/Macro Deformation, Damage, and Failure Prediction for SiC/Ti-15-3 Laminates", NASA/TM 211343, 2001.

26. Bednarcyk B. A., Hopkins D. A. "A Fully Coupled Micro/Macro Theory for Thermo-Electro-Magneto-Elasto-Plastic Composite Laminates", National Aeronautics and Space Administration, Glenn Research Center, 2000.

27. Bednarcyk B. A., Pindera M. J., "An efficient implementation of the generalized method of cells for unidirectional, multi-phased composites with complex microstructures", Composites, Part B 30, Elsevier, 87-105, 1999..

28. Bednarcyk B. A., Pindera M. J., "Inelastic Response of a Woven Carbon/Copper Composite Part 2: Micromechanics Model", Journal of Composite Materials 34(4), 299-331, 2000.

29. Bednarcyk B. A., Steven M., "FEAMAC Beta documentation", NASA/TM

30. Bednarcyk B. A., Steven M., "MAC/GMC 4.0 Keywords Manual", NASA/TM – 2002-212077/Vol2, 2002.

31. Bednarcyk B. A., Steven M., "Transverse tensile and creep modeling of continuously reinforced titanium composites with local debonding", International Journal of Solids and Structures 39, 1987–2017, 2002.

32. Bednarcyk B. A., Steven M., Aboudi J., Pindera M. J., "ACCURATE MICRO/MACRO FIELD SIMULATION FOR COMPOSITES SUBJECT TO FIBER-MATRIX DEBONDING USING HFGM", 15th ASCE Engineering Mechanics Conference June 2-5, 2002.

33. Bednarcyk B. A., Steven M., Aboudi J., Pindera M. J., "Local field effects in titanium matrix composites subject to fiber-matrix debonding", International Journal of Plasticity 20, 1707–1737, 2004.

34. Bell R. L., Hertel Jr. E. S., "A domain decomposition scheme for Eulerian shock physics codes", CED-Vol. 6, High Performance Computing in Computational Dynamics, ASME International Congress and Exposition, 67-72, 1994.

35. Bergeron D., Walker R., and Coffey C., "Detonation of 100-gram anti-personnel mine surrogate charges in sand: A test case for computer code validation", Defense Research Establishment Suffield, SR668, National Defense, Canada, October 1998.

36. Binienda W. K., "High energy impact of composite structures-Ballistic experiments and explicit finite-element analysis", Rep., submitted to NASA Glenn Research Center, The Univ. of Akron, Akron, Ohio, 2004.

37. Bird R., "Protection of vehicles against landmines", Journal of Battlefield Technology, Vol. 4, No. 1, March 2001.

38. Bonorchis D., Nurick G. N., "The analysis and simulation of welded stiffener plates subjected to localized blast loading", International Journal of Impact Engineering 37, 260–273, 2010.

39. Bose K., Hurtado J.A., Snyman M. F., Mars W. V., Chen J. Q., "Modelling of stress softening in filled elastomers", Constitutive Models for Rubber III, pp. 223-230, Busfield and Muhr (eds), Swets & Zeitlinger, Lisse, 2003.

40. Caner F. C., Bazant Z. P., "Size effect on strength of laminate-foam sandwich plates: Finite element analysis with interface fracture", Composites: Part B 40, 337–348, 2009.

41. Chan Y., Correa C. D., "Flow-based Scatter plots for Sensitivity Analysis", Visual Analytics Science and Technology VAST 2010 IEEE Symposium, 2010.

42. Chang F., Chang K., "A progressive damage model for laminated composites containing stress concentrations", J Compos Mater 21, 834–855, 1987.

43. Cheng J., and Binienda W. K., "Simulation of soft projectiles impacting composite targets using an arbitrary Lagrangian-Eulerian Formulation", J. Aircr., 43(6), 1726–1731, 2006.

44. Cugnoni J., Grmur T., Schorderet A., "Inverse method based on modal analysis for characterizing the constitutive properties of thick composite plates", Computers and Structures 85, 1310–1320, 2007.

45. Daniel I. M., "Failure of composite materials", Fracture of nano and engineering materials and structures, 16th European Conference of Fracture, Alexandroupolis, Greece, 2006.

46. Dassault Systems, "ABAQUS User's Manual", Version 6.8, 2008.

47. Doghri I., Adam L., Bilger N., "Mean-field homogenization of elasto-viscoplastic composites based on a general incrementally affine linearization method", International Journal of Plasticity 26, 219–238, 2010.

48. El Wahed A. K., Sproston J. L., Schleyer G. K., "Electrorheological and magnetorheological fluids in blast resistant design applications", Mater. Des., 23(4), 391–404, 2002.

49. Fatt M. S., Sirivolu D., "A wave propagation model for the high velocity impact response of a composite sandwich panel", International Journal of Impact Engineering 37, 117–130, 2010.

50. Fischer H., "United States Military Casualty Statistics: Operation Iraqi Freedom and Operation Enduring Freedom", Congressional Research Service Report number: RS22452, March 25, 2009.

51. Flood I., Bewick B. T., Dinan R. J., Salim H. A., "Modeling blast wave propagation using artificial neural network methods", Advanced Engineering Informatics 23, 418–423, 2009.

52. for longitudinally reinforced titanium composites", Composites Science and Technology 61 705–729, 2001.

53. Gaedner J. P., "micromechanical modeling of composite materials in finite element analysis using an embeddded cell approach", Massachusetts Institute of Technology, 1994.

54. Galarneau M. R., Woodruff S. I., Dye J. L., Mohrle C. R., Wade A. L., "Traumatic brain injury during Operation Iraqi Freedom: findings from the United States Navy-marine Corps Combat Trauma Registry", Naval Research Health Center Report 06-25, 2006.

55. Gan Y. X., "Energy Dissipation Criteria for Surface Contact Damage Evaluation", Continuum Mechanics – Progress in Fundamentals and Engineering Applications, 2012.

56. Ghosh S., "Adaptive concurrent multi-level model for multiscale analysis of composite materials including damage", Multiscale modeling and simulation of composite materials and structures, Springer, 83-164, 2008.

57. Goldberg R. K., Arnold S. M., "A Study of Influencing Factors on the Tensile Response of a Titanium Matrix Composite With Weak Interfacial Bonding", NASA/TM 209798, 2000.

58. Goldberg R. K., Roberts G. D., Gilat A., "Implementation of an associative flow rule including hydrostatic stress effects into the high strain rate deformation analysis of polymer matrix composites", J. Aerosp. Eng., 18(1), 18–27, 2005.

59. González C., LLorca J., "Micromechanical modeling of deformation and failure in Ti-6Al-4V/SiC", composites, Acta Materialia 49, 3505-3519, 2001.

60. Gonzalez C., LLorca J., Week A., "Toughness of fiber-reinforced titanium as a function of temperature: experimental results and micromechanical modeling", Acta Materialia 52, 3929–3939, 2004.

61. Gundel D. B., Wawner F. E., "Experimental and theoretical assessment of the longitudinal tensile strength of unidirectional SiC-Fiber/Titanium-matrix composites", Composites Science and Technology 57, 471-481, 1997.

62. Gunnink J. W., "Laminate stiffnesses and Classical Laminate Theory", Delft University of Technology, Department of Aerospace Engineering, Report LR-477, 1985.

63. Gupta A. D., "Dynamic Elasto-plastic response of a generic vehicle floor model to coupled transient loads", PVP-Vol. 351, Structures under Extreme Loading Conditions, ASME, pp. 81-86, 1997.

64. Gupta A. D., "Estimation of vehicle floor plate loading and response due to detonation of a mine shallow-buried in dry sand and wet turf", US Army Ground Vehicle Survivability Symposium, Monterey, CA, Mar. 29 – April 1, 1999.

65. Gupta A. D., "Modeling and analysis of a blast deflector for a tactical vehicle due to detonation of a mine buried in dry vs. saturated sand", US Army Ground Vehicle Survivability Symposium, 2002.

66. Gupta A.D., Gregory F.H., Bitting R.L., and Bhattacharya S., "Dynamic analysis of an explosively loaded hinged rectangular plate", Computers & Structures, Vol. 26, pp. 339-344, 1987.

67. Gupta A.D., Wisniewski H.L., and Bitting R.L., "Response of a generic vehicle floor model to triangular overpressure loads", Computers & Structures, Vol. 32, No. 3/4, pp. 527-536, 1989.

68. Hale D. K., Kelly A., "Strength of fibrous composite materials", Annual Review of Materials Science Vol. 2: 405-462, 1972.

69. Hassen G., Buhan P. D., Abdelkrim M., "Finite element implementation of a homogenized constitutive law for stone column-reinforced foundation soils, with application to the design of structures", Computers and Geotechnics 37, 40–49, 2010.

70. Helton J. C., "Sampling-Based Methods for Uncertainty and Sensitivity Analysis", Sensitivity Analysis of Model Output, Los Alamos National Laboratory, 2005

71. Hopkinson J., "Original papers", Cambridge University Press, Cambridge, 316–324, 1901.

72. Hwang S. F., Yeh C. K., He R. S., "Characterization of composite materials using an inverse technique", key engineering materials, 1299-1302, 2007.

73. Ilic S., Hackl K., Gillbert R., "Application of the multiscale FEM to the modeling of cancellous bone", Biomech Model Mechanobiol, 9:87–102, 2010.

74. Iyer S. K., Lissenden C. J., Arnold S. M., "Local and overall flow in composites predicted by micromechanics", Composites: Part B 31, 327–343, 2000.

75. Jiang C., Liu G. R., Han X., "A Novel Method for Uncertainty Inverse Problems and Application to Material Characterization of Composites", Experimental Mechanics, 48:539–548, 2007.

76. Jiming Z., Lehua Q., Guoding C., "New inverse methods for identification of constitutice parameters", Trans. nonferrous met. soc. china, 148-152, 2006.

77. Joachin C. E., McMahon G. W., Lunderman C. V., Garner S. B., "Airblast Effects Research: Small-Scale Experiments and Calculations", Technical Report SL-99-5, US Army Corps of Engineers, August 1999.

78. Jones R. M., "Mechanics of Composite Materials, 2nd Ed", Taylor and Francis, Inc., Philadelphia.

79. Karagiozova D., Langdon G. S., Nurick G. N., Chung Kim Yuen S., "Simulation of the response of fibre–metal laminates to localised blast loading", International Journal of Impact Engineering 37, 766–782, 2010.

80. Kim J., Vlahopoulos N., Zhang G., "Development of a blast event simulation process for multi-scale modelling of composite armor for light weight vehicles", International Journal of Vehicle Design, Special issue on 'Modelling and Simulation of Ground Vehicle System.', Vol. 61, 157-176, 2013.

81. Kingery C., and Bulmarsh G., "Airblast parameters from TNT spherical air burst and hemispherical surface burst", ARBRL-TR-02555, US Army Ballistic Research Laboratory, Aberdeen Proving Grounds, MD, 1984.

82. Kroupa J. L., Bartsch M., "Influence of viscoplasticity on the residual stress and strength of a titanium matrix composite after thermomechanical fatigue", Composites Part B 29B, 633–642, 1998.

83. Kwon Y. W., "Analysis of Laminated and Sandwich Composite Structures Using Solid-like Shell Elements", Appl Compos Mater, Springer, June 2012.

84. Kwon Y. W., "Multiscale and multilevel modeling of composites", Multi-scale modeling and simulation of composite materials and structures, Springer, 83-164, 2008.

85. Laine, L., and Sandvik, A. "Derivation of mechanical properties for sand", 4th Asia-Pacific Conference on Shock and Impact Loads on Structures, Singapore, 361-368, November 2001.

86. Langhorst B., Cook C., Schondel J., Chu H. S., Material systems for blast-energy dissipation", INL/CON-10-19383, 2010.

87. Leszczynski J., Shukla M., "Practical aspects of computational chemistry", Springer, 2009.

88. Li D. S., Wisnom M. R., "Factors controlling the transverse tensile properties of unidirectional SiC/Ti-6Al-4V", Composite Engineering, Vol. 5, No.3, 235-255, 1995.

89. Lissenden C. J., Arnold S. M., Iyer S. K., "Flow/Damage surfaces for fiber-reinforced metals having different periodic microstructures", NASA technical memorandum 208805, 1998.

90. Lissenden C. J., Lerch B. A., Ellis J. R., Robinson D. N., "Verification of experimental techniques for flow surface determination", NASA technical memorandum 107053, 1996.

91. Liu G. R., Ma W. B., Han X., "An inverse procedure for determination of material constants of composite laminates using elastic waves", Comput. Methods Appl. Mech. Engrg. 191, 3543–3554, 2002.

92. Liu X., Gu J, Shen Y., Li J., Chen C., "Lattice dynamical finite-element method", Acta Materialia 58, 510–523, 2010.

93. Lopez-Puente J., Arias A., Zaera R., Navarro C., "The effect of the thickness of the adhesive layer on the ballistic limit of ceramic/metal armours. An experimental and numericalstudy", Int. J. Impact Eng., 32, 321–336, 2005.

94. Macek R. W., Aubert B. H., "A mass penalty technique to control the critical time increment in explicit dynamic finite element analyses", Earthquake Engineering and Structural Dynamics, Vol. 24, 1315-1331, 1995.

95. Matsuoka S., "Relaxation Phenomena in Polymers", Hanser, Munich, 1992.

96. McGlaun J. M., Thompson S. L., Elrick M. G., "CTH: a three-dimensional shock wave physics code", Int. J. Impact Engng., Vol. 10, pp. 351-360, 1990.

97. Meyers M. A., "Dynamic behavior of materials", Wiley, New York, 1994.

98. Miyoshi T., et al., "Enhancement of energy absorption in closed-cell aluminum by the modification of cellular structures", J. Phys.: Condens. Matter, 41(10), 1055–1060, 1999.

99. Mullins L., "Rubber Chem. Technol.", 42, 339, 1969.

100. Nesterenko V. F., "Dynamics of heterogeneous materials", Springer, New York, 2001.

101. Nestorovic M. D., Triantafyllidis N., "Onset of failure in finitely strained layered composites subjected to combined normal and shear loading", Journal of the Mechanics and Physics of Solids 52, 941 – 974, 2004.

102. Ochoa O. O., Reddy J. N., "Finite element analysis of composite laminates", Kluwer Academic Publishers, Netherlands, 1992.

103. Ogden R. W., Roxburgh D. G., "A Pseudo-Elastic Model for the Mullins Effect in Filled Rubber", Proceedings of the Royal Society of London, Series A, vol. 455, pp. 2861–2877, 1999.

104. Pahr D. H., Arnold S. M., "The applicability of the generalized method of cells for analyzing discontinuously reinforced composites", Composites, Part B 33, 153-170, 2002.

105. Pahr D. H., Arnold S. M., "The Applicability of the Generalized Method of Cells for Analyzing Discontinuously Reinforced Composites", NASA/TM 211165, 2001.

106. Paige R. E., Mars W. V., "Implications of the Mullins Effect on the Stiffness of a Pre-loaded Rubber Component", ABAQUS Users' Conference, 2004.

107. Paley M., Aboudi J., "Micromechanical Analysis of Composites by the Generalized Cells Model", Mech Mater 14, 127-139, 1992.

108. Peters, S. T., "Handbook of Composites", Chapman & Hall, 2nd ed, 1998.

109. Pindera M. J., Bednarcyk B. A., "An efficient implementation of the generalized method of cells for unidirectional, multi-phased composites with complex microstructures", Composites Part B, 20, 87-105, 1999.

110. Qiao P., Yang M., Bobaru F., "Impact Mechanics and High-Energy Absorbing Materials", Journal of Aerospace Engineering 21:4, 235–248, 2008.

111. Qing H., Mishnaevsky L., "Unidirectional high fiber content composites: Automatic 3D FE model generation and damage simulation", Computational Materials Science 47, 548–555, 2009.

112. Ramault C., Makris A., Sol H., Hemelrjick D. V., Lecompte D., Lamkanfi E., Paepegem W. V., "Development of an Inverse Method for Material Characterization using a Biaxially Loaded Cruciform Composite Specimen", Proceedings of the SEM Annual Conferencem, June 1-4, 2009.

113. Saleeb A. F., Arnold S. M., Castelli M. G., Wilt T. E., Graf W., "A general hereditary multimechanism-based deformation model with application to the viscoelastoplastic response of titanium alloys", International Journal of Plasticity 17, 1305-1350, 2001.

114. Saltelli A., Ratto M., Andres T., Campolongo F., Cariboni J., Gatelli D., Saisana M., Tarantola S., "Global Sensitivity Analysis", Wiley, 2008.

115. Sands C. M., Chandler H. W., Guz I. A., Zhuk Y.A., "Extending the Bodner-Partom model to simulate the response of materials with extreme kinematic hardening", Arch Appl Mech, Vol. 80, 161-173, 2010.

116. Sarva S., Nemat-Nasser S., McGee J., Isaacs J.,"The effect of thin membrane restraint on the ballistic performance of armor grade ceramic tiles", Int. J. Impact Eng., 34(2), 277–302, 2007.

117. Schnur D. S., Zabaras N., "An inverse method for determining elastic material properties and a material interface", international journal for numerical methods in engineering, Vol. 33, 1992.

118. Soutis C., Mohamed G., Hodzic A., "Modelling the structural response of GLARE panels to blast load", Composite Structures 94, 267–276, 2011.

119. Steven M., Bednarcyk B. A., Hussain A., Katiyar V., "Micromechanics-Based Structural Analysis (FEAMAC) and Multi-scale Visualization Within Abaqus/CAE Environment", NASA/TM, 2010-216336.

120. Sun J. S., Lee K. H., Lee H. P., "Comparison of implicit and explicit finite element methods for dynamic problems", Journal of Materials Processing Technology 105, 110-118, 2000.

121. Sun J., Vlahopoulos N., Stabryla T. J., Goetz R., Van De Velde R., "Blast event simulation for a structure subjected to a landmine explosion", 2006 SAE Congress, SAE Paper 2006-01-0931.

122. Suquet P., "Local and global aspects in the mathematical theory of plasticity", Plasticity Today, Modelling, Methods and Applications, 279-310, 1985.

123. Thomas Y. H., Xiao H. W., "A multiscale finite element method for elliptic problems in composite materials and porous media", JOURNAL OF COMPUTATIONAL PHYSICS 134, 169–189, 1997.

124. Tsai S. W., Wu E. M., "A general theory of strength for anisotropic materials", Journal of composite material, Vol. 5, 58-80, 1971.

125. Vedensky D. D., "Multiscale modelling of nanostructures", journal of physics, Vol. 16, 2004.

126. Vlahopoulos N. Zhang G., "Validation of a simulation process for assessing the response of a vehicle and its occupants to an explosive threat", 27th Army Science Conference, Transformational Science and Technology, 2010.

127. Wang S., Zhang M., Quek S. T., "Effect of high strain rate loading on compressive behaviour of fibre-reinforced high-strength concrete", Magazine of Concrete Research, Vol. 63, Issue 11, 813-827, 2011.

128. Weeks C. A., Sun C. T., "Modeling non-linear rate-dependent behavior in fiber-reinforced composites", Composites Science and Technology 58, 603-611, 1998.

129. Westine P. S., Morris B. L., Cox B. L., and Polch E. Z., "Development of computer program for floor plate response from land mine explosions", Technical report No. 13045, US Army Tank-Automotive Command, Warren, MI, 1985.

130. Williams K., and McClennan S., "A numerical analysis of mine blast effects on simplified target geometries: Validation of loading models", Defense R&D Canada-Valcartier, DRDC Valcartier TM 2002-260, 2002.

131. Xia Z., Curtin W. A., "Multiscale modeling of tensile failure in fiber-reinforces composites", Multiscale modeling and simulation of composite materials and structures, Springer, 83-164, 2008.

132. Zhang G., Hart C. J., Vlahopoulos N., Bishnoi K., Goetz R., Rostam F., "Simulation for the Response of a Structure Subjected to a Load from an Explosion", SAE World Congress & Exhibition, Part 2, Apr 2008.